AD

230243

"NOTICE: When Government or other drawings, specifications or other data are used for any purpose other than in connection with a definitely related Government procurement operation, the U.S. Government thereby incurs no responsibility, nor any obligation whatsoever; and the fact that the Government may have formulate furnished, or in any way supplied the said drawings, specifications or other data is not to be regarded by implication or otherwise in any manner licensing the holder or any other person or corpor tion, or conveying any rights or permission to manufacture, use or sell any patented invention that may in any way be related there

DYNAMIC STABILITY ASPECTS OF CYLINDRICAL JOURNAL BEARINGS USING COMPRESSIBLE AND INCOMPRESSIBLE FLUIDS

E. Sternlicht
H. Poritsky
E. Arwas

Contract No. Nonr 2611(00) Proj. No. NR 062 [illegible]

GENERAL ELECTRIC

DOES NOT APPLY.

E.B.A. Dec 22 '59

"Dynamic Stability Aspects of Cylindrical Journal Bearings Using Compressible and Incompressible Fluids" - B. Sternlicht, H. Poritsky, E. Arwas

Errata Sheet

Page	Line	Correction
10	17	should read: " $\frac{R}{C}\frac{V_t}{U} = \frac{\epsilon}{\omega}\frac{d\alpha}{dt} = \frac{\epsilon\dot{\alpha}}{\omega} = \epsilon\alpha'$ "
14	5	" atmosphereic " should read: " atmospheric "
19	11	" equation (12) " should read: " equation (18) "
20	13	" equation (1) " should read: " equation (19) "
20	17	should read: " $z = Ae^{i\lambda t} + Be^{-i\lambda t}$ "
20	18	should read: " where A and B are arbitrary constants and: "
20	19	should read: " $\lambda = \sqrt{\frac{k + ik_1}{m}} = \omega + i\omega_1$
20	20	" $e^{j\lambda t}$ or $e^{-j\lambda t}$ " should read: " $e^{i\lambda t}$ or $e^{-i\lambda t}$ "
27	12	" in Equation (35) " should read: " in Equation (31) "
35	12	Equation (59) should read: " $s^2 + \frac{sE}{f_1(\epsilon)} - \frac{1}{f_2(\epsilon)} = 0$ "
36	9	" $\partial F_r/\partial\epsilon$ " should read: " $\partial F_r/\partial e$ "
37	15	" Equation 34 " should read: "Equation (60) "
40	last line	" Figure 10 " should read: " Figure 30 "
44	17	should read: " direction "
45	3	" Equation (71) " should read: " Equation (73) "
46	16	" Equation (82) " should read: " Equation (84) "
46	20	" Equation (84) " should read: " Equation (83) "
47	3	" Equation (83) " should read: " Equation (85) "
49	1	" of this stability " should read: " of this instability "
51	5	" Sections III, IX and " should read: " Sections IX and "
53	last line	" Figures 22 and 23 " should read: " Figures 28 and 30 "

DYNAMIC STABILITY ASPECTS OF CYLINDRICAL JOURNAL BEARINGS USING COMPRESSIBLE AND INCOMPRESSIBLE FLUIDS

By

B. STERNLICHT

H. PORITSKY

E. ARWAS

GENERAL ENGINEERING LABORATORY
GENERAL ELECTRIC COMPANY
SCHENECTADY, NEW YORK

CONTRACT NO: Nonr - 2844 (00)

TASK NO. NR 097-348

TABLE OF CONTENTS

LIST OF FIGURES

ABSTRACT

~~The paper presents~~ solutions of Reynolds equation for cylindrical journal bearings in which the velocity of the journal center is considered; however, the inertia terms are neglected. Solutions are obtained for ~~both~~ compressible and incompressible fluids. Analysis of the steady state forces that exist in compressible fluid, externally-pressurized cylindrical journal bearings with one plane of feeding is also included. From these analyses the gradients of the radial and tangential forces with respect to displacement and velocity are obtained. The equations of motion for small and large oscillation in terms of these forces and gradients are set up, and stability criteria are established for small oscillations and also for large oscillations of a massless rotor. Sample calculations for threshold of instability are given and, where existing experimental data is available, theoretical predictions are compared with results attained in practice.

I INTRODUCTION

The dynamic characteristics of rotating equipment are becoming very much more important with the present trend towards higher speeds and precision equipment such as turbines, compressors, gyros, grinders, etc. Numerous examples can be cited where equipment was unacceptable or actually failed due to instability, excessive vibrations, operating speed coinciding with system criticals, and other dynamic malfunctions.

In recent years it has been pointed out that bearings have major influence on dynamic response of rotors. They possess both stiffness and damping and thus govern the system criticals and amplitudes of vibration. It has also been shown that forces generated in the fluid films of the bearings may excite lateral vibration in a rotor and cause it to become unstable. This instability may be so violent that the bearings fail within minutes and often damage the whole machine. The importance of this problem, therefore, has attracted many investigators since it was first reported by Newkirk and Taylor in 1925. However, the subject is very complicated and it is not surprising that many observations and even the terminology are controversial.

A brief history may be in order so as to highlight some of these observations. Newkirk and Taylor (1) reported a violent whip of shafts which was caused by the oil film in the bearing. They found that the whip started at speed twice the critical and persisted at higher speeds. Often the instability could be initiated merely by shock. Robertson (2) made certain assumptions and reached the conclusion that the rotor is inherently

unstable at all speeds of rotation. Poritsky (3) showed, by introducing an additional force to the oil film force, that the instability occurs only at speeds exceeding twice the first critical speed. Boeker and Sternlicht (4) pointed out that the additional force introduced by Poritsky (3) in reality does exist and it corresponds to the radial component of the hydrodynamic force. Ref. 4 further points out that the threshold of instability is dependent on the magnitude of this force and that under some conditions instability may start even at zero speed. It also shows that the analysis applies equally to compressible and incompressible hydrodynamic lubrication, provided the hydrodynamic forces are properly calculated for the two cases. This important observation was verified experimentally in Ref. (4) and more recently Fischer, Cherubim and Decker (5) have confirmed this in their experiments. On the other hand, Newkirk and Lewis (6, 7) and Jukis Hori (8) reported experimental cases in which the rotating speed reached five or six times the critical before the instability developed.

Newkirk and Taylor (1, 7) reported also that the violence of whip increases with speeds higher than twice the critical . Hori (8) and Sternlicht (9) observed that in some cases the amplitude of whip decreased as the speed increased. Pinkus (10) found even more complicated examples in which whip disappeared and appeared again as speed was raised.

The effect of fluid viscosity, turbine or motor electrical loads on instability are even more controversial.

Another class of instabilities, often referred to as "Fluid Criticals", are rotor instabilities of limited speed range due to fluid-film action. These have first been discovered by Stodola (11) and further studied by his pupil Hummel (12). Cameron (13) pointed out that aside from the two criticals discussed by Hummel, there also is a third critical in the region of eccentricity ratio less than 0.7.

These observations point out some of the complexities and controversies in the subject. In this study the authors give a more comprehensive theory of stability which explains some of the inconsistencies and gives a better insight into the subject matter.

(In order to clarify the terminology employed in this paper, a section entitled "The Mechanics of Hydrodynamic Instability" is given which defines some of the terms.)

The report gives a number of solutions of Reynolds equation for isothermal compressible and incompressible lubrication of plain cylindrical journal bearings. The analysis neglects inertia terms but considers velocity of the journal center. In the case of compressible lubrication, $p_a = 14.7$ psia is assumed at $z = \pm L/2$. Few cases are also given for 120° partial journal bearing operating with air as lubricant. Results are given in dimensionless form for the radial and tangential forces as functions of $(\varepsilon, \dot{\varepsilon}', L/D)$.

Several cases are also solved for the compressible externally pressurized cylindrical journal bearing with central single plane of feeding, operating under non-rotating steady state condition. Dimensionless force

is given as a function of (ε, L/D, p_s, p_a, $Z_{t\ opt}$).

A brief discussion is next included to show that instability is induced by forces normal to the radial displacement of the journal. Following this, equations and methods of calculation are given for the threshold of half frequency whirl for both vertical and horizontal symmetrical rotors. Equations are also given for calculating the amplitudes of forced vibration of vertical shafts. It is further shown how the fluid film and rotor resonance in rigid vertical shafts can be calculated.

Equations of motion are set up for small oscillations about a position of equilibrium. The equations are in terms of displacements and the hydrodynamic radial and tangential forces. Solutions of these equations exist in which time enters as an exponential. Several solutions are given for a symmetrical rotor supported by an elastic shaft and fluid film. Results give the threshold of resonant whip as a function of eccentricity ratio and dimensionless parameter E.

The more general equations for large displacements are also set up in terms of eccentricity ratio and attitude angle. These equations form a set of two non-linear differential equations, each of order 3. In the case of small rotor mass, the tems involving m can be neglected and the differential equations reduce to a second order non-linear system. The integration of these can be carried out by a graphical method and the steps are outlined.

For several cases where experimental data was available, comparison between theory and practice is given. Explanation is given for several of the reported observations which appear to be irreconcilable. It is shown that in reality they provide consistent verification of the theory and thus enlarge our available knowledge for a better understanding of journal bearing instability.

II THE MECHANICS OF HYDRODYNAMIC INSTABILITY

Hydrodynamic instability is caused by forces generated in the fluid film of the bearing, so directed with respect to the shaft displacement as to propel it in its whirling motion. To visualize better the forces which cause this whirling motion, consider Fig. 1 which shows the equilibrium attitude of a shaft rotating in a bearing and supporting a load W. As this is the position of equilibrium, the resultant force of the fluid film on the shaft is the force F, which must be equal and opposite to W. The important thing to notice in Fig. 1 is that the force F is not in the direction of centers O'O but at an angle Φ to it.

Now let us consider a rotating shaft which carries no load, (W = 0,) and suppose that it is momentarily displaced from O to O', as shown in Fig. 2. The film under these conditions exerts a resultant force F on the shaft, just as it did in Fig. 1. However, in this case there is no opposing force, W, so the force F must be spent in accelerating the shaft and overcoming the frictional drag of its resulting motion. The movement of the shaft center O' in response to the force F obviously will not be toward the shaft center O. Rather, the shaft center will be forced to progress in an orbit around the bearing center and as long as the centers do not coincide, some force F will be generated by the rotation of the shaft and the whirl will continue. Whether the whirling motion becomes more pronounced, continues at the same amplitude, or dies out, depends upon the angle Φ and the damping characteristics of the bearing and shaft system.

The whirl frequency is set by the speed at which the shaft can pump the fluid around in the clearance and maintain the pressure pattern which produces the driving force F. Assuming laminar conditions and neglecting flow due to any pressure gradients (which in a lightly loaded bearing are very small), the average lubricant velocity is half the peripheral speed and in the direction of shaft rotation. Hence, the greatest frequency at which a pressure pattern can progress around the bearing is half the shaft speed. This is the speed and direction at which the shaft vibration occurs. We shall refer to this kind of instability as "Half-Frequency Whirl".

Finally, consider the case illustrated in Fig. 2, in which the shaft supports a load W in the equilibrium position O'. Suppose the shaft, by some external shock, is momentarily given a secondary displacement to a new position O''. The fluid force F corresponding to this new position of the shaft is no longer equal and opposite to W. The vector difference between the forces F and W is a force F_2 which can cause the shaft center to whirl (in the direction of shaft rotation) around its equilibrium position O' at a speed nearly equal to half the shaft rotational speed - just as in the case of the unloaded shaft discussed above. As before, the persistence of such a whirling motion will depend upon the damping characteristics of the system.

Another phenomenon, system resonance, can join with half frequency whirl to produce a vigorous vibration. When the rotational speed is about twice the actual system first critical, the system will build up in resonance at a frequency equal to the system first critical frequency. This form of

resonance is referred to as "Resonant Whip" and may be defined as a resonant vibration of a journal in a fluid film bearing which, for low eccentricity ratios, sets in at approximately twice the actual first system critical and persists at higher speeds with the frequency of vibration approximately equal to the first system critical regardless of running speed. Here too the motion of the shaft center is in the same direction as shaft rotation. Resonant whip is a self-supported vibration, as is half frequency whirl. In the case of resonant whip, the vibration is supported by the fluid film action while the frequency is controlled by the system critical speed.

III CALCULATION OF FLUID FILM FORCES IN SELF ACTING BEARINGS

The general form of the Reynolds equation may be written

$$\frac{\partial}{\partial x}\left[h^3 \rho \frac{\partial p}{\partial x}\right] + \frac{\partial}{\partial z}\left[h^3 \rho \frac{\partial p}{\partial z}\right] = 6\mu \left[U \frac{\partial (h\rho)}{\partial x} + 2 \rho V + 2h \frac{\partial \rho}{\partial t}\right] \quad (1)$$

In this equation U is the relative tangential velocity between the journal and bearing surfaces and V is the relative normal velocity between them.

Equation (1) then contains the terms which determine the instantaneous velocity of the journal center. The fluid inertia terms, however, are neglected in the derivation of Equation (1), in accordance with past analytical and experimental evidence which show their effect to be small, at least at moderate speeds.

The hydrodynamic pressures (and hence, by integration, the fluid film forces) are obtained from the integration of Equation (1) using the appropriate boundary conditions.

For a full circular bearing, Equation (1) is subject to the boundary condition of ambient pressures at the edges. Thus:

$$p(\theta, L/2) = p(\theta, -L/2) = p_a \quad (2)$$

We will now further examine Equation (1), first for the case of an incompressible fluid, then for the case of a compressible fluid under isothermal conditions.

A. Incompressible Fluid

If the fluid is incompressible, the density is assumed constant and can therefore be factored out of Equation (1), which then reduces to:

$$\frac{\partial}{\partial\theta}\left[(1+\varepsilon\cos\theta)^3\frac{\partial p}{\partial\theta}\right]+R^2\frac{\partial}{\partial z}\left[(1+\varepsilon\cos\theta)^3\frac{\partial p}{\partial z}\right]=6\mu\left(\frac{R}{C}\right)^2\left[\varepsilon(\omega-2\dot{\alpha})\sin\theta+2\dot{\varepsilon}\cos\theta\right] \quad (3)$$

Also, in the case of an incompressible fluid, cavitation may occur. If the pressure "p" tends to take on values below ambient over an area A_c extending to the ends of the bearing, then cavitation occurs over A_c. Equation (3) then applies outside A_c, along with the additional boundary conditions:

$$p = p_a \text{ over } A_c$$

$$\frac{\partial p}{\partial n} = 0 \text{ over C, the boundary of } A_c \quad (4)$$

(where n is the directional co-ordinate normal to C)

If cavitation were to occur over an internal area not extending to the bearing ends, pressure below ambient could occur and the onset of cavitation would be governed by the boundary conditions:

$$p = 0 \text{ over } A_c$$

$$\frac{\partial p}{\partial n} = 0 \text{ over C} \quad (4a)$$

It turns out, however, that no such situation occurs and Equation (4) applies.

For incompressible fluids, p in Equation (1) may be used to denote the pressure above ambient (gage pressure) in which case we set p_a(gage) = 0

The integration of Equation (3) yields the pressure distribution in the bearing corresponding to the conditions at which the integration is performed. By a further integration of the pressures outside of C, one obtains the net resultant force which the fluid film exerts on the journal and thus, one may evaluate the components F_r and F_t, of this force in the radial and tangential directions respectively.

From dimensional analysis considerations, these components can be expressed in the following form:

$$F_r = -\mu LU\left(\frac{R}{C}\right)^2 f_r\left(\varepsilon, \frac{V_r}{U}, \frac{V_t}{U}, \frac{L}{D}\right)$$
$$F_t = \mu LU\left(\frac{R}{C}\right)^2 f_t\left(\varepsilon, \frac{V_r}{U}, \frac{V_t}{U}, \frac{L}{D}\right) \qquad (5)$$

where V_r ($= C\dot{\varepsilon}$) and V_t ($= C\varepsilon\dot{\alpha}$) are the radial and tangential components, respectively, of the journal center velocity, and where f_r and f_t are dimensionless and depend on the dimensionless variables shown.

Note that the dimensionless quantities V_r/U and V_t/U may be replaced as follows:

$$\frac{R}{C}\cdot\frac{V_r}{U} = \frac{1}{\omega}\frac{d\varepsilon}{dt} = \frac{\dot{\varepsilon}}{\omega} = \varepsilon'$$

$$\frac{R}{C}\cdot\frac{V_t}{U} = \frac{1}{\omega}\frac{d\alpha}{dt} = \frac{\dot{\alpha}}{\omega} = \alpha'$$

For any given L/D ratio then, Equation (5) may be written:

$$F_r = -\mu LU\left(\frac{R}{C}\right)^2 f_r\left(\varepsilon, \varepsilon', \alpha'\right)$$
$$F_t = \mu LU\left(\frac{R}{C}\right)^2 f_t\left(\varepsilon, \varepsilon', \alpha'\right) \qquad (5a)$$

The negative sign in the F_r equation is due to the fact that F_r is measured positive in the direction of increasing radial displacement, while (at least for $V_t = 0$) the radial force turns out to point in the direction opposing the radial displacement.

The right hand member of Equation (3) is linear in ω, $\dot{a}$, $\dot{\varepsilon}$. It would appear from this that Reynolds equation for incompressible fluids can be integrated separately first for a stationary journal center, ($\omega \neq 0$, $\dot{\varepsilon} = \dot{a} = 0$), then for a radial velocity of the journal center ($\omega = \dot{a} = 0$, $\dot{\varepsilon} \neq 0$), and finally for a tangential velocity of the journal center ($\omega = \dot{\varepsilon} = 0$, $\dot{a} \neq 0$), and hence by superposition, the pressures (and thus the forces F_r and F_t) obtained for the joint effects of U, V_r and V_t. This condition, however, is vitiated by the non-linear requirement of the boundary condition given in Equation (4) and the fact that the curve C will, in general, change in a manner depending on all three velocities U, V_r and V_t.

Nevertheless, examination of the right hand side of Equation (3) shows that at least U and V_t enter in the form $(\varepsilon CU - 2RV_t) \sin\theta$, or its equivalent form, $(\omega - 2\dot{a}) \sin\theta$. Suppose that Equation (3) is integrated for a given L/D and the forces F_r and F_t evaluated for $V_t = 0$ yielding

$$\begin{aligned} F_r &= -\lambda \omega f_r(\varepsilon, \varepsilon') \\ F_t &= \lambda \omega f_t(\varepsilon, \varepsilon') \end{aligned} \tag{6}$$

where $\lambda \omega$ has the dimensions of a force, λ being defined by:

$$\lambda = \frac{\mu L R}{\pi} \left(\frac{R}{C}\right)^2 \tag{7}$$

Then, for non-zero V_t or $\dot{a}$, the forces may be derived, without further integration, by replacing ω by $\omega (1 - 2a')$. At the same time, the dimensionless parameter ε' must be divided by $(1 - 2a')$. Hence, for $V_t \neq 0$, the fluid film forces become:

$$F_r = -\lambda \omega (1 - 2a') f_r (\varepsilon; \bar{\varepsilon}') \quad \text{and} \quad F_t = \lambda \omega (1 - 2a') f_t (\varepsilon, \bar{\varepsilon}') \tag{8}$$

where

$$\bar{\varepsilon}' = \frac{\varepsilon'}{1 - 2a'} \tag{8a}$$

For the case of a full circular bearing and incompressible fluids, discussed above, numerical integrations of the Reynolds equation have been carried out for L/D ratios of 0.5, 1.0 and 1.5, and for a wide range of journal center speeds. The resulting fluid film forces are given in Tables 1 and 1a, the symbols in these tables corresponding to the nomenclature given in Figure 4.

For the case of L/D = 1, these forces and attitude angles have also been plotted in Figures 5 and 6, on the eccentricity ratio-journal center velocity plane Note that these curves represent an extension of the conventional one parameter steady-state solution to the two parameter dynamic condition. The conventional steady-state solution appears in this more general representation as the particular case where $\bar{\varepsilon}' = 0$.

B. Compressible Fluids - Isothermal Conditions

When the bearing fluid is a gas and the ratio of the film to ambient pressures is large, compressibility effects may no longer be neglected and the more general form of the Reynolds equation given in Equation (1) applies.

The right hand side of Equation (1) includes the non-steady flow term:

$$12 \mu h \frac{\partial \rho}{\partial t}$$

This term may be of importance in cases of high frequency oscillations of the journal center. At low frequency oscillations of the journal center, however, it is of smaller magnitude than the other terms on the right hand side of the equation. Furthermore, its inclusion in the analysis would greatly complicate the work by introducing a third parameter (time) in the solutions. In the present analysis for compressible fluids, the non-steady flow term has been neglected. More rigorous examination of its effect on bearing stability is planned for the future.

We have also assumed in the present analysis that isothermal conditions prevail in the fluid film and this conforms with the results of numerous experiments (see, for example, References 5, 15 and 16).

Under isothermal conditions, the equation of state is:

$$p = R T \rho \tag{9}$$

where R is the gas constant and T, the absolute temperature.

Eliminating ρ from Equation (1) by means of Equation (9) and dropping out the non-steady flow term, the Reynolds equation becomes:

$$\frac{\partial}{\partial x}\left[h^3 p \frac{\partial p}{\partial x}\right] + \frac{\partial}{\partial z}\left[h^3 p \frac{\partial p}{\partial z}\right] = 6\mu\left[U \frac{\partial (ph)}{\partial x} + 2 p V\right] \tag{10}$$

This equation is non-linear. Thus, the method of superposition (which was proved to be invalid in the incompressible case on account of the non-linear boundary condition, Equation (4)) is invalid here too because of the non-linearity of Equation (10).

The boundary condition of atmosphereic pressure at the bearing ends, Equation (2), still holds, however, absolute pressure in the bearing region may now become sub-atmospheric (though, of course, never negative). Once again, as in the incompressible case, the fluid film forces may be expressed in terms of their radial and tangential components F_r and F_t, respectively. Here, of course, the dimensionless functions f_r and f_t have to be calculated anew, this time by integration of the non-linear Reynolds equation (Equation 10).

Numerical integrations have been carried out for full circular bearings (with compressible, isothermal flow) for L/D ratios of 0.5, 1.0 and 1.5, and a wide range of journal center velocities. These are given in Table II. For purposes of comparison, similar additional cases have been calculated for a 120 deg. partial bearing with an L/D ratio of 0.5 and these are given in Table III.

IV CALCULATION OF FORCES ON JOURNAL IN EXTERNALLY-PRESSURIZED BEARINGS

Analyses have been made based on (Ref. 15, 16) for the resultant hydrostatic force acting on a journal in a cylindrical bearing with central plane of feeding. Results are given in terms of L/D ratio, supply pressure p_s, ambient pressure p_a and Z_t.

The governing equation which applies for an incompressible fluid non-rotating journal and small eccentricity ratio is:

$$\frac{\partial^2 p}{\partial x^2} + \frac{\partial^2 p}{\partial z^2} + \frac{3}{h}\frac{\partial h}{\partial x}\frac{\partial p}{\partial x} = 0 \qquad (11)$$

Since $\frac{\partial p}{\partial x} \longrightarrow 0$ as $\varepsilon \longrightarrow 0$, for small ε, $\frac{\partial p}{\partial x}$ is of the same order of magnitude as ε. This means that $\frac{3}{h}\frac{\partial h}{\partial x}\frac{\partial p}{\partial x}$ is of the order of $(\varepsilon)^2$. Thus for $\varepsilon << 1$, equation (11) reduces to

$$\frac{\partial^2 p}{\partial x^2} + \frac{\partial^2 p}{\partial z^2} = 0 \qquad \varepsilon << 1 \qquad (11a)$$

In the case of compressible fluids under isothermal flow conditions equation (11) is of the form

$$\frac{\partial}{\partial x}\left[p\, h^3 \frac{\partial p}{\partial x}\right] + h^3 \frac{\partial}{\partial z}\left[p \frac{\partial p}{\partial z}\right] = 0 \qquad (12)$$

Performing the indicated operations, the equation expands to

$$\frac{1}{p}\left[\left(\frac{\partial p}{\partial x}\right)^2 + \left(\frac{\partial p}{\partial z}\right)^2\right] + \left[\frac{\partial^2 p}{\partial x^2} + \frac{\partial^2 p}{\partial z^2}\right] + \frac{3}{h}\frac{\partial h}{\partial x}\frac{\partial p}{\partial x} = 0 \qquad (12a)$$

The film thickness equation may be written as

$$h = C(1 - \varepsilon \cos\theta)$$

Equation (12a) may now be written as

$$\frac{1}{p}\left[\left(\frac{\partial p}{\partial x}\right)^2+\left(\frac{\partial p}{\partial z}\right)^2\right]+\left[\frac{\partial^2 p}{\partial x^2}+\frac{\partial^2 p}{\partial z^2}\right]+\left[\frac{3\varepsilon \sin\frac{x}{R}}{R\left(1-\varepsilon\cos\frac{x}{R}\right)}\right]\frac{\partial p}{\partial x}=0 \qquad (12b)$$

Now, for small ε, $\frac{\partial p}{\partial x}$ becomes of the order of magnitude of ε, so that Equation (12b) may be reduced to

$$\frac{1}{p}\left[\left(\frac{\partial p}{\partial x}\right)^2+\left(\frac{\partial p}{\partial z}\right)^2\right]+\frac{\partial^2 p}{\partial x^2}+\frac{\partial^2 p}{\partial z^2}=0 \qquad (12c)$$

By defining a new dependent variable, $\hat{p}$, such that

$$p=\sqrt{\hat{p}}$$

Equation (12b) can be rewritten as

$$\frac{\partial^2 \hat{p}}{\partial x^2}+\frac{\partial^2 \hat{p}}{\partial z^2}=0 \qquad (12d)$$

This equation is of the same form as Equation (12a)

Applying the separation technique to Equation (12d) yields two ordinary differential equations which can be solved for $\hat{p}$ (x, z).

It should be pointed out that for rigorous analysis of the externally-pressurized bearing, the equation of continuity of flow between the feeders and the bearing must also be satisfied. Since the feeders and bearing clearance are restrictors in series, they jointly affect the bearing performance. The calculations presented here take account of this and, therefore, the results are in terms of the dimensionless feeding parameter Z_t.

In general one is interested in getting maximum stiffness from a hydrostatic bearing. This is accomplished by optimising the parameter Z_t versus the dimensionless spring constant $\bar{k}$. On the left hand side of the optimum too much restriction is present in the feeding system, while the reverse is true on the right hand side of $Z_{t\,opt}$.

The procedure for calculations is outlined in order to clarify the subject matter:

1) Given L/D, p_s and p_a

2) Assume values of Z_t

3) Calculate

$$Y = \sqrt{\frac{\frac{L}{D}(1 + Z_t)}{Z_t\left[\left(\frac{p_s}{p_a}\right)^2 - 1\right]}} \qquad (13)$$

4) Find g (Y, L/D)

$$g\,(Y,\ L/D) = \frac{3\pi D}{4YL}\left\{e^{-Y^2}\left[\psi\sqrt{Y^2+\frac{L}{D}} - \psi\,(Y)\right] - \frac{\sqrt{\pi}}{2}\,e^{Y^2}\left[\bar{\Phi}\sqrt{Y^2+\frac{L}{D}} - \bar{\Phi}(Y)\right]\right\} \qquad (14)$$

where ψ and $\bar{\Phi}$ are the error functions

$$\psi\,(x) = \int_o^x e^{t^2}\,dt$$

$$\bar{\Phi}\,(x) = \frac{2}{\pi}\int_o^x e^{-t^2}\,dt$$

5) Calculate dimensionless stiffness $\bar{k}$.

$$\bar{k} = \frac{g\,(Y,\ L/D)}{\cosh\frac{L}{D} + \frac{Z_t\,D}{2\,L}\sinh\frac{L}{D}} \qquad (15)$$

and optimize $\bar{k}$ by varying Z_t (see Figure 7).

Stiffness can be calculated from

$$k = \bar{k} p_a \frac{DL}{C} \qquad (16)$$

6) Calculate dimensionless pressure, $\bar{p}$ vs ε

$$\bar{p}_{opt} = \frac{p_{opt}}{p_a} = \bar{k}_{opt} \varepsilon \qquad (17)$$

The results are given in Fig. 8-10 for three different supply pressures and three L/D ratios.

7) Restrictor calculations

$$\frac{2Z_t}{L} \sqrt{\frac{p_s^2 - p_a^2}{1 + Z_t}} = \frac{3\mu C_d d^2 n}{D C^3} \sqrt{\frac{g R T}{m}} \qquad (18)$$

where

C_d = discharge coefficient (≈ 0.6)

d = orifice diameter

n = number of feeders/bearing

(14) m = number of orifices/feeder

Several important conclusions can be drawn from this analysis.

a) For a non-rotating externally pressurized journal bearing, the displacement is in the direction of load (attitude angle is zero).

b) The displacement is proportional to load for low eccentricity ratios $\varepsilon < 0.5$. Thus, the fluid stiffness is a constant. This leads to the conclusion that for a given mass rotor the critical speed of the system is independent of eccentricity ratios for $\varepsilon < 0.5$.

c) The critical speed can be raised by increasing the supply pressure. This is confirmed by our experiments and those reported in Ref. 5.

d) From the standpoint of maximum load, it appears that there is an optimum L/D ratio. This shows up clearly in Figure 9, where it is seen that (for the values of the parameters used in that figure) $(L/D)_{opt} = 1$. Thus, Figure 9 shows that a bearing with L/D = 2 which has twice the area of the optimum bearing, carries only 67% of its load. Similarly, a bearing with L/D = 1/2, which has half the area of the optimum bearing, carries 89% of its load.

e) Once the optimum $\bar{F}_t$ is obtained one has still free choice of several parameters in equation (12), e.g., d, C, n and m.

It has been shown by several investigators that the hydrodynamic effects are very small when superimposed on the hydrostatic effects. This is especially true when the hydrostatic supply pressure is high ($p_s/p_a > 3$). There is, however, a small attitude angle when rotation is considered. The attitude angle decreases with increase in supply pressure for under this condition hydrostatic effects predominate. Experimental results confirming this point are shown in Fig. 11.

From Fig 8-11 one can calculate the optimum force and stiffness as a function of ε, L/D, p_s/p_a. From Fig. 11 one can estimate the attitude angle as a function of p_s and in turn obtain the radial and tangential force and stiffness for the hydrostatic bearing in which hydrodynamic effects due to rotation are considered.

V INSTABILITY INDUCED BY FORCES NORMAL TO RADIAL DISPLACEMENT

In the preceding sections we have obtained the fluid film forces that act on the journal. Before proceeding to use these in the stability investigations, it is of interest to point out the effect of the force component normal to the radial displacement.

The equations of motion of a balanced rotor with a restraining force and a force normal to the displacement from equilibrium and proportional to it are:

$$\begin{aligned} m\ddot{x} &= -kx + k_1 y \\ m\ddot{y} &= -ky - k_1 x \end{aligned} \tag{19}$$

Let:

$$z = x + iy \quad (\text{where } i = \sqrt{-1}\,) \tag{20}$$

Multiplying the second equation (1) and adding it to the first one, there results:

$$m\ddot{z} = -(k + ik_1)\, z$$

whose solutions are:

$$z = A\, e^{j\lambda t} + B\, e^{-j\lambda t}$$

where A and B are arbitrary constants, j indicates complex components, and

$$\lambda = \sqrt{\frac{k_1 + i\,k_2}{m}} = \omega + i\,\omega_1$$

Since λ is a complex number, it follows that either $e^{j\lambda t}$ or $e^{-j\lambda t}$ will become infinite with time. Hence, a rotor with a force normal to its displacement is inherently unstable.

VI THRESHOLD FOR HALF FREQUENCY WHIRL

Employing the hydrodynamic forces generated within the fluid film, it has been shown (Ref. 3 and 4) that the threshold of instability may be represented by

$$m\omega^2\left(\frac{1}{k}+\frac{1}{K_2}\right) < 4 \tag{21}$$

where $1/K_2$ is the radial fluid film resiliance. In Ref. 4, it was shown that this inequality applies to bearings which possess a high degree of symmetry. It was also shown in that reference that the results apply to both compressible and incompressible fluids. This point was further confirmed experimentally in Ref. 5.

In Ref. 2 it is shown that neglecting friction forces, the resultant film force due to journal rotation in a plain bearing is at right angles to the eccentricity, and is just balanced by resultant force due to whirling when the whirling frequency is one-half rotational frequency. This result represents the upper limit of whirling frequency for an unloaded ideal bearing. The same result can be deduced more directly by considering the continuity condition that the volume of lubricant passing through the film at some point A, Fig. 12 must equal the volume passing point B plus the volume required to fill the void of the receding journal. In the limiting condition no pressure can exist in the film, hence side leakage is zero, and it follows that

$$\frac{R\omega}{2}(C+e) = \frac{R\omega}{2}(C-e) + 2R\Omega e$$

Hence:

$$\Omega = \omega/2 \tag{22}$$

The same result is obtained regardless of where points A and B are taken.

VII FORCED VIBRATION OF VERTICAL ROTOR (SIMPLIFIED ANALYSIS)

Let us consider a vertical rotor supported by two plain journal bearings as shown in Fig. 13. The rotor consists of a flywheel fitted to a shaft and, to simplify the analytical work, it will be assumed that the rotor mass is concentrated at a point situated half-way between the bearings and, further, that the bearings are identical. The center of gravity of the rotor is offset a distance δ from the center of the shaft.

For the amplitudes of vibration of the center line of the shaft at the points 1, 2 and 3 we will use the symbols e_1, e_2 and e_3, respectively. The actual bending deflections of the shaft will be noted by y. The relation between the displacements at various points on the shaft will be as indicated by the displacement diagram of Figure 14. The amplitude of whirl at the point 2 is partly due to the displacement of the shaft in the bearings and partly due to the deflection of the shaft. Further, it will be seen that the amplitude of vibration of the center of gravity of the rotor is the vector sum of e_2 and δ.

Figure 15 shows the force diagram for the rotor. Let us denote the angular velocity of the shaft by ω and the centrifugal force acting on the rotor will be given by the following expression:

$$C.F. = m\omega^2 (e_2 + \delta) \qquad (23)$$

Since there is no damping in the shaft, the phase angle of the shaft deflection must be the same as that of the applied centrifugal force and the vectors representing these two quantities must be parallel. As shown by the force diagram, the centrifugal force is composed of the two components

$m\omega^2\delta$ and $m\omega^2 e_2$ parallel to the amplitudes δ and e_2 respectively.

The centrifugal force acting on the rotor is equally divided between the bearings at 1 and 3 and the force acting on each of these bearings will therefore be equal to C.F./2. Since the bearings are assumed to be identical, the shaft displacements must be the same in both bearings. We will therefore drop the suffices and write $e_1 = e_3 = e$.

Since the forces applied to the bearings are of constant magnitude and rotate with a constant angular velocity, the relation between force and displacement can be determined from the constant load characteristics of the bearings. From Equation (3) it is apparent that introducing a value for $\dot{\alpha}$ makes no difference to the principle of the solution of the equation. Consequently, the use of curves obtained from the constant load calculations can be extended to cover the case of a constant rotating load.

If we consider the disturbing force as the unbalance force then it rotates with the same angular velocity as the journal, i.e., $\dot{\alpha} = \omega$. Making use of the load number, f (Tables I and II), and taking into account the rotation, the force C.F. will be given by the following expression:

$$\frac{C.F.}{2} = \frac{1}{2\pi} \mu \omega L D (R/C)^2 f e^{i(\omega t + \phi)} \qquad (24)$$

For convenience, the attitude angle ϕ has been chosen to be positive when the force on the fluid film leads the displacement, i.e., for negative load numbers. Here, f and ϕ are a function of the eccentricity ratio ϵ as given in Tables I and II.

Let us introduce the symbol β for the phase angle difference between vectors δ and $(e_2 + \delta)$ as shown in Figure 14.

By resolving the displacement vectors in the x and y direction, we arrive at the following two equations:

$$e \sin \phi = \delta \sin \beta \tag{25a}$$

$$\delta + e_2 = e \cos \phi + \delta \cos \beta + y \tag{25b}$$

The deflection of the shaft is obtained from simple beam theory and is given by:

$$y = \frac{C.F.\, \ell^3}{48\, EI} \tag{26}$$

Making use of Equations (23), (24) and (26), Equation (25b) can now be written:

$$\frac{1}{\pi}\, \mu\, LD\, (R/C)^3\, f\, \left(\frac{1}{m\omega} - \frac{\ell^3\, \omega}{48\, EI}\right) = e \cos \phi + \delta \cos \beta \tag{27}$$

The unknown β can be eliminated between Equations (25a) and (27) and as a result we obtain the following relation between the frequency and the amplitude of whirl:

$$\left\{\frac{1}{\pi}\mu\, LD\, (R/C)^3\, f\, \left(\frac{1}{m\omega} - \frac{\ell^3\, \omega}{48\, EI}\right)\right\}^2 - \frac{2}{\pi}\mu\, LD\, (R/C)^2\, f\, \left(\frac{1}{m\omega} - \frac{\ell^3\, \omega}{48\, EI}\right) e \cos \phi + e^2 = \delta^2 \tag{28}$$

For a further study it will be convenient to introduce in the above equation a new variable defined by:

$$\gamma = \frac{1}{m\omega} - \frac{\ell^3\, \omega}{48\, EI} \tag{29}$$

This leads to a simple quadratic equation, the solution of which is:

$$\gamma = \frac{\pi}{f\, \mu\, LD}\left(\frac{C}{R}\right)^2 \left\{e \cos \phi \pm \left[e^2 \cos^2 \phi + (\delta^2 - e^2)\right]^{1/2}\right\}$$

Making use of Table I and the above equation, values can be found for γ as a function of any eccentricity e.

The frequency ω is defined in terms of γ by Equation (29). Rearranging and solving for ω we get the following formula:

$$\omega = -\frac{24\ EI\ \gamma}{l^3} \pm \left[\left(\frac{24\ EI\ \gamma}{l^3}\right)^2 + \frac{48\ EI}{l^3\ m}\right]^{1/2}$$

VIII FLUID FILM AND ROTOR RESONANCE

Fluid film resonance is a consequence of the quasi-elastic properties of the oil film. The phenomenon may therefore be studied by assuming that the rotor is rigid. The conditions of a rigid rotor may be simulated by setting $\ell^3/EI = 0$ in Equation (29). Thus, we obtain the following relation:

$$\gamma = 1/m\omega$$

By substituting the expression for γ in the above equation we obtain the following equation for ω:

$$\omega = \frac{\mu LD (R/C)^2 f}{\pi m \left\{ e \cos \phi \pm \left[e^2 \cos^2 \phi + (\delta^2 - e^2) \right]^{1/2} \right\}} \qquad (30)$$

By considering the forces acting on the journal it is possible to derive the frequency response characteristics for the system and predict the variation in amplitude of "fluid resonance" with speed. Referring to Fig. 15, we shall denote the disturbing force by the vector P, the instantaneous position of the journal by the vector e, and the force in which the fluid film exerts on the journal by F. The inertia force acting on the journal will be given by $m\ddot{e}$.

If the journal is vertical and there are no other external forces acting we can express the conditions of force equilibrium for the journal by the following vector equation.

$$m\ddot{e} + F = P \qquad (31)$$

Let $m\delta$ denote the out-of-balance of the rotor and ω its angular velocity. The disturbing force acting on the rotor will then be given by:

$$P = m \delta \omega^2 e^{i(\beta + \omega t)} \qquad (32)$$

Where β is the phase angle of the disturbing force relative to the displacement vector e.

If we assume that the journal center moves in a circular path around the bearing center, we can write

$$e = e_o e^{i\omega t}$$

where e_o is constant over any complete revolution.

The inertia force acting on the journal can, therefore, be expressed by

$$m\ddot{e} = -m\omega^2 e_o e^{i\omega t} \tag{33}$$

If we assume that a single bearing is taking the total load, Equation (30) becomes

$$F = \frac{1}{2\pi} \mu \omega LD (R/C)^2 f e^{i(\omega t + \phi)} \tag{34}$$

Making use of Equations (32), (33), and (34) in Equation (35), we obtain:

$$-m\omega^2 e_o e^{i\omega t} + \frac{1}{2\pi} \mu\omega LD \left(\frac{R}{C}\right)^2 f e^{i(\omega t + \phi)} = m\delta\omega^2 e^{i(\omega t + \beta)}$$

The real components in the above equation give:

$$-m\omega e_o + \frac{1}{2\pi} \mu\omega LD (R/C)^2 f \cos\phi = m\delta\omega\cos\beta$$

and from the imaginary components we get:

$$\frac{1}{2\pi} \mu LD (R/C)^2 f \sin\phi = m\delta\omega\sin\beta$$

Eliminating β between the above two equations and rearranging we finally obtain the following equation in ω:

$$\omega^2 - \left\{\frac{m e_o \mu LD (R/C)^2 f \cos\phi}{\pi\left[(m e_o)^2 - (m\delta)^2\right]}\right\}\omega + \frac{\left[\mu LD (R/C)^2 f\right]}{4\pi^2\left[(me_o)^2 - (m\delta)^2\right]} = 0$$

The condition for resonance is that the two roots of the above equation coincide. This will lead to the following relation:

$$\cos^2 \phi = 1 - \left(\frac{m\delta}{me_o} \right) \tag{35}$$

and the resonance frequency will be given by

$$\omega_{res} = \frac{m\, e_o\, \mu\, LD\, (R/C)^2\, f \cos \phi}{2\, \pi\, (m\, e_o)^2 - (m\delta)^2} \tag{36}$$

IX EQUATIONS OF SMALL OSCILLATIONS

In Sections III and IV, the fluid film forces that act on the journal were obtained. We will now consider the equations of motion for small oscillations about a position of equilibrium corresponding to some particular external, steady load, making use of these forces.

Introduce fixed rectangular (x, y) axes as in Fig. 16. Suppose now that under a certain external steady load on the journal, it is running at eccentricity ratio ε_o which corresponds to position A_o, which we choose as the direction of positive y. Then Equation 6 yields for the steady load on the journal

$$\begin{aligned} F_r &= -\lambda\,\omega f_r(\varepsilon_o, 0) \\ F_t &= \lambda\,\omega f_t(\varepsilon_o, 0) \end{aligned} \tag{37}$$

Consider next a small (variable) deflection $d\alpha$, $d\varepsilon$ of the journal center to A, near the position A_o, and let X, Y be the added forces on the journal in the x, y direction resulting from this displacement. From Equations 8 due to changes in magnitude of F_r, F_t, we obtain (since ω is constant)

$$\begin{aligned} dF_r &= \lambda\left[2\,d\dot{\alpha}\, f_r - \omega\left(\frac{\partial f_r}{\partial \varepsilon}\,d\varepsilon + \frac{\partial f_r}{\partial \varepsilon'}\,d\varepsilon'\right)\right] \\ dF_t &= \lambda\left[-2d\dot{\alpha}\, f_t + \omega\left(\frac{\partial f_t}{\partial \varepsilon}\,d\varepsilon + \frac{\partial f_t}{\partial \varepsilon'}\,d\varepsilon'\right)\right] \end{aligned} \tag{38}$$

where f_r, f_t, $\frac{\partial f_r}{\partial \varepsilon}$, $\frac{\partial f_t}{\partial \varepsilon}$, $\frac{\partial f_r}{\partial \varepsilon'}$, $\frac{\partial f_t}{\partial \varepsilon'}$ are evaluated at $\varepsilon = \varepsilon_o$, $\varepsilon' = 0$.

These forces contribute directly to Y, X respectively. In addition, there are also contributions to X, Y due to the directional changes $d\alpha$, given by

$$\begin{aligned} F_r\,d\alpha &= -\lambda\,\omega f_r\,d\alpha \\ -F_t\,d\alpha &= -\lambda\,\omega f_t\,d\alpha \end{aligned} \tag{39}$$

where f_r, f_t are also evaluated at ε_o, 0. Hence

$$X = \lambda \left[- \omega \, da \, f_r - 2 d\dot{a} \, f_t + \omega \left(\frac{\partial f_t}{\partial \varepsilon} \, d\varepsilon + \frac{\partial f_t}{\partial \varepsilon'} \, d\varepsilon' \right) \right]$$

$$Y = \lambda \left[- \omega \, da \, f_t + 2 d\dot{a} \, f_r - \omega \left(\frac{\partial f_r}{\partial \varepsilon} d\varepsilon + \frac{\partial f_r}{\partial \varepsilon'} \, d\varepsilon' \right) \right] \qquad (40)$$

Since f_r, f_t are positive and increasing functions of ε as well as of ε', both f_r, f_t and the various derivatives $\frac{\partial f_r}{\partial \varepsilon}$, $\frac{\partial f_r}{\partial \varepsilon'}$ are positive.

Let the components of the displacement $A_o A$ along the x, y direction be ξ, η (see Fig. 16) and let a be measured from y-axis. Then for small ξ, η and a, there results from Fig. 16.

$$d\varepsilon = \frac{\eta}{C}, \qquad da = \frac{\xi}{\varepsilon_o C},$$

$$d\varepsilon' = \frac{d\dot{\xi}}{\omega} = \frac{\dot{\eta}}{C\omega}, \qquad d\dot{a} = \frac{\dot{\xi}}{\varepsilon_o C} \qquad (41)$$

Equations (40) yield

$$X = \lambda \left[- \frac{\omega f_r \xi}{\varepsilon_o C} - \frac{2 f_t \dot{\xi}}{\varepsilon_o C} + \omega \frac{\partial f_t}{\partial \varepsilon} \frac{\eta}{C} + \frac{\partial f_t}{\partial \varepsilon'} \frac{\dot{\eta}}{C} \right]$$

$$Y = \lambda \left[- \frac{\omega f_t \xi}{\varepsilon_o C} + \frac{2 f_r \dot{\xi}}{\varepsilon_o C} - \omega \frac{\partial f_r}{\partial \varepsilon} \frac{\eta}{C} - \frac{\partial f_r}{\partial \varepsilon'} \frac{\dot{\eta}}{C} \right] \qquad (42)$$

Because of the assumption of small a, Equations 41 and 42 are not valid for small ε.

Now, suppose, as in Fig. 17, that a rotor, consisting of a single disk is symmetrically mounted on a shaft, which is carried in two similar and symmetrically placed bearings. Let k be the shaft stiffness constant. We assume that the deflections of the shaft in each bearing, both for the steady load deflection ε_o and for small further deflections are symmetrical about

the middle plane of the rotor, and that steady load and the added forces X, Y on each journal are equal. The shaft segment to the left of the rotor has the force X, Y_o+Y exerted on it by the lubricant on its journal, and must have an equal and opposite force exerted on it by the rotor mass (which also exerts a similar force on the shaft segment to the right). Thus the shaft center deflects relative to the journal centers an amount

$$x = -2X/k, \qquad y = -2Y/k \tag{43}$$

giving rise to a net displacement of the rotor center

$$x + \xi, \qquad y + \eta \tag{44}$$

We suppose that the steady force $-2Y_o$ is an external load on the rotor (gravity). The remaining forces, 2X and 2Y, assuming that the rotor is balanced, can only be used up as "inertia forces". Hence

$$\begin{aligned} 2X &= m(\ddot{x} + \ddot{\xi}) = -kx \\ 2Y &= m(\ddot{y} + \ddot{\eta}) = -ky \end{aligned} \tag{45}$$

and substituting from Equations (42) we get

$$\begin{aligned} X &= \lambda\left[-\frac{\omega f_r \xi}{\varepsilon_o C} - \frac{2 f_t \dot{\xi}}{\varepsilon_o C} + \frac{\omega \partial f_t}{\partial \varepsilon}\frac{\eta}{C} + \frac{\partial f_t}{\partial \varepsilon'}\frac{\dot{\eta}}{C}\right] = \frac{m}{2}(\ddot{x} + \ddot{\xi}) = -\frac{kx}{2} \\ Y &= \lambda\left[-\frac{\omega f_t \xi}{\varepsilon_o C} + \frac{2 f_r \dot{\xi}}{\varepsilon_o C} - \frac{\omega \partial f_r}{\partial \varepsilon}\frac{\eta}{C} - \frac{\partial f_r}{\partial \varepsilon'}\frac{\dot{\eta}}{C}\right] = \frac{m}{2}(\ddot{y} + \ddot{\eta}) = -\frac{ky}{2} \end{aligned} \tag{46}$$

Here the functions f_r, f_t and their derivatives with respect to ε, ε' are all evaluated at the equilibrium eccentricity ratio, and for $\varepsilon' = 0$. They are given in Fig. 18-21 for the incompressible cases and in Fig. 22-25 for the compressible cases.

The differential equations (46) are linear in the variable ξ, η; x, y and solutions of them exist in which time enters as an exponential. These may be expressed in dimensionless form as

$$e^{\nu\tau}, \text{ where } \tau = \omega_o t, \qquad \omega_o = \sqrt{\frac{k}{m}} \tag{47}$$

Here ω_o is the critical speed of the rotor mass m with a shaft stiffness k.

From the right hand equation pair of equation (46), there results

$$x = -\frac{m(\nu\omega_o)^2}{k + m(\nu\omega_o)^2}\,\xi, \qquad y = -\frac{m(\nu\omega_o)^2}{k + m(\nu\omega_o)^2}\,\eta \tag{48}$$

Equation (46) now leads to the determinantal equation

$$\begin{vmatrix} \left[\omega f_r + 2\nu\omega_o f_t + \frac{k m \varepsilon_o C (\nu\omega_o)^2}{2\lambda\left[k + m(\nu\omega_o)^2\right]}\right] & \left[\omega\frac{\partial f_t}{\partial\varepsilon} + \nu\omega_o\frac{\partial f_t}{\partial\varepsilon'}\right] \\ \left[-\omega f_t + 2\nu\omega_o f_r\right] & \left[\omega\frac{\partial f_r}{\partial\varepsilon} + \nu\omega_o\frac{\partial f_r}{\partial\varepsilon'} + \frac{k m C (\nu\omega_o)^2}{2\lambda\left[k + m(\nu\omega_o)^2\right]}\right] \end{vmatrix} = 0 \tag{49}$$

if we now introduce the dimensionless ratio

$$s = \frac{\omega}{\omega_o} \tag{50}$$

we obtain, on dividing through by ω_o:

$$f(\nu) = \begin{vmatrix} \left[s f_r + 2\nu f_t + \frac{E\varepsilon_o\nu^2}{1+\nu^2}\right] & \left[s\frac{\partial f_t}{\partial\varepsilon} + \nu\frac{\partial f_t}{\partial\varepsilon'}\right] \\ \left[-s f_t + 2\nu f_r\right] & \left[\frac{E\nu^2}{1+\nu^2} + s\frac{\partial f_r}{\partial\varepsilon} + \nu\frac{\partial f_r}{\partial\varepsilon'}\right] \end{vmatrix} = 0 \tag{51}$$

where

$$E = \frac{k C^3 \pi}{2\mu L R^3 \omega_o} \tag{52}$$

Onset of Instability

It may be shown that for small values of s, all six roots of Equation (51) lie in the left half of the complex ν plane. This means that the solutions of the small displacement equations (46), about the position of equilibrium corresponding to the given constant load on the rotor, are stable. On the other hand, if s is large, it can be shown that some of the roots lie in the real half of the complex plane, so that the solutions of Equation (46) become unstable. The transition from stability to instability, one may further show, can never take place by a root crossing at $\nu = 0$. Therefore, this transition can only occur as a result of roots crossing the pure imaginary ν axis, as illustrated in Figure 26. We now proceed to find when this crossing takes place. (Note first that to study the roots of Equation (51), it is convenient to keep constant the value of ε_o at which f_r and f_t and their derivatives are evaluated.)

Writing

$$\zeta = \frac{E \nu^4}{1 + \nu^4} \tag{53}$$

Equation (51) becomes

$$\begin{vmatrix} s f_r + 2 \nu f_t + \varepsilon \zeta & s \dfrac{\partial f_t}{\partial \varepsilon} + \nu \dfrac{\partial f_t}{\partial \varepsilon'} \\ -s f_t + 2 \nu f_r & s \dfrac{\partial f_r}{\partial \varepsilon} + \nu \dfrac{\partial f_r}{\partial \varepsilon'} + \zeta \end{vmatrix} = 0 \tag{54}$$

To find the threshold of instability, we seek pure imaginary roots of (51). For such a root, both the real part and the pure imaginary part of $f(\nu)$ in (51) must vanish separately.

Equating to zero the imaginary part of Equation (54), we have:

$$\nu \begin{vmatrix} 2 f_t & s \dfrac{\partial f_t}{\partial \varepsilon} \\ 2 f_r & s \dfrac{\partial f_r}{\partial \varepsilon} + \zeta \end{vmatrix} + \nu \begin{vmatrix} s f_r + \varepsilon \zeta & \dfrac{\partial f_t}{\partial \varepsilon'} \\ -s f_t & \dfrac{\partial f_r}{\partial \varepsilon'} \end{vmatrix} = \rho$$

Since $\nu \neq 0$:

$$\zeta \left(2 f_t + \varepsilon \frac{\partial f_r}{\partial \varepsilon'}\right) + s \left[f_r \frac{\partial f_r}{\partial \varepsilon'} + f_t \frac{\partial f_t}{\partial \varepsilon'} \right] + 2s \left(f_t \frac{\partial f_r}{\partial \varepsilon} - f_r \frac{\partial f_t}{\partial \varepsilon} \right) = 0$$

This is linear in ζ and yields for ζ/s an explicit function of ε which turns out negative:

$$\frac{\zeta}{s} = \frac{-2 \left(f_t \dfrac{\partial f_r}{\partial \varepsilon} - f_r \dfrac{\partial f_t}{\partial \varepsilon} \right) - \left(f_r \dfrac{\partial f_r}{\partial \varepsilon'} + f_t \dfrac{\partial f_t}{\partial \varepsilon'} \right)}{2 f_t + \varepsilon \dfrac{\partial f_r}{\partial \varepsilon'}} = -f_1(\varepsilon) \qquad (55)$$

Next, equating to zero the real part of Equation (54), we have:

$$\begin{vmatrix} s f_r + \varepsilon \zeta & s \dfrac{\partial f_t}{\partial \varepsilon} \\ -s f_t & s \dfrac{\partial f_r}{\partial \varepsilon} + \zeta \end{vmatrix} + 2 \nu^2 \begin{vmatrix} f_t & \dfrac{\partial f_t}{\partial \varepsilon'} \\ f_r & \dfrac{\partial f_r}{\partial \varepsilon'} \end{vmatrix} = 0$$

Upon dividing by s^2, substituting for ζ/s from (55), and solving for $(\nu/s)^2$, there results:

$$-\left(\frac{\nu}{s}\right)^2 = \frac{\varepsilon \left[f_1(\varepsilon) \right]^2 - f_1(\varepsilon) \left(f_r + \varepsilon \dfrac{\partial f_r}{\partial \varepsilon} \right) + \left(f_r \dfrac{\partial f_r}{\partial \varepsilon} + f_t \dfrac{\partial f_t}{\partial \varepsilon} \right)}{2 \left[f_t \dfrac{\partial f_r}{\partial \varepsilon'} - f_r \dfrac{\partial f_t}{\partial \varepsilon'} \right]} = f_2(\varepsilon) \qquad (56)$$

This is a function of ε only, and turns out to be positive, yielding a pure imaginary value of

$$\nu = i\,\nu'$$

where

$$\left(\frac{\nu'}{s}\right) = \pm\sqrt{f_2(\varepsilon)} \tag{57}$$

The quantity $\left(\frac{\nu'}{s}\right)$ is the ratio of the oscillation frequency of the journal center to the shaft running frequency at the limit of stability. Note that it is independent of E and depends only on ε.

We now return to Equation (53) and put it in the form:

$$s^2\left(\frac{\Omega}{s}\right)\left(\frac{\nu}{s}\right)^4 - s\,E\left(\frac{\nu}{s}\right)^3 + \frac{\Omega}{s} = 0 \tag{58}$$

Recalling (55), (56) and dividing (58) by $f_1(\varepsilon) \cdot f_2(\varepsilon)$, we obtain:

$$s + \frac{s\,E}{f_1(\varepsilon)} - \frac{1}{f_2(\varepsilon)} = 0 \tag{59}$$

The solution s ($= \omega/\omega_o$) of this quadratic equation depends both on ε and on E and is thus dependent (see Equation 52) on the bearing geometry, fluid viscosity, rotor mass and shaft stiffness. The value of s, obtained by solving Equation (59), expresses the rotor speed at the limit of stability as a function of ω_o, the mass-shaft critical speed.

It should be kept in mind, however, that the critical speed of a mass-shaft-bearings system should be calculated using the combined stiffness of the shaft and lubricant film. For a symmetrical 2-bearings system, this critical speed may be calculated as follows:

a) Shaft Stiffness = k

b) Lubricant film stiffness = $\frac{dF}{de} = \frac{\mu L \omega R (R/C)^2}{\pi C} \frac{df}{d\varepsilon}$

$$= \frac{sk}{2E} \frac{df}{d\varepsilon}$$

The critical speed of the system is then:

$$\omega^2_{CR} = \frac{1}{m\left(\frac{1}{k} + \frac{1}{2} \cdot \frac{2E}{ks} \Big/ \frac{df}{d\varepsilon}\right)} = \frac{\frac{k}{m}}{\left(1 + \frac{E}{s} \Big/ \frac{df}{d\varepsilon}\right)}$$

Its ratio to the shaft-mass critical, ω_o, is

$$\frac{\omega_{CR}}{\omega_o} = \sqrt{\frac{\frac{df}{d\varepsilon}}{\frac{df}{d\varepsilon} + \frac{E}{s}}} \qquad (60)$$

In defining the lubricant film stiffness as above, it is customary to use the radial film stiffness $\partial F_r/\partial \varepsilon$.

Now, the ratio of the rotor speed at the limit of stability to the critical speed of the rotor-shaft-bearings system can be obtained:

$$\frac{\omega}{(\omega_{CR})_{rad}} = \frac{\omega}{\omega_o} \Big/ \frac{(\omega_{CR})_{rad}}{\omega_o} = \frac{s}{\sqrt{\frac{\frac{df_r}{d\varepsilon}}{\frac{df_r}{d\varepsilon} + \frac{E}{s}}}}$$

The value of s used in this equation being that obtained from the solution of Equation (59).

Example:

Consider the rotor-shaft-bearings system of Figure 27.

R = 1 inch

$\frac{L}{D}$ = 0.5 and 1

$\frac{C}{R}$ = 10^{-3}

k = 1.25×10^6 lb./in. (From Fig. 27 for a steel rotor + shaft)

m = 0.1 lb.-sec.^{2}/in. (From Fig. 27 for a steel rotor + shaft)

The dimensionless number E (defined in Equation 52), is a function of bearing geometry, shaft stiffness and fluid viscosity. In the example worked out here, the range: $0.1 \leq E \leq 100$ is covered. For the rotor shown in Fig. 27 this corresponds to a viscosity ranging from order 10^{-9} to order 10^{-6} lb.-sec.^{2}/in. The range of eccentricity ratios covered in this example is $0.1 \leq \varepsilon \leq 0.8$.

The film stiffness used in calculating the natural frequency (per Equation 34) is that due to the radial restoring force. The natural frequencies calculated below will then be those along the radial direction $(\omega_{CR})_r$.

The values of f_r, f_t, $\frac{\partial f_r}{\partial \varepsilon}$, $\frac{\partial f_t}{\partial \varepsilon}$, $\frac{\partial f_r}{\partial \varepsilon'}$ and $\frac{\partial f_t}{\partial \varepsilon'}$, were obtained from the solution of the dimensionless Reynolds Equation. These are given in Table I and Figures 18 through 21 for the incompressible cases and Table II and Figures 22 through 25 for the compressible cases.

Introducing these values into Equations 52, 55, 59, and 60, we obtain: (for the incompressible cases):

Bearing L/D = 0.5

ε	E	$\frac{\zeta}{s}$	$\left(\frac{v}{s}\right)_s$	$\frac{1}{i}\left(\frac{v}{s}\right)$	s	$\frac{(\omega_{CR})_r}{\omega_o}$	$\frac{\omega}{(\omega_{CR})_r}$
0.2	0.1	- 0.9429	-0.1411	0.3756	2.6096	0.9852	2.6488
0.5	0.1	- 3.1968	-0.1252	0.3538	2.8104	0.9974	2.8177
0.8	0.1	-13.4452	-0.05543	0.2354	4.2438	0.9998	4.2446
0.2	1.0	- 0.9429	-0.1411	0.3756	2.1842	0.8533	2.5597
0.5	1.0	- 3.1968	-0.1252	0.3538	2.6739	0.9741	2.7450
0.8	1.0	-13.4452	-0.05543	0.2354	4.2105	0.9985	4.2168
0.2	10.0	- 0.9429	-0.1411	0.3756	0.6307	0.2723	2.3162
0.5	10.0	- 3.1968	-0.1252	0.3538	1.6659	0.7325	2.2743
0.8	10.0	-13.4452	-0.05543	0.2354	3.8919	0.9839	3.9556
0.2	100.0	- 0.9429	-0.1411	0.3756	0.06678	0.02910	2.2948
0.5	100.0	- 3.1968	-0.1252	0.3538	0.2533	0.1315	1.9262
0.8	100.0	-13.4452	-0.05543	0.2354	1.9267	0.7751	2.4857

Bearing L/D = 1

ε	E	$\frac{\zeta}{s}$	$\left(\frac{v}{s}\right)^2$	$\frac{1}{i}\left(\frac{v}{s}\right)$	s	$\frac{(\omega_{CR})_r}{\omega_o}$	$\frac{\omega}{(\omega_{CR})_r}$
0.2	0.1	- 2.6761	-0.1377	0.37	2.6763	0.9948	2.6903
0.3	0.1	- 4.324	-0.1338	0.37	2.7224	0.9971	2.7303
0.7	0.1	-18.484	-0.0846	0.29	3.4179	0.9998	3.4186
0.8	0.1	-29.2005	-0.04898	0.22	4.5169	0.9999	4.5173
0.2	1.0	- 2.6761	-0.1377	0.37	2.5146	0.9488	2.6503
0.3	1.0	- 4.324	-0.1338	0.37	2.620	0.9704	2.7000
0.7	1.0	-18.483	-0.0846	0.29	3.3936	0.9974	3.4024
0.8	1.0	-29.2005	-0.04898	0.22	4.5016	0.9992	4.5052
0.2	10.0	- 2.6761	-0.1377	0.37	1.4108	0.5798	2.4332
0.3	10.0	- 4.324	-0.1338	0.37	1.8120	0.7263	2.4950
0.7	10.0	-18.483	-0.0846	0.29	3.1603	0.9737	3.2457
0.8	10.0	-29.2005	-0.04898	0.22	4.3506	0.9917	4.3872
0.2	100.0	- 2.6761	-0.1377	0.37	0.1951	0.0834	2.3420
0.3	100.0	- 4.324	-0.1338	0.37	0.3198	0.1390	2.300
0.7	100.0	-18.483	-0.0846	0.29	1.6353	0.7000	2.3647
0.8	100.0	-29.2005	-0.04898	0.22	3.1199	0.8998	3.4675

The ratios $\frac{\omega}{(\omega_{CR})_{rad}}$ for these (incompressible) cases are plotted in Figure 28 as a function of the eccentricity ratio, L/D and dimensionless number E. The figure indicates that while for low eccentricity ratios the instability occurs at approximately twice the critical speed, this number increases with increase in

eccentricity ratio. Thus the onset of instability for eccentricity ratios of 0.8 is around three to four times the critical speed. This conclusion agrees with observations which show that stability increases with increase in eccentricity ratio. However, it also shows that instability may occur even at very high eccentricity ratios. These have not been observed for very few machines in practice operate at speeds much above twice the first critical.

The number $\frac{1}{i}\left(\frac{\nu}{s}\right)$, shown in the above table (where $i = \sqrt{-1}$), represents the ratio of the frequency of the oscillation of the shaft center to the running frequency of the shaft, calculated at the onset of instability, as discussed on page 35. This ratio, which was shown to be independent of E, is plotted in Figure 29 as a function of the eccentricity ratio. Note from this figure that for a wide band of eccentricity ratios (between 0.2 and 0.5), the frequency of the shaft oscillations at the onset of instability is between 35% and 40% of the running frequency of the shaft.

Calculations were also made, using the analysis described above, for bearings with an L/D of 1 and using compressible theory. The forces and gradients used in these calculations are those given in Table II and Figures 22-25. From these calculations, the ratio $\frac{\omega}{(\omega_{CR})_{rad}}$ is plotted in Figure 30 as a function of eccentricity ratio and for values of E = 10 and 100. Note, from this figure, that for the compressible case too, the limit of stability increases with increase in eccentricity ratio At low eccentricities, however, instability sets in at very low speed. In fact, Figure 10 suggests that at

zero eccentricity ratio, oscillations will be unstable at all speeds. Some experimental verification of this is given in Reference 4, where it is shown that for vertical rotors ($\varepsilon = 0$) instability exists at all speeds.

It must be pointed out here that the mesh size used (in the digital computer calculations of the fluid film forces and gradients) for the incompressible cases, was approximately three times as coarse as that used for the compressible cases. The reason for this is the much greater complexity of the non-linear, compressible fluid Reynolds equation. Checks were made in a few calculations, using a finer circumferential grid and these showed that the values of total dimensionless force ($f = \sqrt{f_r^2 + f_t^2}$) are obtained with good accuracy in both the compressible and incompressible cases. However, the calculated values of the attitude angle ($\Phi = \mathrm{Tan}^{-1} \frac{f_t}{f_r}$) may be in error by two or three degrees in some of the compressible cases. Since the relative values of the tangential and radial components of fluid film forces are very critical in stability investigations, it is planned to review the results given in Figure 30 using more accurate computations.

The difficulty in obtaining accurate numerical solutions of the non-linear, compressible fluid Reynolds equation illustrates the advisability of evaluating the order of magnitude of each term of the equation. This allows those terms whose order of magnitude can be shown to be small (relative to the other terms of the equation), to be omitted from the equation before numerical solutions are obtained for a wide range of cases. Failure to do this greatly increases the difficulty and computation expense required to obtain accurate results.

X EQUATIONS OF MOTION FOR LARGE DISPLACEMENTS

We now consider the general equations of motion of the journal center and the rotor center, without making the assumption used in section IX that this motion is close to the steady-state position.

Suppose that under a certain applied steady load on the rotor, such as gravity, the journal center is deflected to Q_o, corresponding to $\varepsilon = \varepsilon_o$, and that coordinate axes are chosen as in Figure 31 so that y axis passes through Q_o.

Then the coordinates of Q_o are

$$\xi = 0 \qquad \eta = C\,\varepsilon_o \tag{61}$$

The forces exerted by the lubricant on the journal at each bearing (half the applied steady load) are given by

$$F_{xo} = \lambda\,\omega\, f_t(\varepsilon_o, 0), \qquad F_{yo} = -\lambda\,\omega\, f_r(\varepsilon_o, 0) \tag{62}$$

These forces also cause a steady deflection Q_oA_o of the shaft center and rotor center of amounts

$$x_o = -2\,F_{xo}/k, \qquad y_o = -2\,F_{yo}/k \tag{63}$$

Consider now a general motion of the journal center to the point Q specified by the polar coordinates $(\varepsilon C, \alpha)$. The journal center is now at

$$\xi = C\,\varepsilon \sin\alpha, \qquad \eta = C\,\varepsilon\cos\alpha \tag{64}$$

The forces on the journal in the radial and tangential directions are (from Eq. 8 and 8a)

$$\begin{aligned} F_r &= -\lambda\,(\omega - 2\dot{\alpha})\, f_r(\varepsilon, \bar{\varepsilon}') \\ F_t &= \lambda\,(\omega - 2\dot{\alpha})\, f_t(\varepsilon, \bar{\varepsilon}') \end{aligned} \tag{65}$$

where

$$\bar{\varepsilon}' = \frac{\varepsilon'}{(1 - 2\alpha')} \tag{65a}$$

and along x, y directions

$$F_x = \lambda(\omega - 2\dot{a})\left[-f_r(\varepsilon, \bar{\varepsilon}')\sin a + f_t(\varepsilon, \bar{\varepsilon}')\cos a\right]$$
$$F_y = -\lambda(\omega - 2\dot{a})\left[f_r(\varepsilon, \bar{\varepsilon}')\cos a + f_t(\varepsilon, \bar{\varepsilon}')\sin a\right] \quad (66)$$

The shaft center deflection is

$$x = -2F_x/k = \frac{-2\lambda}{k}(\omega - 2\dot{a})\left[-f_r \sin a + f_t \cos a\right]$$
$$y = -2F_y/k = \frac{2\lambda}{k}(\omega - 2\dot{a})\left[f_r \cos a + f_t \sin a\right] \quad (67)$$

and the net deflections of the rotor center are:

$$\xi + x = C\varepsilon \sin a + \frac{2\lambda}{k}(\omega - 2\dot{a})\left[f_r \sin a - f_t \cos a\right]$$
$$\eta + y = C\varepsilon \cos a + \frac{2\lambda}{k}(\omega - 2\dot{a})\left[f_r \cos a + f_t \sin a\right] \quad (68)$$

Subtracting the steady force components Equation (62) from Equation (66) we obtain:

$$F_x - F_{xo} = -\lambda\omega f_t(\varepsilon_o, 0) + \lambda(\omega - 2\dot{a})\left[-f_r \sin a + f_t \cos a\right]$$
$$F_y - F_{yo} = \lambda\omega f_r(\varepsilon_o, 0) - \lambda(\omega - 2\dot{a})\left[f_r \cos a + f_t \sin a\right] \quad (69)$$

These forces can only be used up in producing acceleration of the rotor mass. Thus,

$$\frac{m}{2}(\ddot{x} + \ddot{\xi}) = F_x - F_{xo}, \qquad \frac{m}{2}(\ddot{y} + \ddot{\eta}) = F_y - F_{yo} \quad (70)$$

or more explictly,

$$\left(\frac{m}{k}\frac{d^2}{dt^2} + 1\right)\left[(\omega - 2\dot{a})(-f_r \sin a + f_t \cos a)\right] = \omega f_t(\varepsilon_o, 0) + \frac{mCd^2}{2\lambda\, dt^2}(\varepsilon \sin a)$$
$$\left(\frac{m}{k}\frac{d^2}{dt^2} + 1\right)\left[(\omega - 2\dot{a})(f_r \cos a + f_t \sin a)\right] = \omega f_r(\varepsilon_o, 0) - \frac{mC}{2\lambda}\frac{d^2}{dt^2}(\varepsilon \cos a) \quad (71)$$

Massless Rotor

If we consider the case of massless rotor, the terms involving m can be deleted from Equation 71 which then reduces to:

$$\left(1 - \frac{2\dot{a}}{\omega}\right)\left[-f_r(\varepsilon, \bar{\varepsilon}')\sin a + f_t(\varepsilon, \bar{\varepsilon}')\cos a\right] = f_t(\varepsilon_o, 0)$$
$$\left(1 - \frac{2\dot{a}}{\omega}\right)\left[f_r(\varepsilon, \bar{\varepsilon}')\cos a + f_t(\varepsilon, \bar{\varepsilon}')\sin a\right] = f_r(\varepsilon_o, 0) \qquad (72)$$

These are differential equations from which $\dot{a}$, $\dot{\varepsilon}$ can be solved as functions of ε, a.

The steady state solution is given by $\varepsilon = \varepsilon_o$, $a = 0$. Equations 72 may be transformed by multiplying first by - sin a, cos a and adding; then by cos a, sin a, and adding. There results

$$\left(1 - \frac{2\dot{a}}{\omega}\right) f_r(\varepsilon, \bar{\varepsilon}') = -f_t(\varepsilon_o, 0)\sin a + f_r(\varepsilon_o, 0)\cos a$$
$$\left(1 - \frac{2\dot{a}}{\omega}\right) f_t(\varepsilon, \bar{\varepsilon}') = f_t(\varepsilon_o, 0)\cos a + f_r(\varepsilon_o, 0)\sin a \qquad (73)$$

Introducing as in Figure 32, the resultant force f given in dimensionless form

$$f(\varepsilon, \bar{\varepsilon}') = \sqrt{f_r^2 + f_t^2} \qquad (74)$$

and the direction angle ψ that this force makes with the (inner) radial direc

$$\psi = \tan^{-1} f_t/f_r \qquad (75)$$

We note also the relation

$$f_r = f\cos\psi, \qquad f_t = f\sin\psi \qquad (76)$$

71)

)

Denote by f_o, ψ_o the values of f and ψ at the positions of equilibrium.

$$f_o = f(\varepsilon_o, 0), \qquad \psi_o = \psi(\varepsilon_o, o) \tag{77}$$

Thus, by taking the square root of the sum of squares of Equations (71) and their ratio, one obtains the following equivalent form for these equations:

$$\left(1 - \frac{2\delta}{\omega}\right) f(\varepsilon, \bar{\varepsilon}') = f_o \tag{78}$$

$$\tan \psi = \tan (\alpha + \psi_o) \tag{79}$$

Hence

$$\psi = \alpha + \psi_o \tag{80}$$

Introduce the parameter τ by means of

$$\tau = \omega t \tag{81}$$

Then Equation (78) can be replaced by

$$(1 - 2\alpha') f(\varepsilon, \bar{\varepsilon}') = f(\varepsilon_o, 0) = f_o \tag{82}$$

By means of plots of f and ψ in the $\varepsilon - \bar{\varepsilon}'$ plane, such as those of Figures 5 and 6, the locus of a shaft center initially displaced from its equilibrium position (ε_o, ψ_o) to some other position (ε, ψ), can be obtained numerically.

The equations required for this and a description of the procedure follow:

From Equation (80) we have

$$\alpha = \psi - \psi_o \tag{83}$$

and from Equation (82) we have

$$\alpha' = \frac{1}{2} - \frac{1}{2} \frac{f_o}{f} \tag{84}$$

For a small dimensionless time increment

$$\Delta\tau = \tau_{n+1} - \tau_n$$

we can write

$$\varepsilon_{\tau=\tau_{n+1}} \doteq \varepsilon_{\tau=\tau_n} + \varepsilon'_{\tau=\tau_n} \cdot \Delta\tau \tag{85}$$

and

$$\alpha_{\tau=\tau_{n+1}} \doteq \alpha_{\tau=\tau_n} + \alpha'_{\tau=\tau_n} \cdot \Delta\tau \tag{86}$$

Now, consider a shaft center whose static equilibrium position is $(\varepsilon_o, 0)$ and let it be displaced to a position $(\varepsilon_{\tau=\tau_o}, \alpha_{\tau=\tau_o})$ at the instant $\tau = \tau_o$. Its locus can then be traced as follows (See Figure 33a):

1. From Figures 5 and 6, obtain the dimensionless force f_o and the angle ψ_o which correspond to the position of static equilibrium ($\varepsilon = \varepsilon_o$ $\bar{\varepsilon}' = 0$).
2. From Equation 83, calculate $\psi_{\tau=\tau_o} = \psi_o + \alpha_{\tau=\tau_o}$
3. Locate the point $(\varepsilon_{\tau=\tau_o}, \psi_{\tau=\tau_o})$ in Figure 6 and hence read off $\bar{\varepsilon}'_{\tau=\tau_o}$.
4. Locate the point $(\varepsilon_{\tau=\tau_o}, \bar{\varepsilon}'_{\tau=\tau_o})$ in Figure 5 and read off $f_{\tau=\tau_o}$.
5. By means of Equation (82), calculate

$$\alpha'_{\tau=\tau_o} = \frac{1}{2} - \frac{1}{2} \cdot \frac{f_{\tau=\tau_o}}{f_o}$$

6. For a small time increment $\Delta\tau = \tau_1 - \tau_o$, calculate from Equation (86)

$$\alpha'_{\tau=\tau_1} \doteq \alpha_{\tau=\tau_o} + \alpha'_{\tau=\tau_o} \cdot \Delta\tau$$

7. From Equation (84) calculate

$$\psi_{\tau=\tau_1} = \psi_o + \alpha_{\tau=\tau_1}$$

8. From Equation (65a) obtain

$$\varepsilon'_{\tau=\tau_o} = \left[\bar{\varepsilon}' (1 - 2a')\right]_{\tau=\tau_o}$$

9. From Equation (83) calculate

$$\varepsilon_{\tau=\tau_1} = \varepsilon_{\tau=\tau_o} + \varepsilon'_{\tau=\tau_o} \cdot \Delta\tau$$

The new location of the shaft center ($\varepsilon_{\tau=\tau_1}$, $a_{\tau=\tau_1}$) is now defined. The procedure is repeated for a new time interval $\Delta t = \tau_2 - \tau_1$ and the location of the shaft center at time $\tau = \tau_2$ is similarly obtained. Stepwise repetition of this procedure will then define the complete locus of the shaft center. Figures 33 (b), (c) and (d) show three possible loci.

In Figure 33 (b), the shaft center leads back to the position of static equilibrium so that the condition is stable.

In Figure 33 (c), the shaft center describes a closed loop. This is a condition of stable oscillation. The period of these oscillations is given by $\frac{1}{\omega}(\tau_{final} - \tau_o)$.

In Figure 33 (d), the locus of the shaft center spirals out and the oscillations are unstable.

As an example of this procedure, a numerical integration was carried out for the case where the journal center was displaced radially from its steady state position at $\varepsilon = 0.1$ to an initial position at $\varepsilon = 0.4$. The fluid film forces used were those obtained from incompressible theory for a bearing with an L/D of 1. The results of this integration, carried through for the first loop, are shown in Figure 34. These indicate that, for the conditions assumed, the journal center spirals in towards the steady state position.

XI EXPERIMENTAL VERIFICATION

Several observations may be cited which verify the theory, and to some extent clarify this very difficult and controversial subject.

Figure 35 shows the amplitude and frequency obtained experimentally on a vertical 700 HP canned rotor motor. The first system critical for this motor was also measured by excitation and was found to be at 28.6-29 cycles/sec. Similar results were obtained on four other units of same construction. This illustration is given for it cites two forms of instability and shows that there is actually transition between them. The amplitude of the Half Frequency Whirl in general is quite small and, therefore, the rotor speed may be increased without causing damage to the bearings. On the other hand, the amplitude of Resonant Whip is too large for satisfactory operation. Ref. 4 gives a number of examples of Half Frequency Whirl. It also points out that compressible fluid bearings are also susceptible to this form of instability. This point was further verified more recently in Ref. 5.

Figure 35 shows that, depending on the speed of operation, one may find different forms of instability. It is not, therefore, surprising that conflicts in observation exist. The Half Frequency Whirl has not been observed too often because its amplitude of vibration in general is small and may not cause severe problems to the equipment. This form of instability is more common for vertical rotors and lightly loaded machines especially of the compressible fluid type. The Resonant Whip on the other hand which occurs in general at speeds twice the first system critical has large amplitude. It has been shown

however (Fig. 28 and 30) that the occurance of this stability is dependent on eccentricity ratio and the parameter E. Thus, once the instability occurs its frequency may increase or decrease with increase in speed depending on the actual position of journal center and the value of E at the specific speed. For as speed increases, the eccentricity and the viscosity decrease and they both influence the threshold of instability. If the damping increases with speed, the tendency is to decrease the Resonant Whip Frequency; the reverse is also true.

As stated previously, observations have also been made on the inception of instability with turbine or motor load. This is to be expected for, if we refer to the torque on a turbine or motor, we find that there is an eccentricity between the rotor and the stator. Thus, uneven torques are present, see Figure 36. In the case of a turbine, at the point of closest approach the steam or gas leakage path is decreased and therefore, the force at that point is larger than that 180° away. In the case of a motor or a generator, the flux increases and this has a similar effect. Thus, there is a resultant force at O' which is at right angles to the displacement. It acts in the same way as the tangential fluid film force and, therefore, must be included in the stability analysis.

In sections IX and X it has been shown that instability is dependent on the fluid film properties within the bearing clearance. It is therefore essential to evaluate these properties accurately. These sections show that the inception of instability depends to a very large extent on eccentricity

ratio and system critical. A general statement can be made that the threshold of instability increases with increase in eccentricity ratio.

Since the stiffness of the fluid film is extremely important in predicting system criticals and also frequencies of instability, the point deserves a brief discussion. It has been shown in Ref. 4 and confirmed further in Ref. 5 that Equation 21 will predict accurately the threshold of Half Frequency Whirl. This equation, however, contains the radial fluid film stiffness which has to be obtained accurately either by theory or from tests. In Table III of Ref. 5 good comparison is given between the measured and calculated Whirl Frequencies. The correlation between the two is further improved if compressible theory is used. Figure 37 employs compressible theory and shows the radial component of force vs eccentricity ratio for bearing B discussed in Ref. 5 (Figure 1 and Table 3). For the load corresponding to point (a) the radial stiffness for the compressible case is actually lower than that obtained from Ref. 5, Figure 1. This will, therefore, lower the calculated threshold of Whirl. The reverse is true for the two higher loads b and c.

Figure 37 was plotted to show another relevent point. Note that the radial component of force is a function of both eccentricity ratio and speed.

Since increased load produces both an increase in eccentricity and threshold of instability, the question arises as to where does one calculate the radial stiffness, e.g., at b or b', c, c' or c''. It is fortunate that the stiffness does not vary too much between point b and b' or c and c'' as shown

in Figure 37. Further, since stiffness enters to the one half power in Equation 21, the errors in threshold of whirl will be relatively small.

In the calculation of system criticals, the fluid film stiffness must be considered. In the use of hydrodynamic bearings, there is some question as to which stiffness should be used. For, as shown in sections III, IX and X, there are both a radial and a tangential stiffness and, in general, the two are not equal. In rigorous analysis one must use the derivative of force with respect to displacement. The increment of force must contain coupling terms. Since the stiffness varies with attitude, there will be a number of criticals which will cover a band of frequencies. Large variation in radial and tangential stiffness will yield a wide frequency band. Conversely, in the case where the stiffnesses are nearly equal in all directions, the critical frequency band will be narrow.

In the case of hydrostatic bearings, the problem of calculation of critical speed is very much simpler, as shown in section IV. For such bearings, the stiffness as a function of load remains constant at least up to eccentricity ratio of 0.5. Thus natural frequency is independent of external force. This simplifies the calculation of the natural frequency. Experimental verification of calculated natural frequency was made recently on a Helium/Nitrogen compressor whose rotor mass was 2×10^{-2} lb.-sec.^{2}/in. and whose rotor stiffness was 3×10^6 lb./in. The measured natural frequency with 100 psia supply pressure was 698 cycles/sec.

Bearing No. 1	Bearing No. 2
$L = 1.25''$	$L = 1.25''$
$D = 1.25''$	$D = 2.50''$
$C = 0.0005''$	$C = 0.0010''$
$m = 8 \times 10^{-3}$ lb.-sec.^{2}/in.	$m = 12.4 \times 10^{-3}$ lb.-sec.^{2}/in.
k calculated from Fig. 7	k calculated from Fig. 7
$= 1.43 \times 10^5$ lb./in.	$= 2.12 \times 10^5$ lb./in.
Therefore	Therefore
$f_n = \frac{1}{2\pi}\sqrt{\frac{k}{m}} = 675$ ~/sec.	$f_n = 695$ ~/sec.

These compared very favorably with the experimental value of 698 cycles/sec.

The above clarifies some of the observations and shows comparatively good agreement between theory and practice in the calculation of critical speeds and frequencies of instability.

XII CONCLUSIONS AND RECOMMENDATIONS

It was shown that if the Reynolds Equation is integrated and the film forces on the journal computed for zero tangential velocity, then the effects of a tangential velocity can also be obtained. This is done by correcting the radial velocity ($V_r = C\omega\varepsilon'$) and the radial and tangential force components (F_r and F_t) using the factor $(1-2a')$, as shown in Equations (8 and 8a).

Solutions for radial and tangential forces as functions of ε, ε' and L/D were obtained for both compressible and incompressible journal bearings. Likewise, the derivatives of these forces with respect to ε and ε' were obtained.

Calculations were also made of the forces generated in externally pressurized compressible fluid bearings. It was shown that stiffness in this type of bearing is constant for at least small eccentricity ratios. The critical speed is independent of external load. It was further shown that the optimum bearing from the standpoint of maximum stiffness exists at L/D ratios around unity. Maximum stiffness is a function of p_s/p_a, L/D, and Z_t.

Equations of motion were set up for small oscillations about a position of equilibrium corresponding to some particular external, steady load. These equations contain functions f_r, f_t and their derivatives with respect to ε and ε'. These differential equations are linear in the variable ξ, η, x, y and solutions exist in which time enters as an exponential. Solutions have been obtained for both compressible and incompressible cases to show the effect of ε and E on the threshold of instability.

Results show that the threshold of instability increases with increase in external load. Refer to Figures 22 and 23.

The calculation of critical speed deserves additional attention for cases when the stiffness in all directions around an equilibrium point is unequal.

The equations of large displacements have also been set up in terms of ε and α. Method for obtaining the path of the journal center for the case of a massless rotor have been outlined.

The threshold for Half Frequency Whirl and other forms of dynamic disturbance have been treated in sections VI through VIII and equations are given for the frequencies of disturbance.

Wherever data was available, theory and experiment has been compared. The results appear to have good agreement. Several of the controversial observations have been clarified.

The subject is by no means completely covered and it still demands considerable study. Several of these studies are enumerated below:

1) Study the behavior of rotors for small oscillations at very low eccentricity ratios and where the angular increment $d\alpha$ may not be neglected.
2) Find methods for solution of the equations of motion for large displacements. Preferably try to obtain closed solutions.
3) For the case of large displacements study the special cases where
   a) the eccentricity is small
   b) the rotor mass is small (method of solution is outlined in section X)
   c) the bearing clearance in small compared to the shaft bending deflections.

4) Study the above three points in cases where the rotor or bearings are not symmetrical.

5) Study methods for predicting critical speeds of rotors where unequal stiffnesses in two directions exist.

6) Conduct experiments to verify all the above points.

7) Perform experiments on externally pressurized bearings to determine how closely theory agrees with practice with regard to constant stiffness, optimum L/D ratio and critical speed as function of eccentricity ratio and p_s.

8) Study pocketed externally pressurized journal bearings under the same condition.

9) Study other forms of instability which have been reported by several investigators.

10) Establish charts and tables to aid engineers in the design of stable bearings.

ACKNOWLEDGEMENT

This paper is based on the work performed under Contract Number Nonr - 2844 (00), Task Number NR 097-348 administered by the Office of Naval Research and jointly sponsored by the Department of Defense, Atomic Energy Commission, Maritime Administration, and the General Electric Company. The authors are especially indebted to Messrs. J. J. Laffan and H. J. Gneck for their assistance in the preparation of this report. The authors are also indebted to Miss M. E. Haas for programming and performing some of the calculations.

REFERENCES

1) B. L. Newkirk and H. D. Taylor, "Shaft Whipping Due to Oil Action in Journal Bearing", General Electric Review, August 1925, pp 559-568.

2) D. Robertson, "Whirling of a Journal in a Sleeve Bearing", Philosophical Magazine, series 7, vol 15, January 1933, pp 113-130.

3) H. Poritsky, "Contribution of the Theory of Oil Whip", Trans. ASME, vol 75, 1953, pp 1153-1161.

4) G. F. Boeker and B. Sternlicht, "Investigation of Translatory Fluid Whirl in Vertical Machines", Trans. ASME, vol 78, 1956, pp 13-20.

5) G. K. Fischer, J. L. Cherubim and O. Decker, "Some Static and Dynamic Characteristics of High-Speed Shaft Systems Operating with Gas-Lubricated Bearings", ONR Gas Bearing Symposium, 1959.

6) B. L. Newkirk and J. F. Lewis, "Oil Film Whirl - An Investigation of Disturbances Due to Oil Film on Journal Bearings", Trans. ASME, vol 78, 1956, pp 21-27.

7) B. L. Newkirk, "Varieties of Shaft Disturbances Due to Fluid Films in Journal Bearings", Trans. ASME, vol 78, 1956, pp 985-988.

8) Jukin Hori, "A Theory of Oil Whip", Journal of Applied Mechanics, June 1959, pp 189-198

9) B. Sternlicht, "Experimental Verification of Theoretical Investigations into Half Frequency Whirl", ASME Paper 55-LUB-20.

10) O. Pinkus, "Experimental Investigation of Resonant Whip", Trans. ASME, vol 78, 1956, pp 975-983.

11) A. Stodola, "Kritische Wellenstorung Infolge der Nadgiebegkeit des Delpolstere im Lager", Schweizerische Bauzeitung, vol 85, pp 265-266, 1925.

12) C. Hummel, "Kritische Drehzahlen als Folge der Nachgiebigkeit des Schmiermittels in loger", Forschungsarbiten aug dem Gibiet des Ingeineurwesens, No 287, 48 pp (1926)

13) A. Cameron, "Oil Whip in Bearings - Theoretical Deduction of a Further Criterion", Engineering, February 25, 1955, pp 237-239.

14) B. Sternlicht, "Elastic and Damping Properties of Cylindrical Journal Bearings", ASME Trans., Series D, June 1959.

15) G. Heinrich, "Das Zylindrische Stromungslager" und "Das Stromunp-Spurlager", Maschinenbau und Warmewirtschaft, Wien, Jg 3, Heft 8, s 136-143 (1950), Jg 6, s 57-60 and 78-87 (1951).

16) A. Slibar and H. J. Sneck, "Optimum Power Requirements for Externally-Pressurized Cylindrical Gas Journal Bearings", General Electric TIS Report 57GL49, February, 1957.

E

0.1

0.3

TABLES

0.5

0.7

INCOMPRESSIBLE CASE - FULL CIRCULAR BEARING

(Equal Radial and Tangential Shaft Center Velocities)

TABLE I

E	$\pi\varepsilon a'$ / $\pi\varepsilon'$	L/D = 0.5				L/D = 1.0				L/D = 1.5			
		f_r	f_t	f	180-ϕ	f_r	f_t	f	180-ϕ	f_r	f_t	f	180-ϕ
0.1	6.0	11.2	9.2	14.5	140.4	33.2	31.5	45.9	136.8	64.9	56.5	86.0	138.9
	4.0	7.4	6.4	9.8	139.1	23.9	21.4	32.1	138.2	43.0	38.0	57.4	138.5
	2.0	3.6	3.4	4.9	137.0	11.7	10.9	16.0	137.0	20.0	20.5	28.6	134.3
	1.0	1.4	1.6	2.2	130.3	4.5	4.9	6.7	132.6	8.4	10.8	13.7	127.9
	0	0	0.2	0.2	98.3	0.1	0.7	0.7	100.1	0.3	1.3	1.3	102.4
0.3	6.0	20.3	13.0	24.1	147.4	62.0	40.0	73.8	147.2	104.0	72.0	126.5	145.3
	4.0	13.5	9.0	16.2	146.3	41.2	27.5	49.5	146.3	68.5	48.5	83.9	144.7
	2.0	7.2	5.0	8.8	145.4	19.5	15.0	24.6	142.4	34.0	26.0	42.8	142.6
	1.0	3.6	2.8	4.6	142.0	7.8	7.8	11.0	135.2	17.5	15.3	23.2	138.8
	0	0.3	0.8	0.8	111.8	0.8	2.4	2.5	108.2	1.6	4.0	4.3	112.1
	-0.6	-0.3	-0.1	0.3	342.3	-0.6	-0.4	0.8	330.5	-1.0	-0.5	1.1	331.5
	-2.0	-1.0	-1.7	2.0	300.8	-2.0	-4.3	4.8	295.5	-3.2	-8.5	9.1	290.6
	-4.0	-2.0	-4.2	4.6	295.5	-4.4	-12.8	13.5	288.8	-6.0	-21.0	21.8	286.0
	-18.0	-8.7	-20.5	22.3	293.0	-19.6	-65.0	67.9	286.8	-26.0	-105.0	108.2	283.9
0.5	6.0	45.0	19.6	49.1	156.5	123.0	56.0	135.3	155.5	182.0	91.5	203.7	153.3
	4.0	30.0	13.8	33.0	155.3	80.0	39.5	89.2	153.7	122.0	63.5	137.5	152.5
	2.0	15.6	7.8	17.4	153.6	39.0	21.8	44.7	150.8	62.5	35.0	71.6	150.7
	1.0	8.1	4.7	9.4	149.9	17.3	11.9	21.0	145.5	31.8	22.0	38.7	145.3
	0	1.1	1.6	1.9	125.6	2.9	4.8	5.6	121.3	4.8	7.4	8.8	122.8
	-0.6	-0.2	0.2	0.3	35.6	-0.6	0.6	0.8	47.5	-0.7	0.8	48.3	48.0
	-2.0	-0.8	-1.2	1.4	303.2	-1.5	-2.3	2.7	303.0	-2.2	-6.0	6.4	289.7
	-4.0	-1.4	-2.2	2.6	301.2	-2.8	-10.6	11.0	284.8	-3.6	-17.0	17.4	282.0
	-18.0	-4.8	-19.2	19.8	284.0	-10.3	-58.5	59.4	280.0	-13.7	-95.0	96.0	278.2
0.7	6.0	136.0	36.5	140.7	165.0	290.0	87.0	302.8	163.3	420.0	125.0	438.2	163.4
	4.0	92.5	26.0	96.1	164.3	205.0	62.5	214.2	163.0	278.0	90.0	292.2	162.1
	2.0	45.0	15.0	47.4	161.6	96.0	36.5	104.4	159.6	139.0	53.5	149.0	159.0
	1.0	19.5	9.6	21.7	153.8	42.5	21.0	47.4	153.7	67.5	32.0	74.7	154.6
	0	4.1	3.5	5.4	139.7	9.7	9.1	13.3	136.8	13.1	13.0	18.5	135.5

TABLE I (Cont'd)

		L/D = 0.5				L/D = 1.0				L/D = 1.5			
E	$\pi\varepsilon'$	f_2	f_t	f	180-ϕ	f_r	f_t	f	180-ϕ	f_r	f_t	f	180-ϕ
0.8	6.0	332.0	58.0	337.6	170.1	650.0	124.0	661.8	169.2	780.0	165.0	797.5	168.0
	4.0	220.0	42.0	224.0	169.2	425.0	88.0	433.6	168.3	520.0	118.0	532.9	167.2
	2.0	113.0	25.0	115.8	167.5	215.0	52.5	221.4	166.3	265.0	71.0	274.4	165.0
	1.0	56.5	16.0	58.7	163.5	112.0	34.3	116.6	163.0	133.0	46.5	140.7	160.8
	0	8.8	5.8	10.5	146.5	18.3	13.1	22.5	144.4	23.6	18.0	29.7	142.7
	-0.6	0.1	0.9	0.9	96.3	0.2	2.4	2.4	93.0	0.3	3.5	3.5	94.2
	-2.0	-0.5	-0.6	0.7	309.2	-1.1	-1.3	1.7	309.6	-1.5	-2.5	2.9	301.0
	-4.0	-0.8	-2.4	2.6	288.7	-2.0	-7.2	7.5	285.4	-2.5	-11.2	11.5	282.5
	-18.0	-0.6	-18.6	18.6	271.8	-0.4	-54.5	54.5	270.5	-0.1	-84.0	84.0	270.0

TABLE IA

INCOMPRESSIBLE CASE - FULL CIRCULAR BEARING

(No Tangential Shaft Center Velocity)

ε	$w\varepsilon'$	f_r	f_t	f	$180-\phi$
0.01	2.0	10.0	0.090	10.0	179.5
	1.5	7.30	0.089	7.30	179.3
	1.0	4.80	0.088	4.80	179.0
	0.5	2.25	0.087	2.25	177.8
	0	0.001	0.075	0.075	91.0
	-1.0	- 5.00	0.067	5.00	0.8
	-2.0	-10.00	0.065	10.00	0.4
0.3	2.0	20.0	3.10	20.2	171.2
	1.5	15.0	3.08	15.3	168.4
	1.0	10.0	3.00	10,5	163.3
	0.5	5.00	2.96	5.81	149.4
	0	0.798	2.43	2.56	108.2
	-1.0	- 2.50	1.75	3.05	35.0
	-2.0	- 5.50	1.69	5.75	17.1
0.5	2.0	40.00	7.30	40.7	169.7
	1.5	29.50	6.80	30.3	167.0
	1.0	19.50	6.45	20.5	161.7
	0.5	10.50	5.70	12.0	151.5
	0	2.90	4.77	5.58	121.3
	-1.0	- 1.55	2.66	3.08	59.8
	-2.0	- 3.90	2.48	4.63	32.4

TABLE IA (cont.)

ε	$\pi\varepsilon'$	f_r	f_t	f	$180-\phi$
0.7	2.0	102	15.0	103.3	171.6
	1.5	80.0	14.5	81.4	169.7
	1.0	52.0	13.7	53.9	165.2
	0.5	27.0	12.0	30.1	156.0
	0	9.67	9.08	13.3	136.8
	-0.5	1.60	5.75	5.97	105.5
	-1.0	- 1.00	3.80	3.93	75.3
	-1.5	- 1.85	3.24	3.73	60.3
	-2.0	- 2.98	3.06	3.33	45.7
0.95	2.0	2000	70.0	2000	178.0
	1.5	1495	69.0	1496	177.4
	1.0	1000	67.0	1002	176.2
	0.5	545	58.0	548	173.9
	0	112	38.0	118	161.3
	-0.5	13.0	13.5	19.4	133.9
	-1.0	5.5	6.50	7.38	118.3

TABLE II

COMPRESSIBLE CASE - FULL CIRCULAR BEARING
(Equal Radial and Tangential Shaft Center Velocities)

P_a = 14.7 psia

ϵ	$\frac{\dot{r}_{max}}{r\omega\epsilon'}$	L/D = 0.5				L/D = 1.0				L/D = 1.5			
		f_r	f_t	f	$180-\phi$	f_r	f_t	f	$180-\phi$	f_r	f_t	f	$180-\phi$
0.1	2	0.0155	0.4489	0.4491	92.0	0.1405	1.4000	1.4071	95.7	0.3727	2.2742	2.3045	99.3
0.1	0	0.0118	0.4496	0.4498	91.5	0.1032	1.4051	1.4100	94.2	0.2697	2.3130	2.3286	96.7
0.1	-2	0.0080	0.4501	0.4502	91.0	0.0625	1.4100	1.4114	92.5	0.1521	2.3393	2.3443	93.7
0.3	2	0.0997	1.4889	1.4922	93.8	0.7660	4.4084	4.4744	99.9	1.7821	6.9394	7.1646	104.4
0.3	0	0.0610	1.4978	1.4990	92.3	0.4926	4.5138	4.5403	96.2	1.1960	7.2375	7.3356	99.4
0.3	-2	0.0199	1.5043	1.5045	90.8	0.1657	4.5880	4.5910	92.1	0.4047	7.4633	7.4743	93.1
0.5	2	0.5155	3.0860	3.1288	99.5	2.8218	8.1584	8.6326	109.1	5.2901	12.0288	13.1406	113.7
0.5	0	0.2665	3.1496	3.1609	94.8	1.7145	8.7340	8.9007	101.1	3.5365	13.2594	13.7229	104.9
0.5	-2	-0.0219	3.1871	3.1872	89.6	-0.05807	9.1019	9.1021	89.6	-0.0234	14.2294	14.2294	89.9
0.7	2	3.2410	6.0216	6.8383	118.3	10.1720	12.6841	16.2579	128.7				
0.7	1	2.9510	6.4931	7.1322	114.4	9.21	13.92	16.69	123.5	14.1642	19.3002	23.9400	126.3
0.7	0	1.7796	6.8279	7.0560	104.6	7.2401	15.9058	17.4761	114.5	11.6732	22.1466	25.0347	117.8
0.7	-1	0.2131	6.9064	6.9097	91.8	3.54	16.24	16.62	102.3	3.4692	24.9177	25.1580	97.9
0.7	-2	-1.6671	7.0261	7.2212	76.7	-8.5003	17.3560	19.3258	63.9	-19.0716	25.0067	31.9629	51.5
0.8	0	6.1970	11.1694	12.7733	119.0	17.5781	22.3809	28.4700	128.2	24.3184	29.4273	38.1753	129.6

TABLE III

COMPRESSIBLE CASE - 120° PARTIAL BEARING

(Equal Radial and Tangential Shaft Center Velocities)

$L/D = 0.5$, $p_a = 14.7$ psia

ε	$\frac{\pi\varepsilon\alpha'}{\pi\varepsilon'}$	f_r	f_t	f	$180-\beta$
0.1	2	0.0092	0.0461	0.0470	101.3
	0	0.0030	0.0477	0.0478	93.6
0.3	2	0.0837	0.2250	0.2401	110.4
	1	0.0583	0.2351	0.2422	103.9
	0	0.0261	0.2431	0.2445	96.1
0.5	2	0.4871	0.6184	0.7872	128.2
	0	0.1687	0.7818	0.7997	102.2
0.7	0	1.5312	2.5655	2.9876	120.8

FIGURES

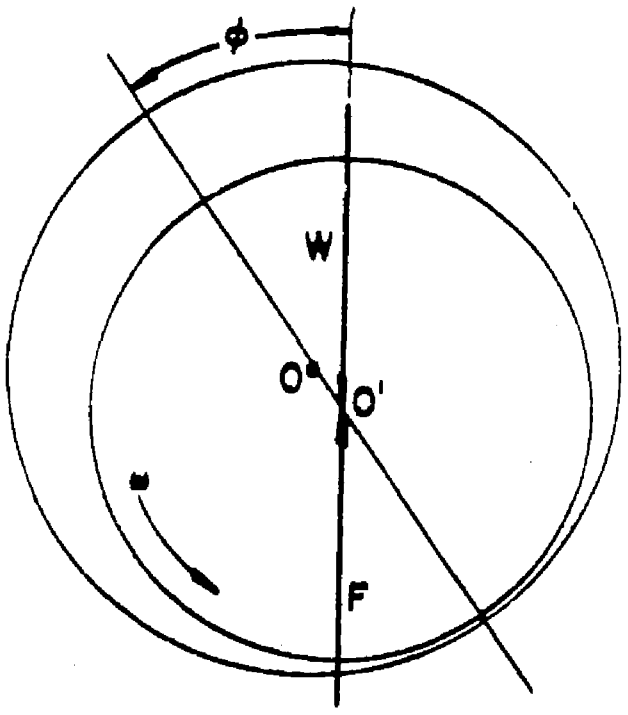

Fig. 1. Rotating shaft in equilibrium position.

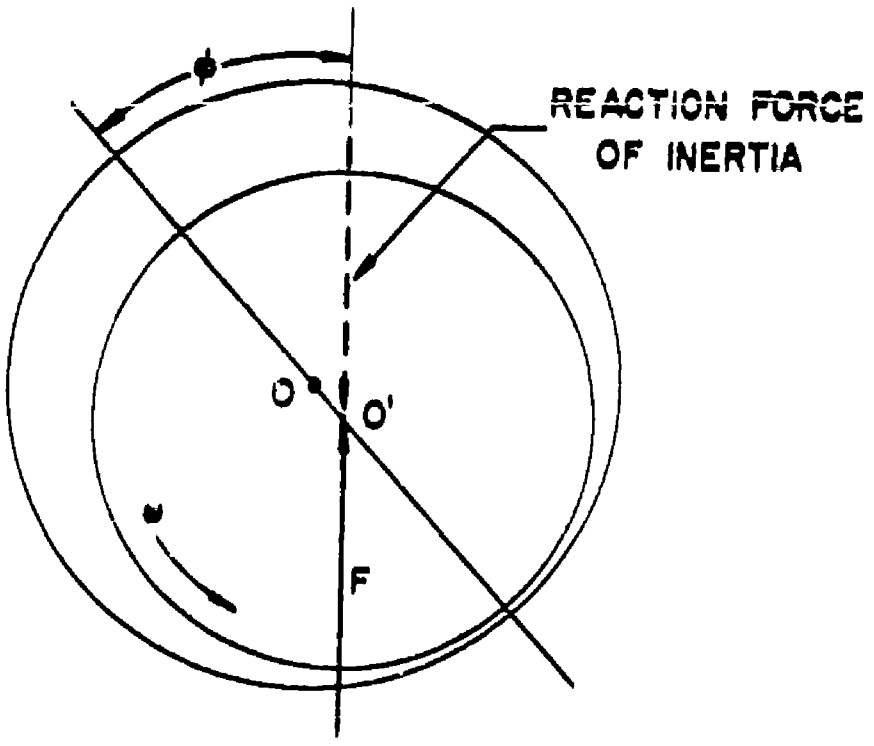

Fig. 2. Unloaded shaft displaced from the bearing center.

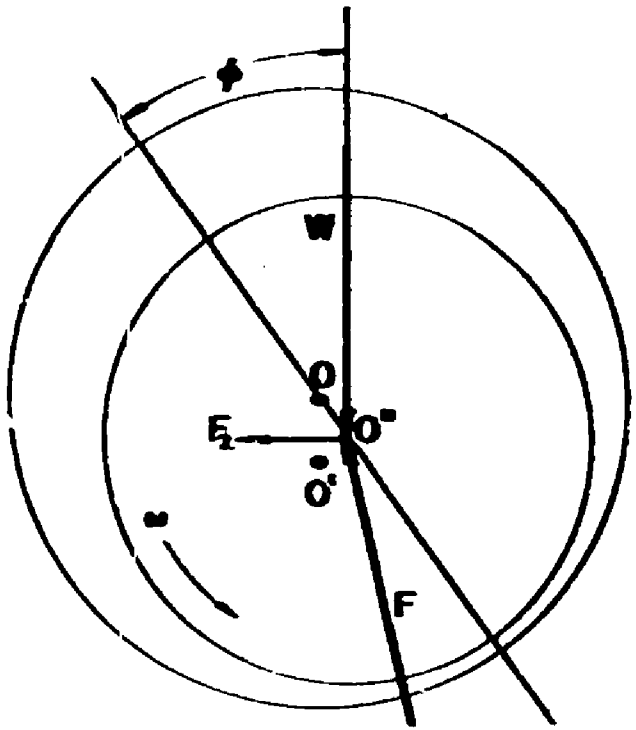

Fig. 3. Loaded shaft displaced from its equilibrium position.

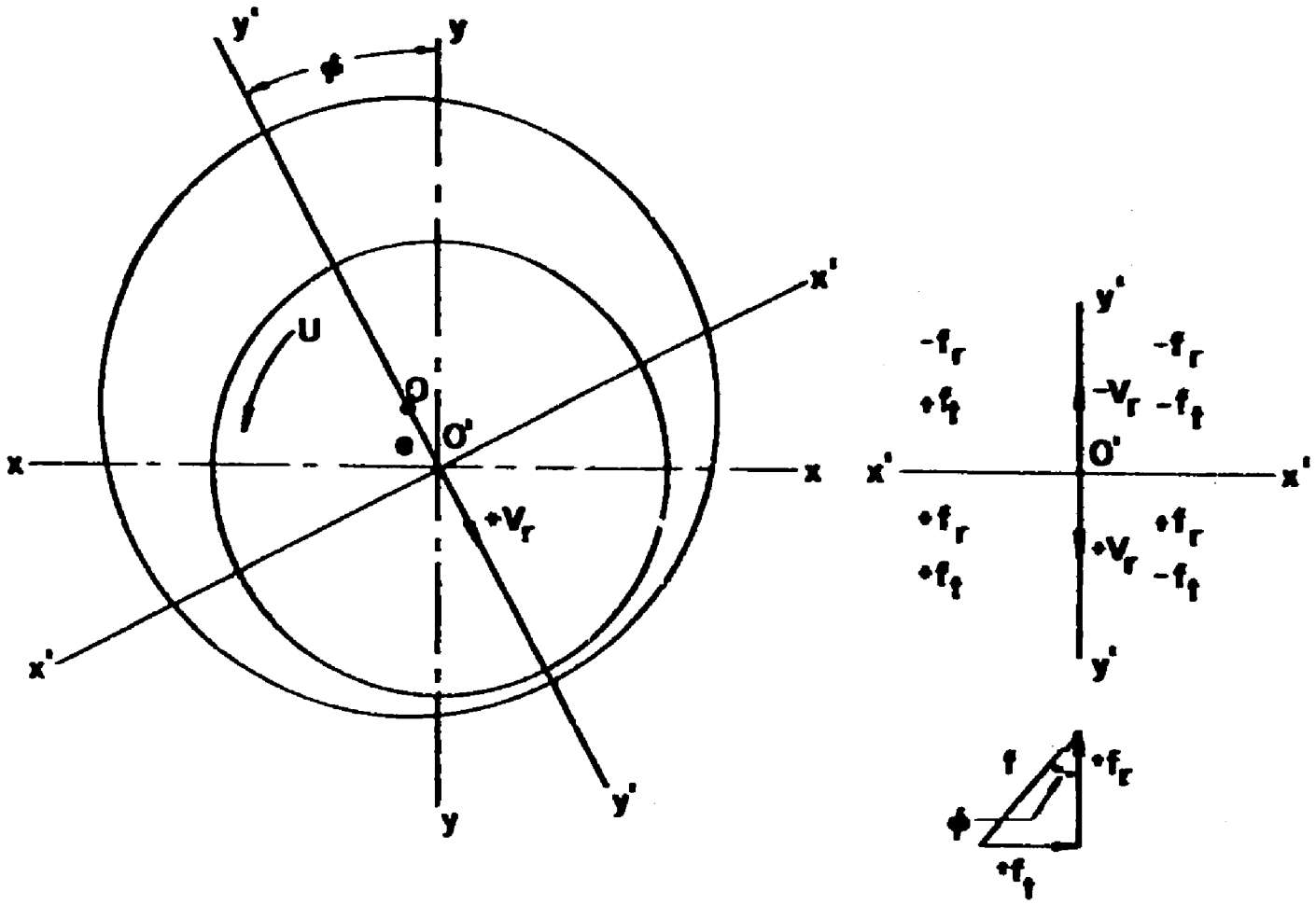

Fig. 4. Nomenclature

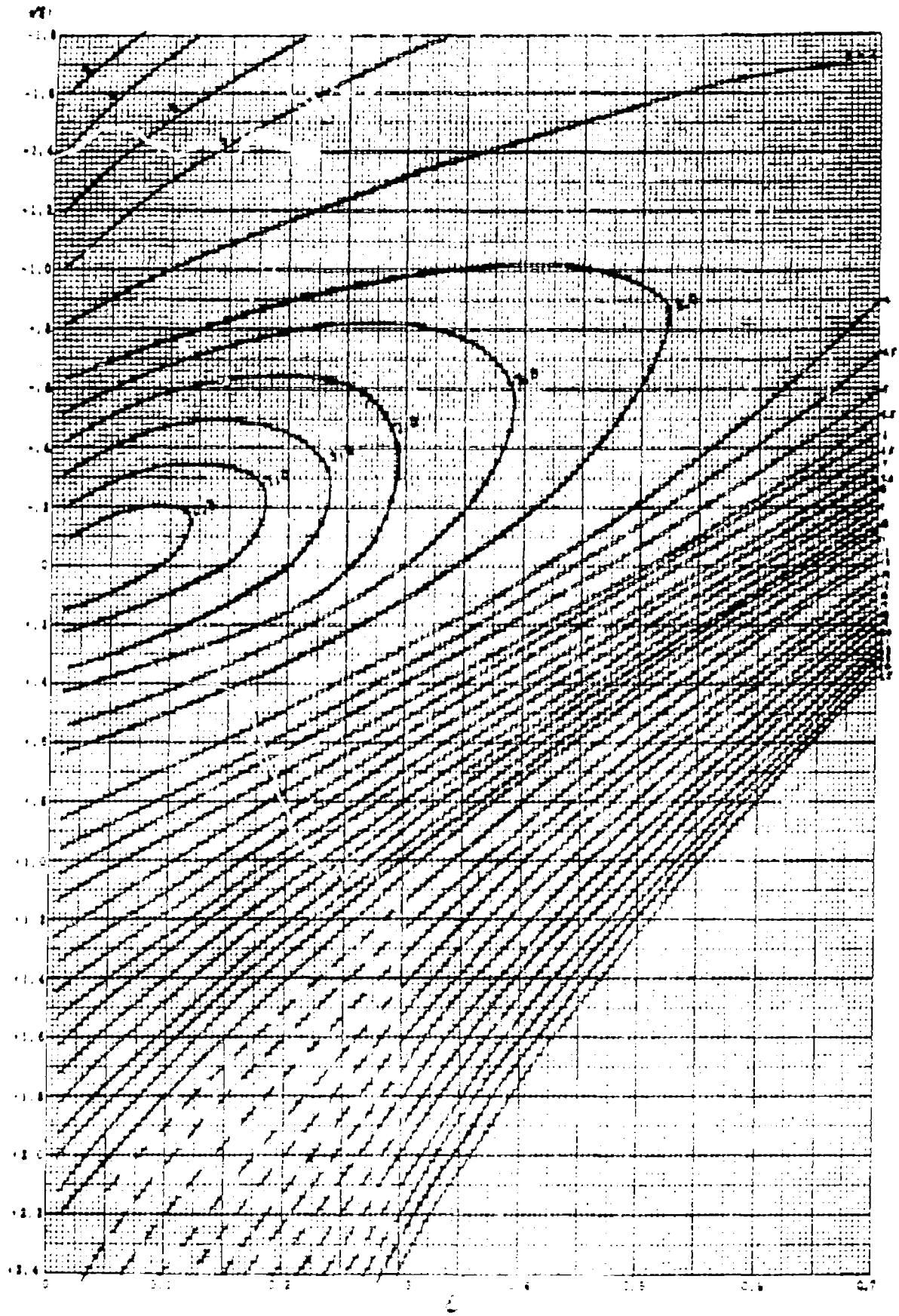
$\pi\bar{\varepsilon}'$
ξ

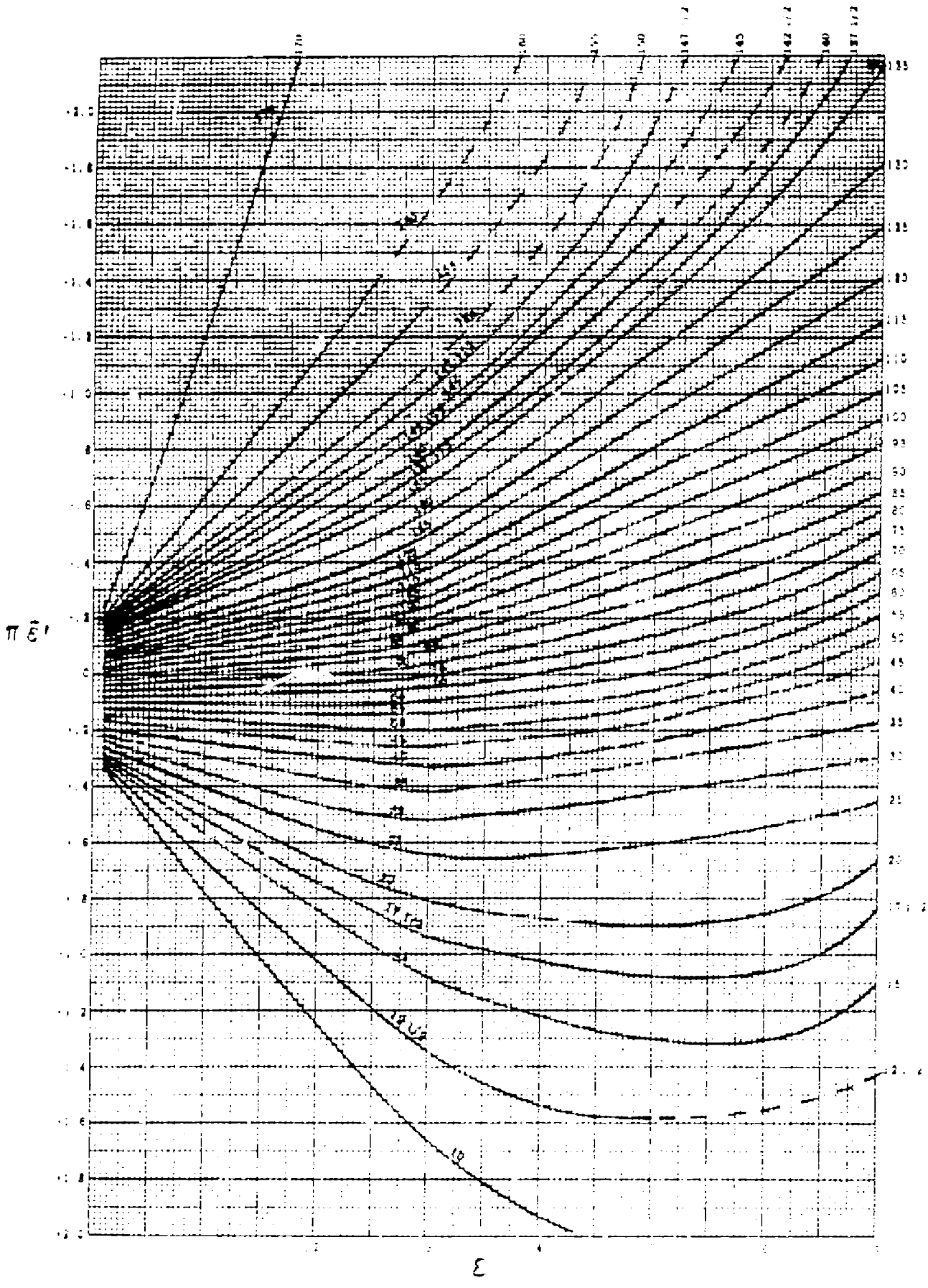
$\pi\,\tilde{\varepsilon}'$
ε

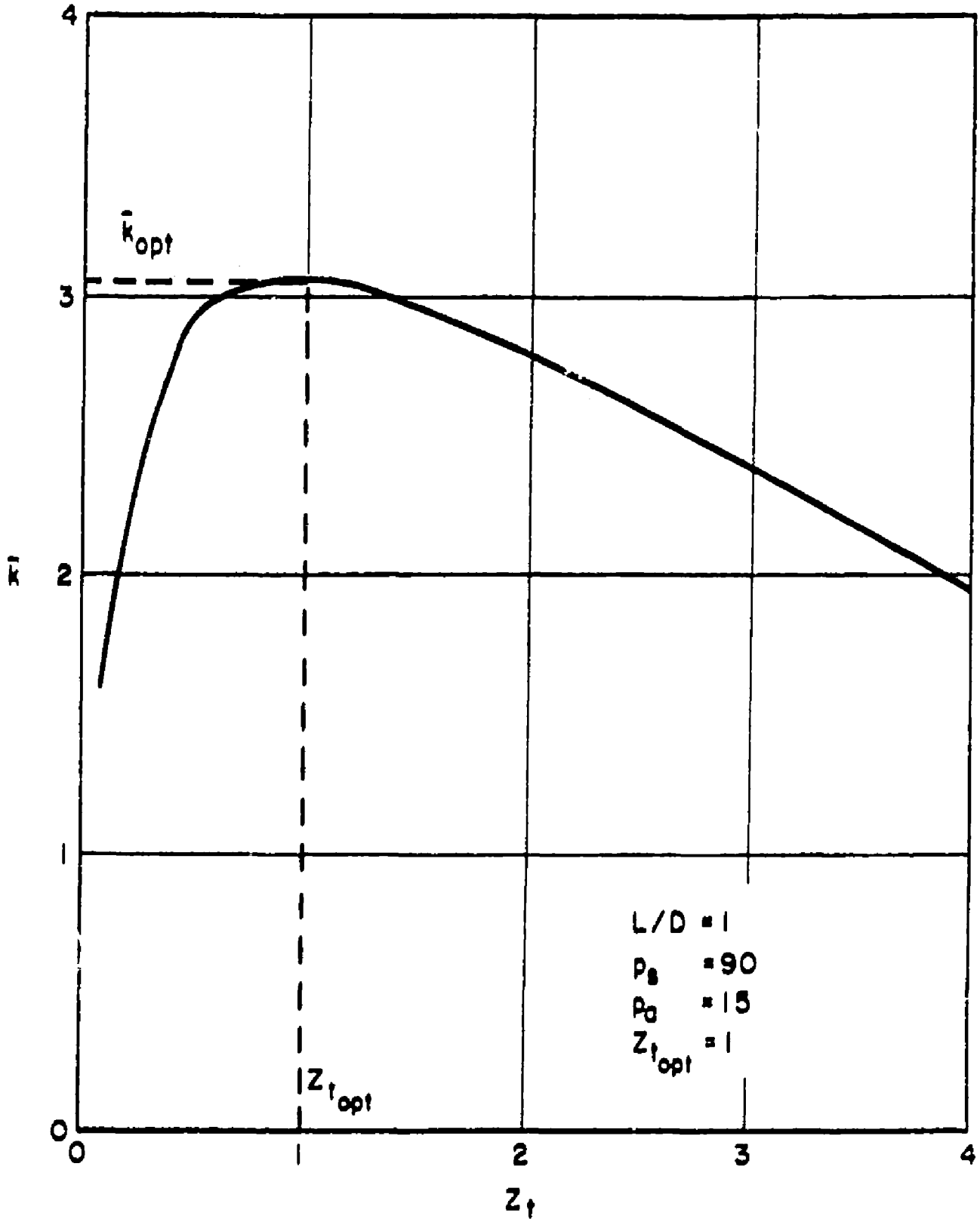

Fig. 7. Dimensionless feeding parameter Z_t vs dimensionless stiffness $\bar{k}$.

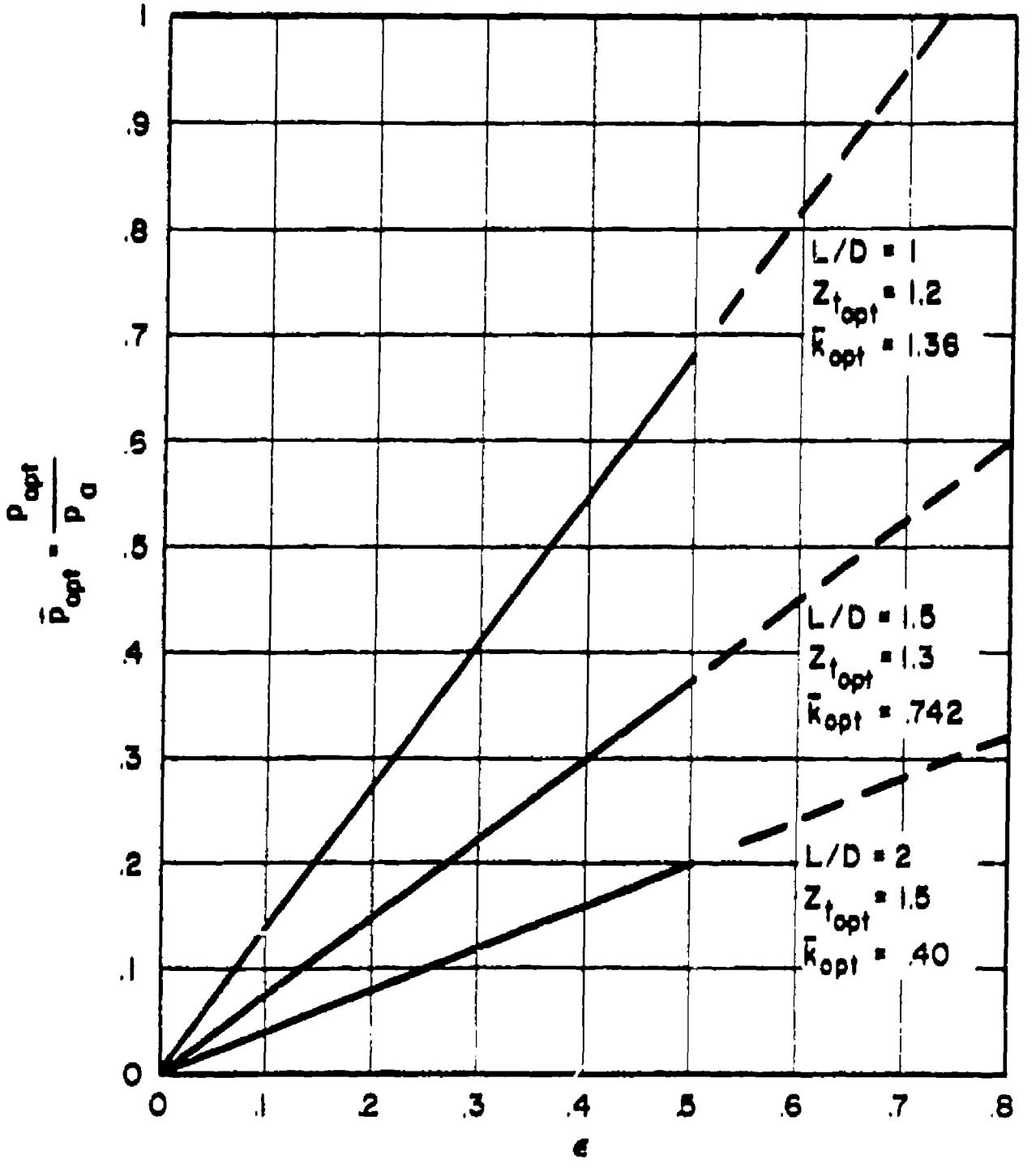

Fig. 8. Dimensionless pressure vs eccentricity ratio
$p_s / p_a = 3$

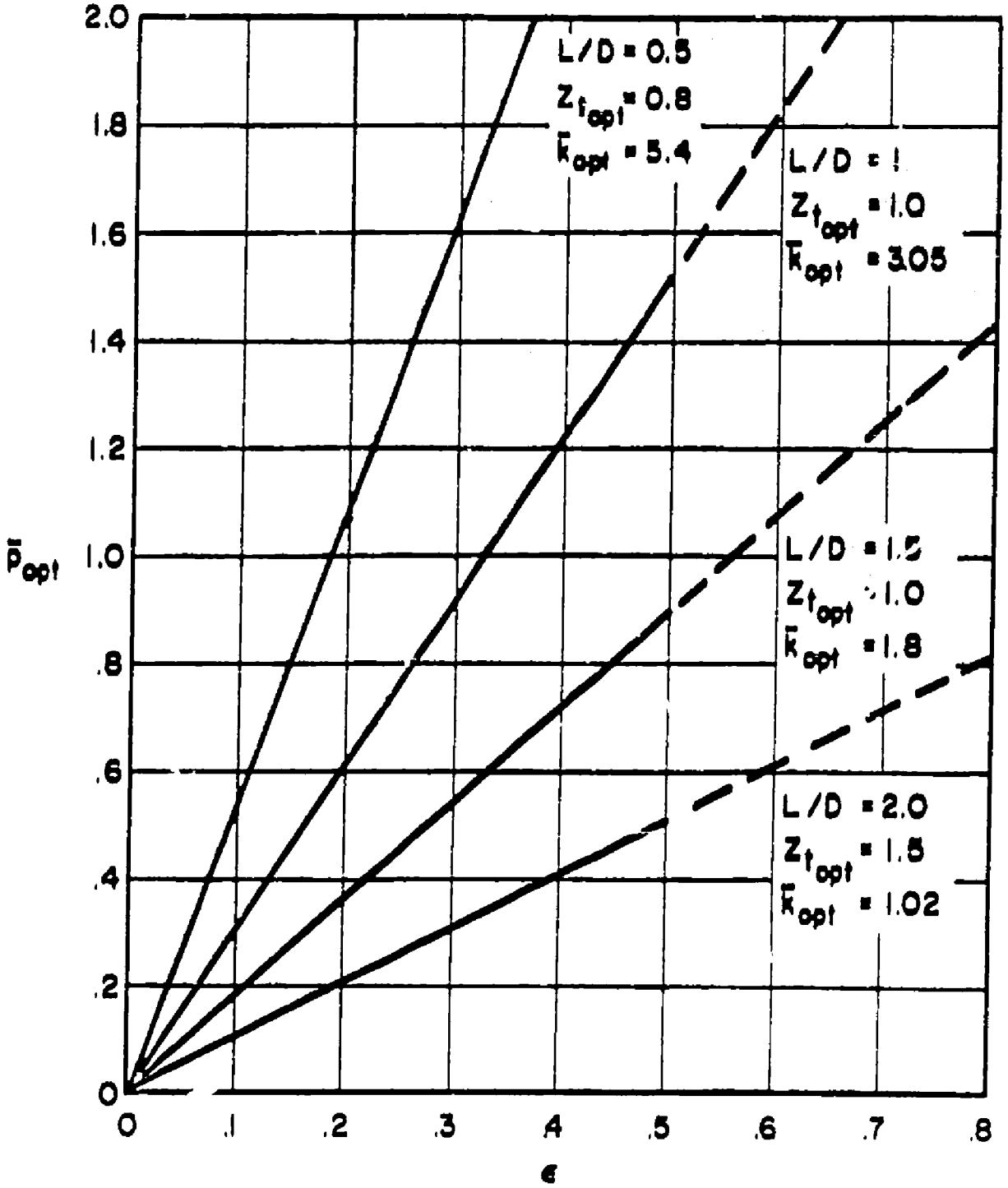

Fig. 9. Dimensionless pressure vs eccentricity ratio $p_s/p_a = 6$.

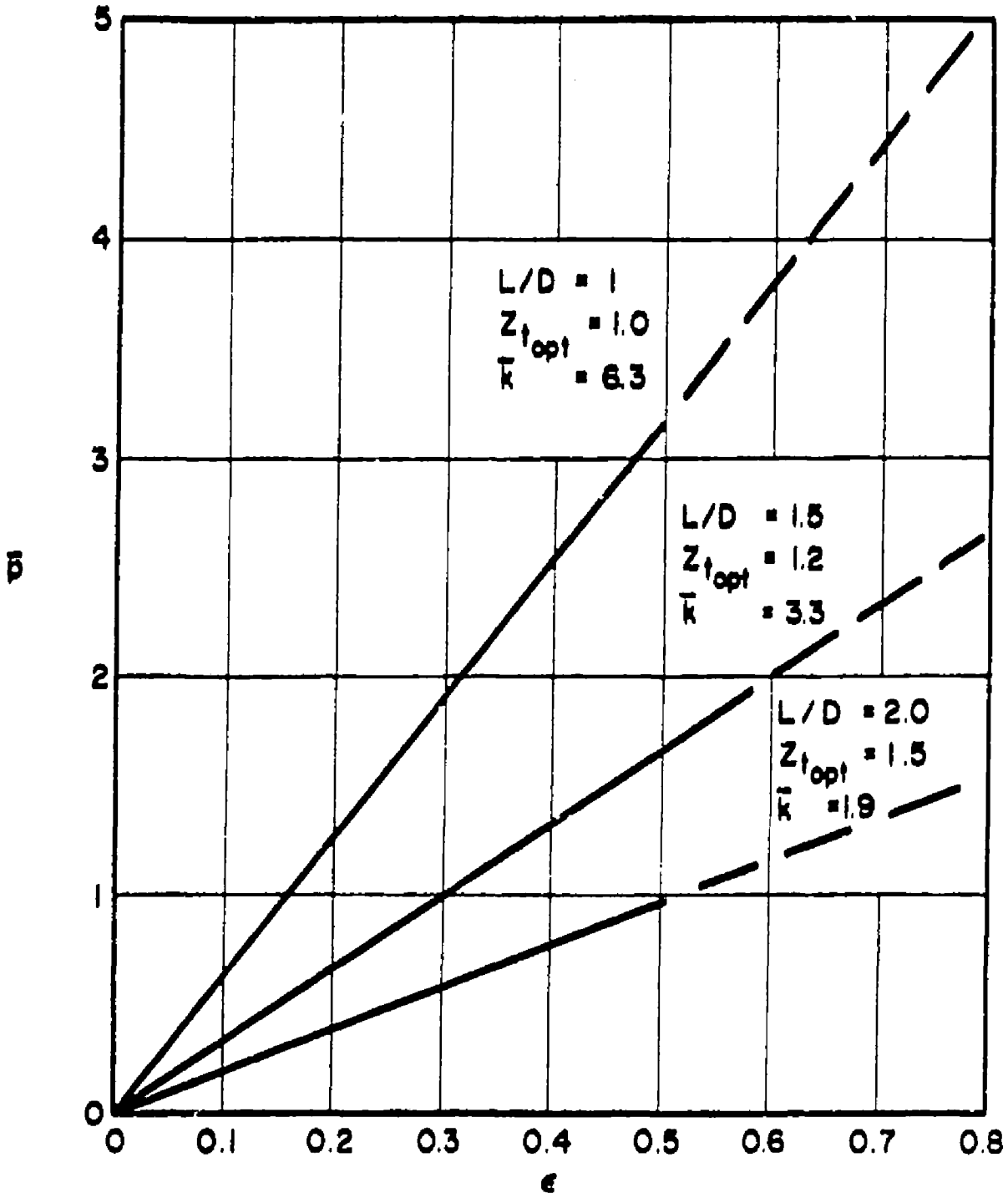

Fig. 10 Dimensionless pressure vs eccentricity ratio $p_s/p_a = 12$.

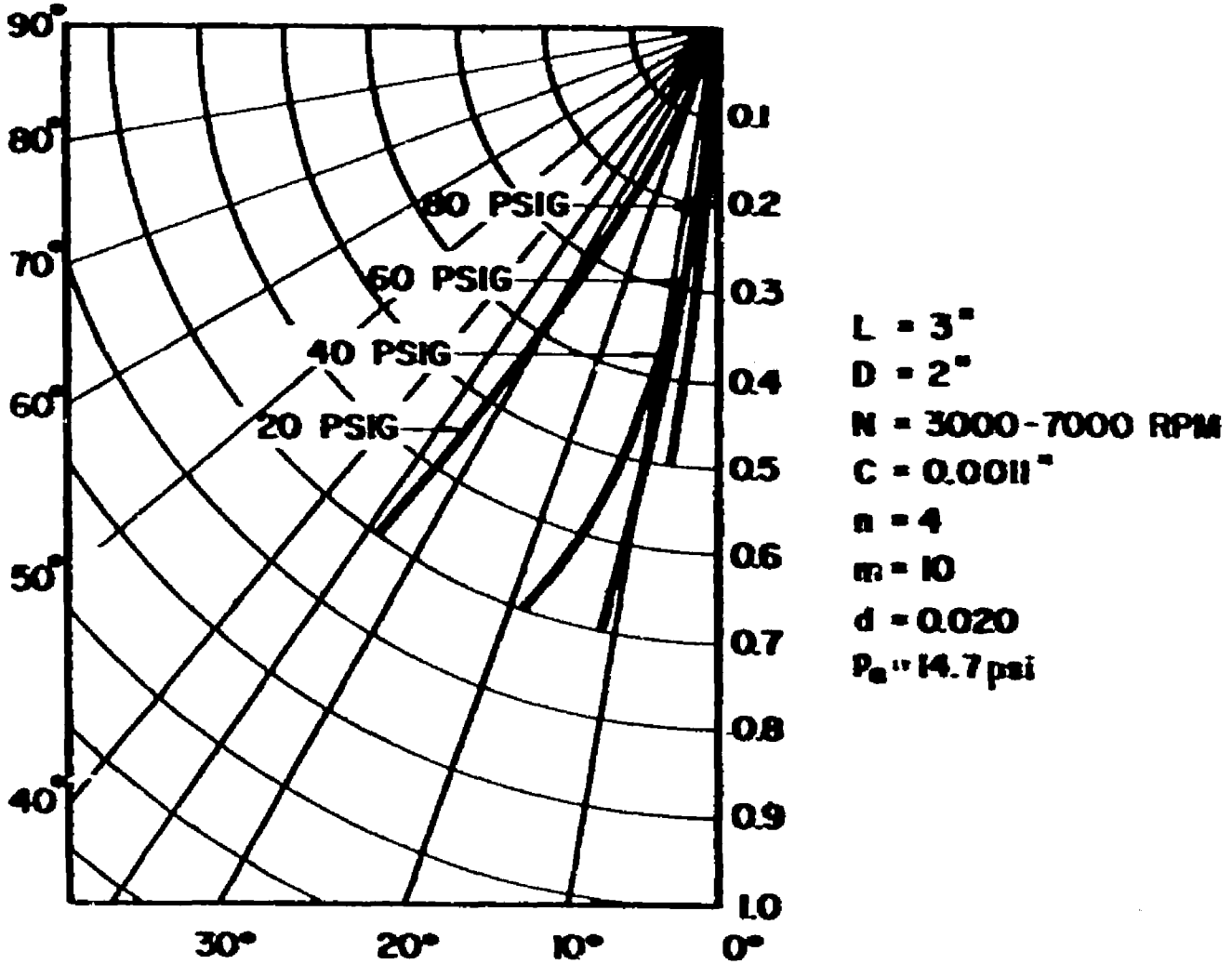

Fig. 11 Attitude angle vs eccentricity ratio for several P_s/P_a.

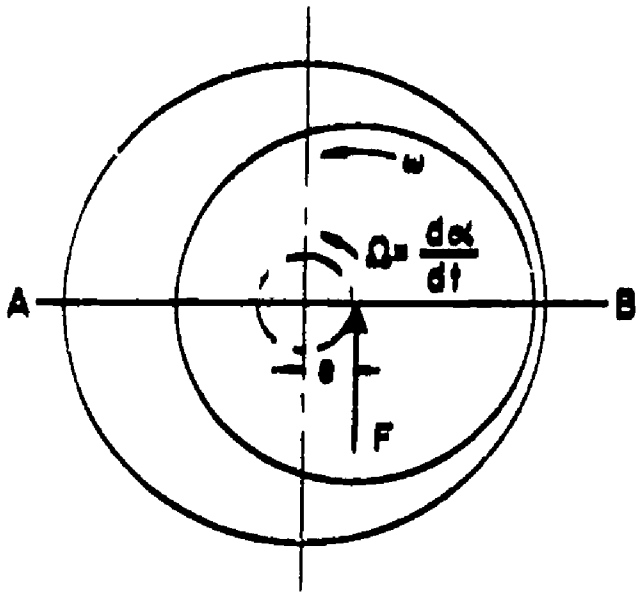

Fig. 12. Whirling journal.

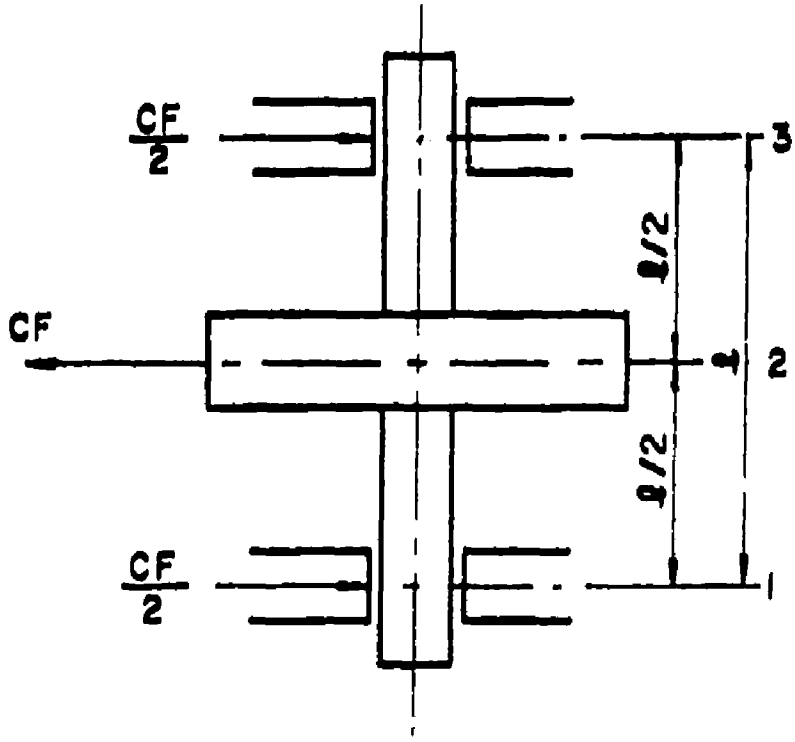

Fig. 13. Vertical rotor in symmetrical journal bearings.

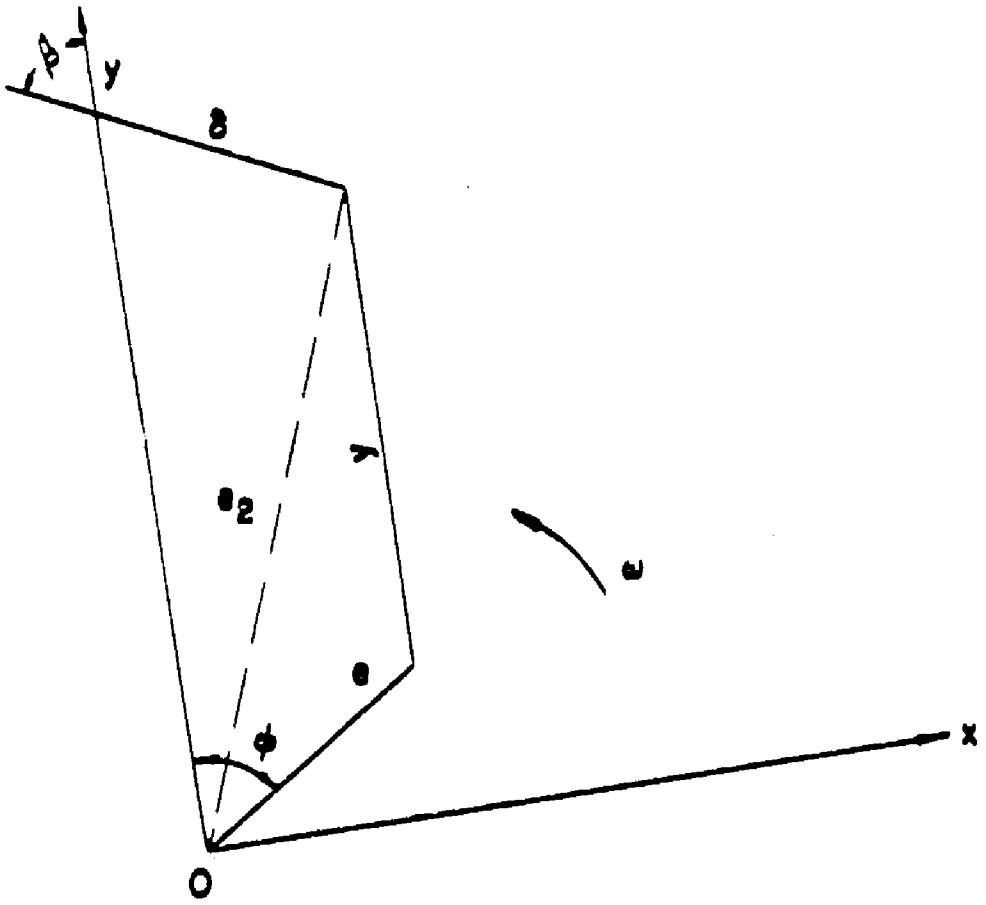

Fig. 14 Displacement diagram.

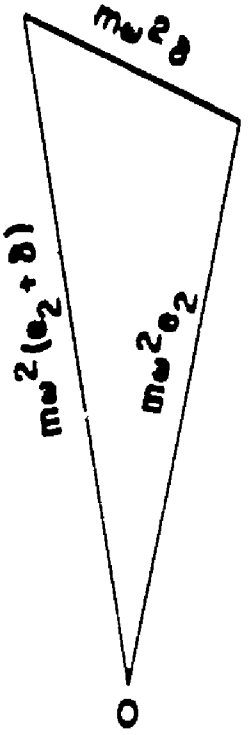

Fig. 15. Force diagram.

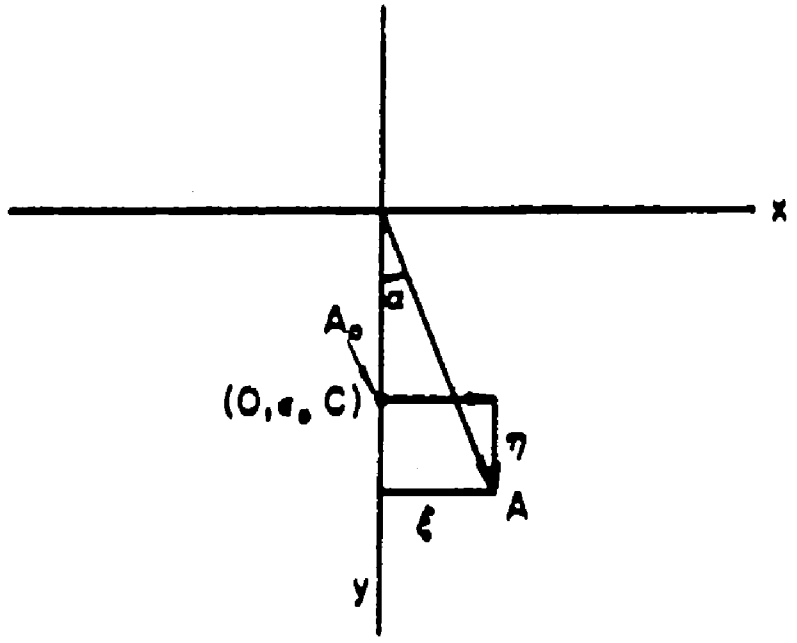

Fig. 16. Small displacement from equilibrium.

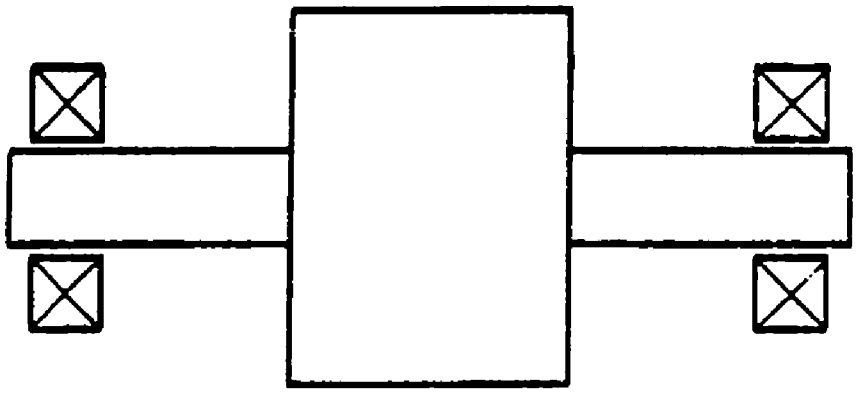

Fig. 17. Symmetrical rotor.

100

$\frac{\partial f_r}{\partial \alpha}$ 10

1

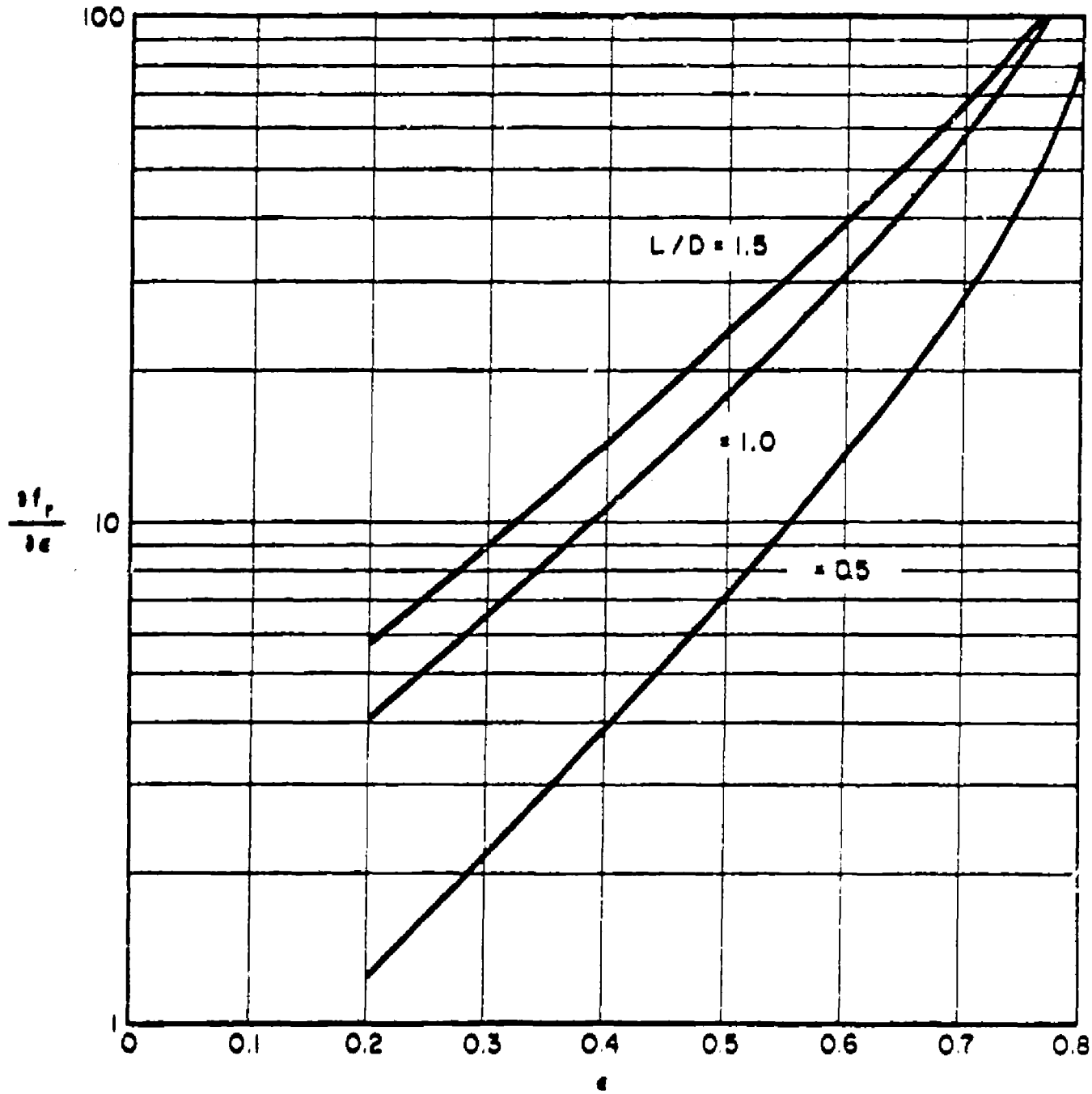

Fig. 18. $\frac{\partial f_r}{\partial \epsilon}$ vs ε (incompressible).

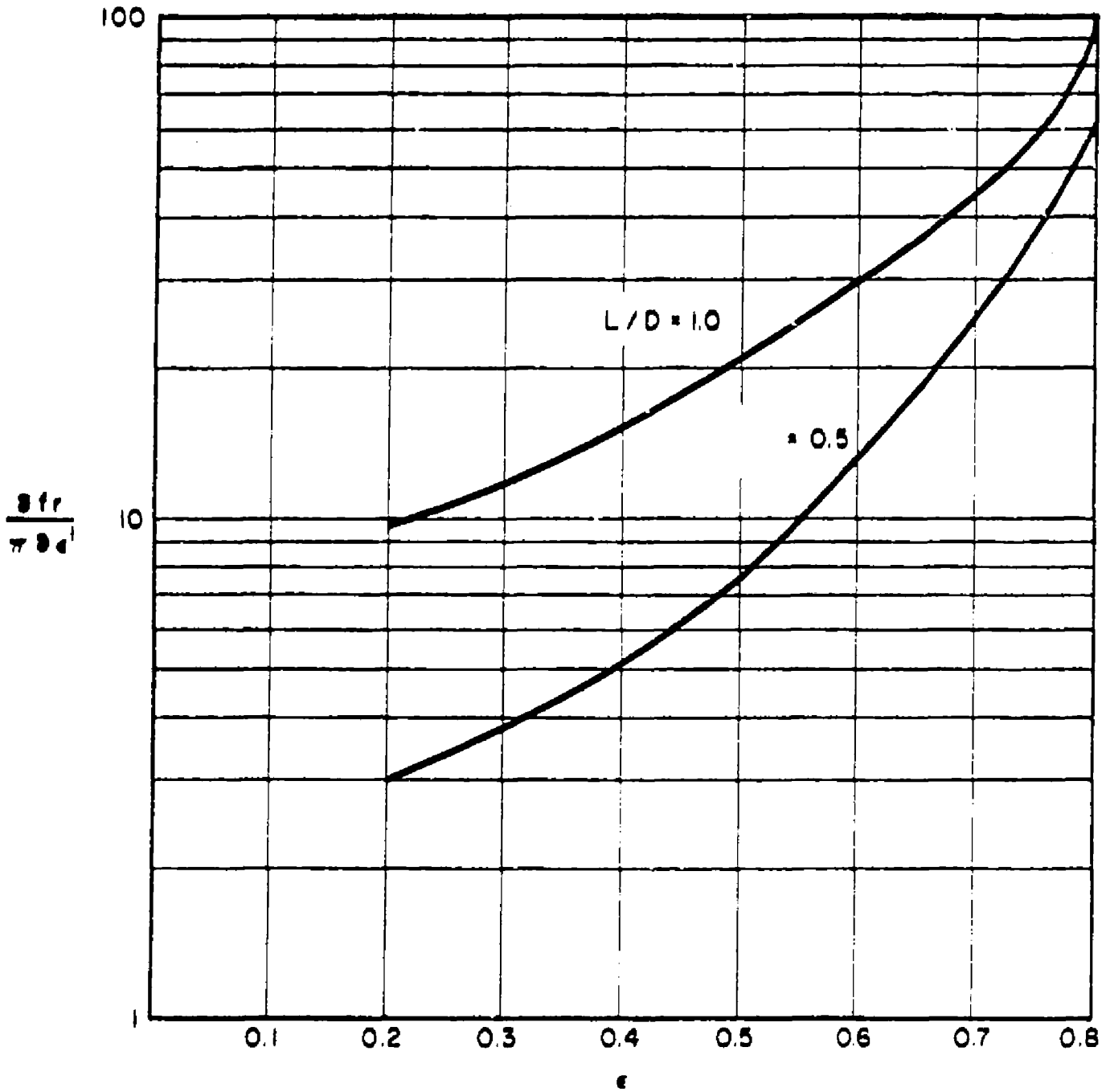

Fig. 19. $\frac{\partial f_r}{\pi \partial \epsilon'}$ vs ϵ (incompressible).

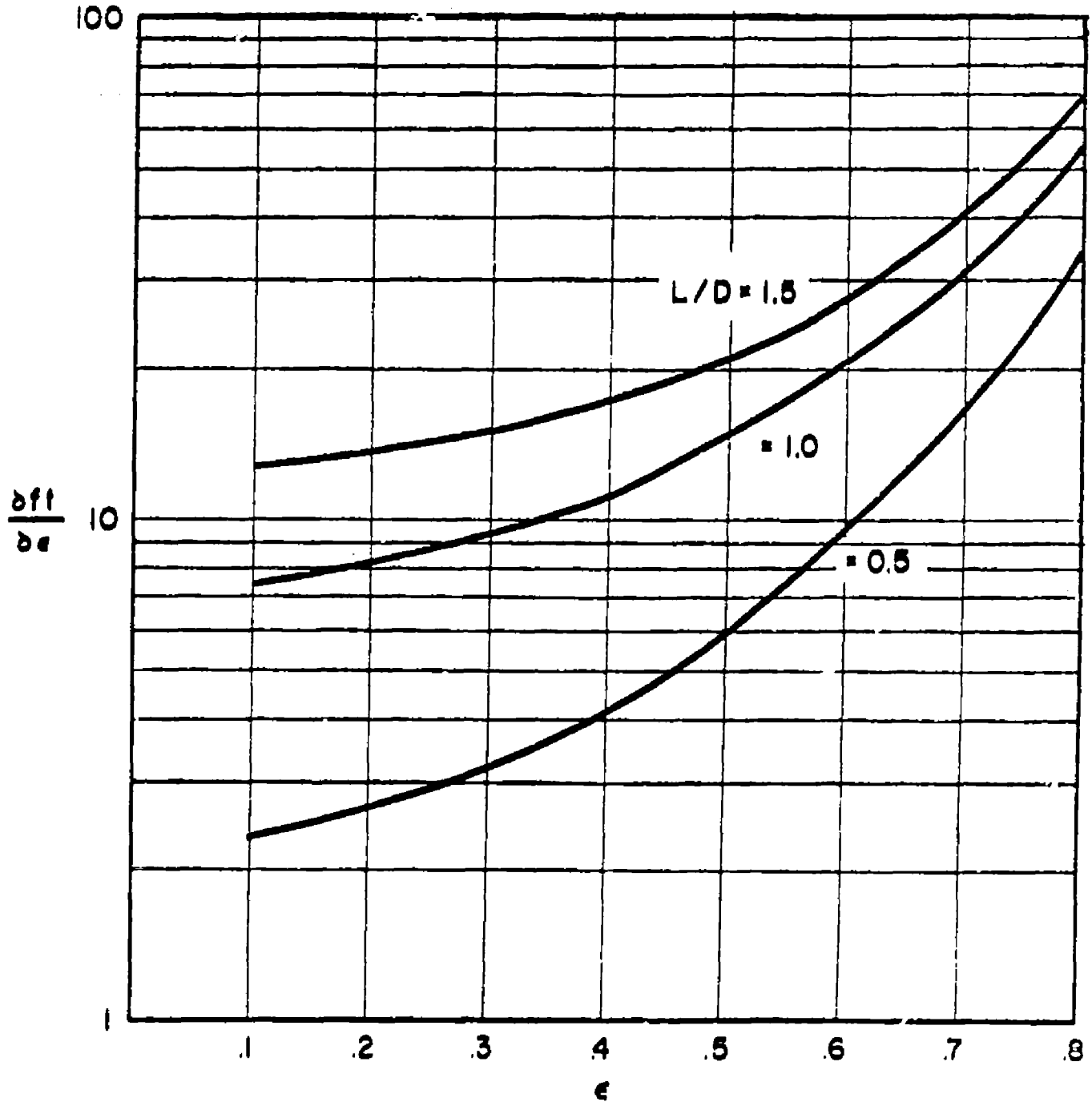

Fig. 20. $\frac{\partial f_1}{\partial \epsilon}$ vs ϵ (Incompressible)

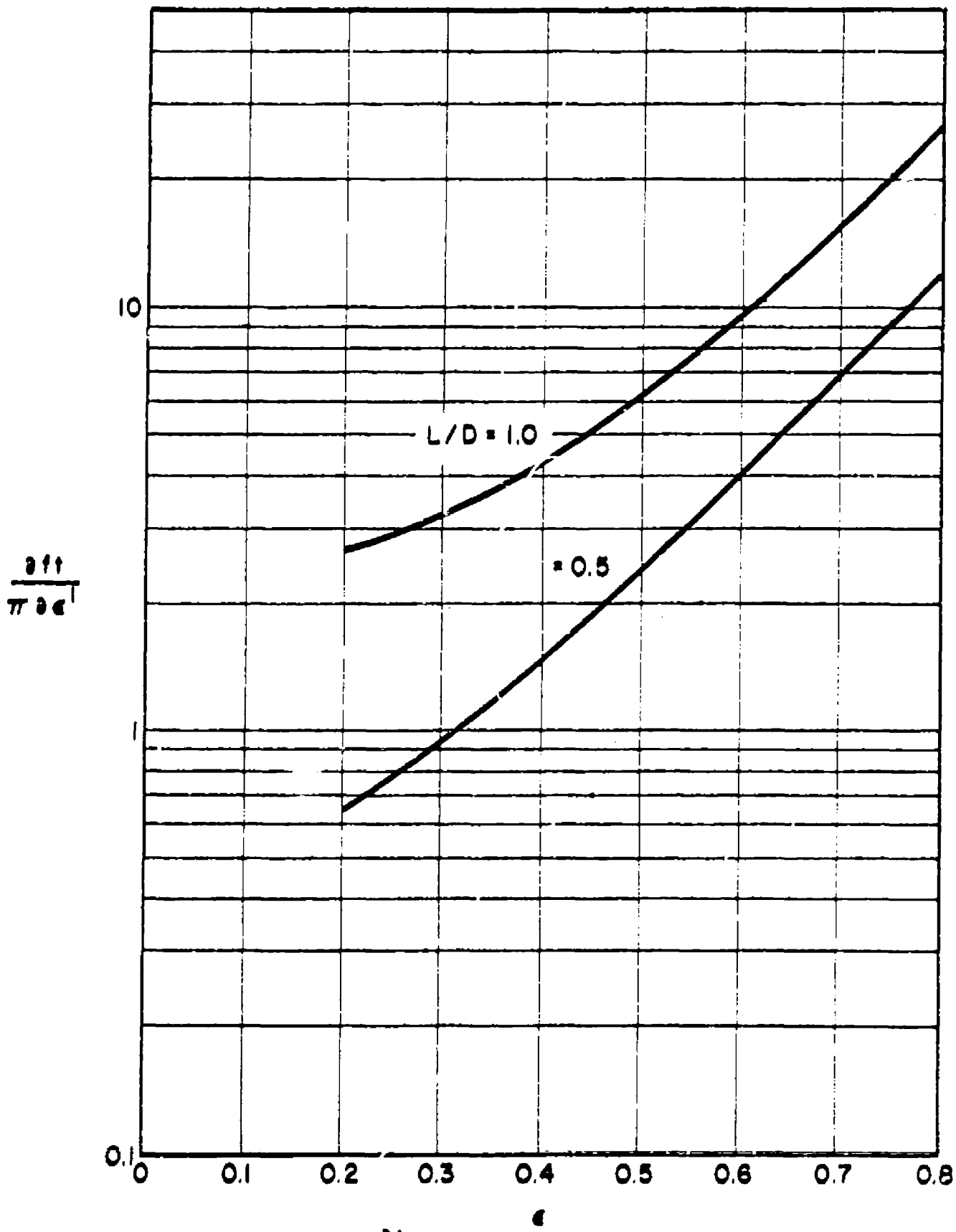

Fig. 21. $\frac{\partial f_t}{\pi \partial \epsilon'}$ vs ε (incompressible).

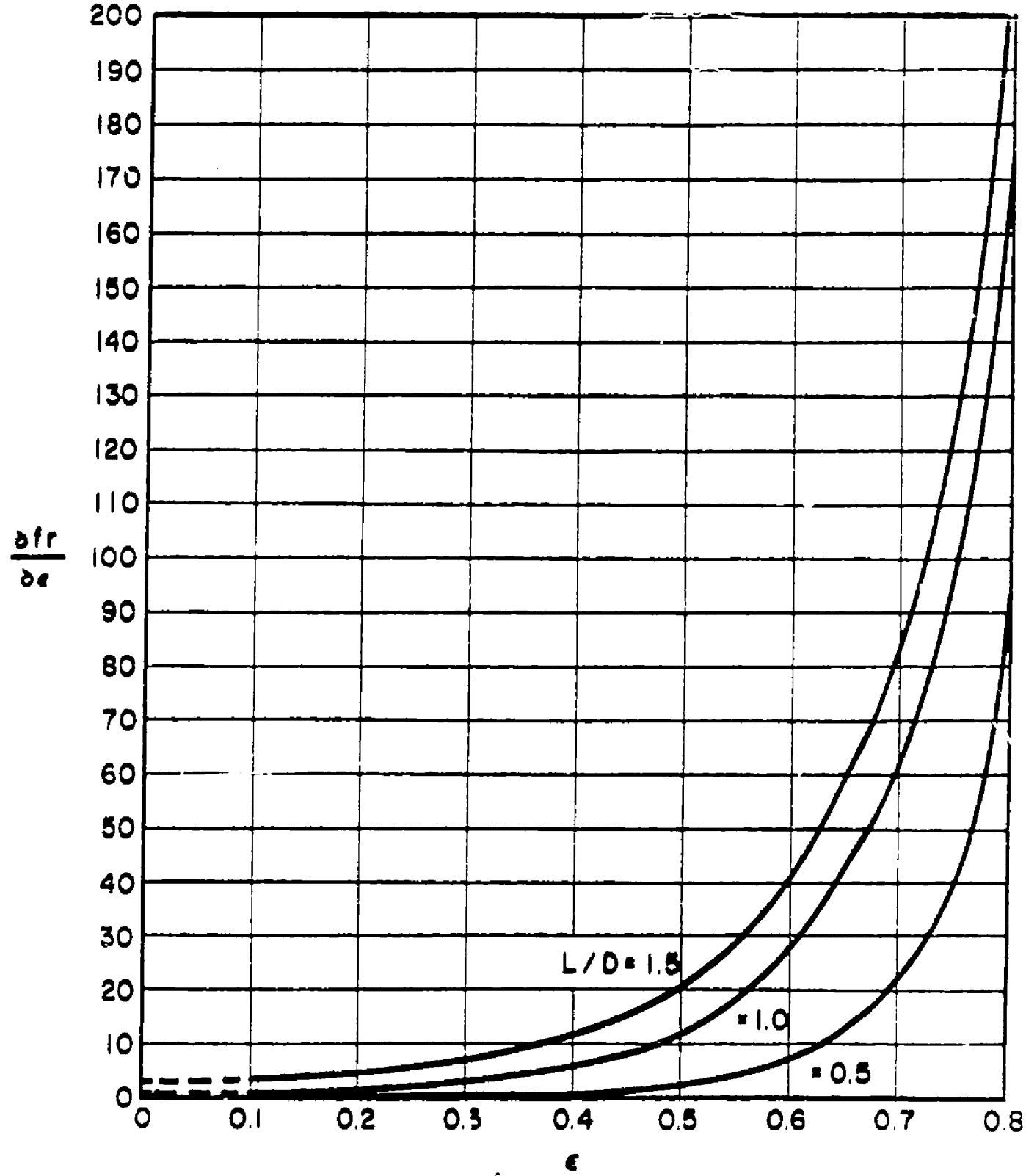

Fig. 22. $\frac{\partial f_r}{\partial \varepsilon}$ vs ε (Compressible)

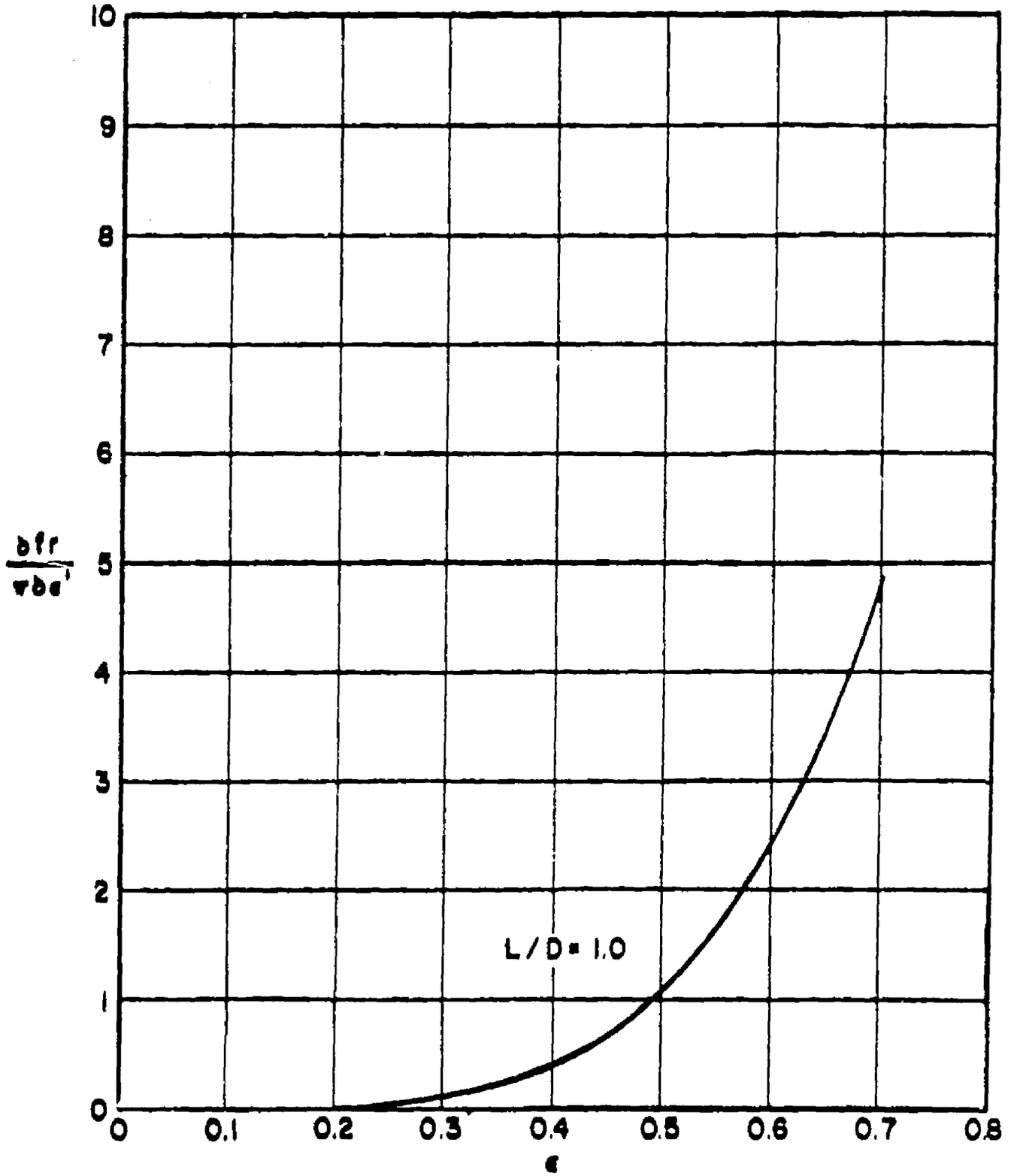

Fig. 23. $\frac{\partial f_r}{\pi \partial \varepsilon'}$ vs ε (Compressible)

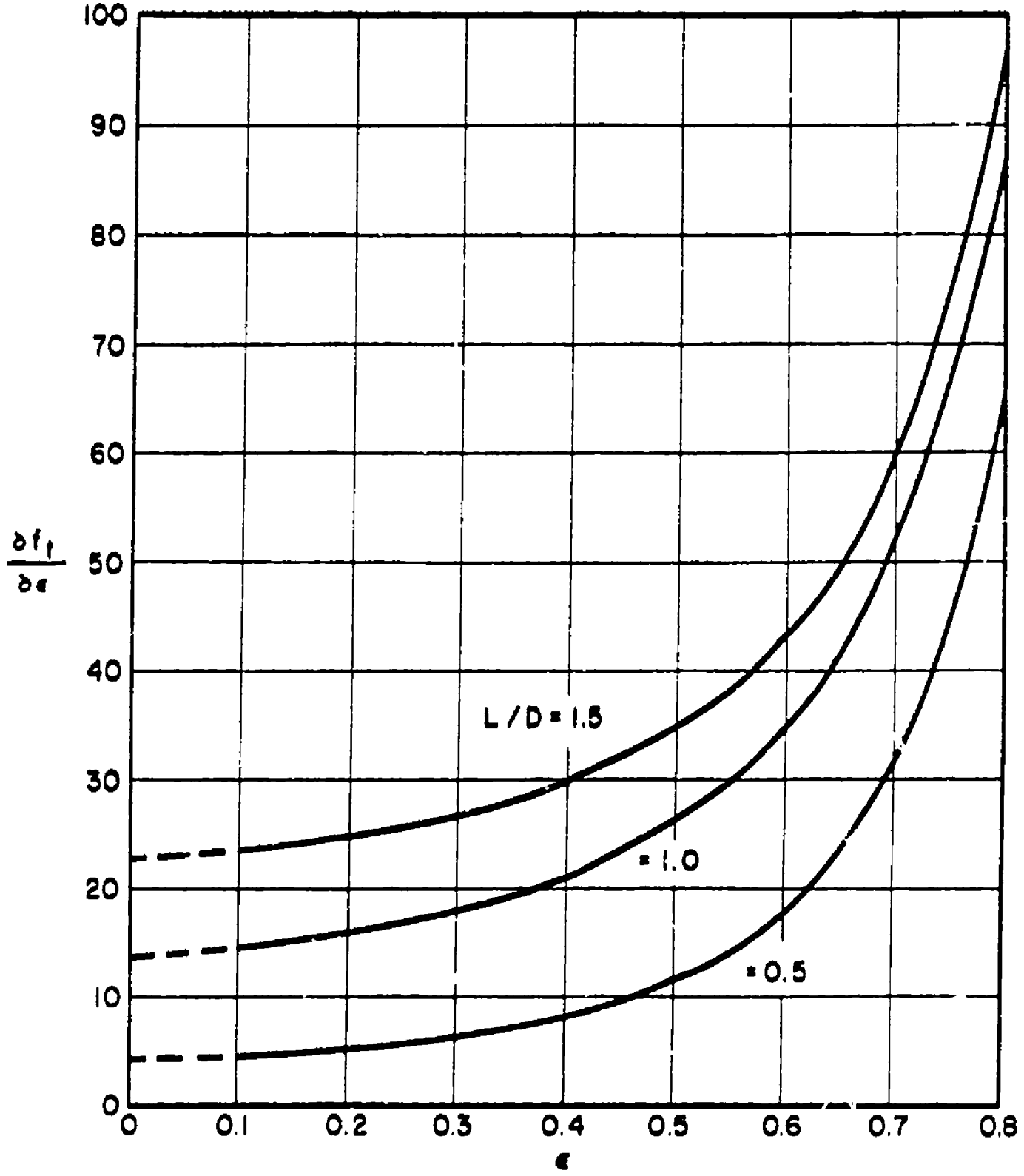

Fig. 24. $\frac{\partial f_1}{\partial \epsilon}$ vs ϵ (Compressible)

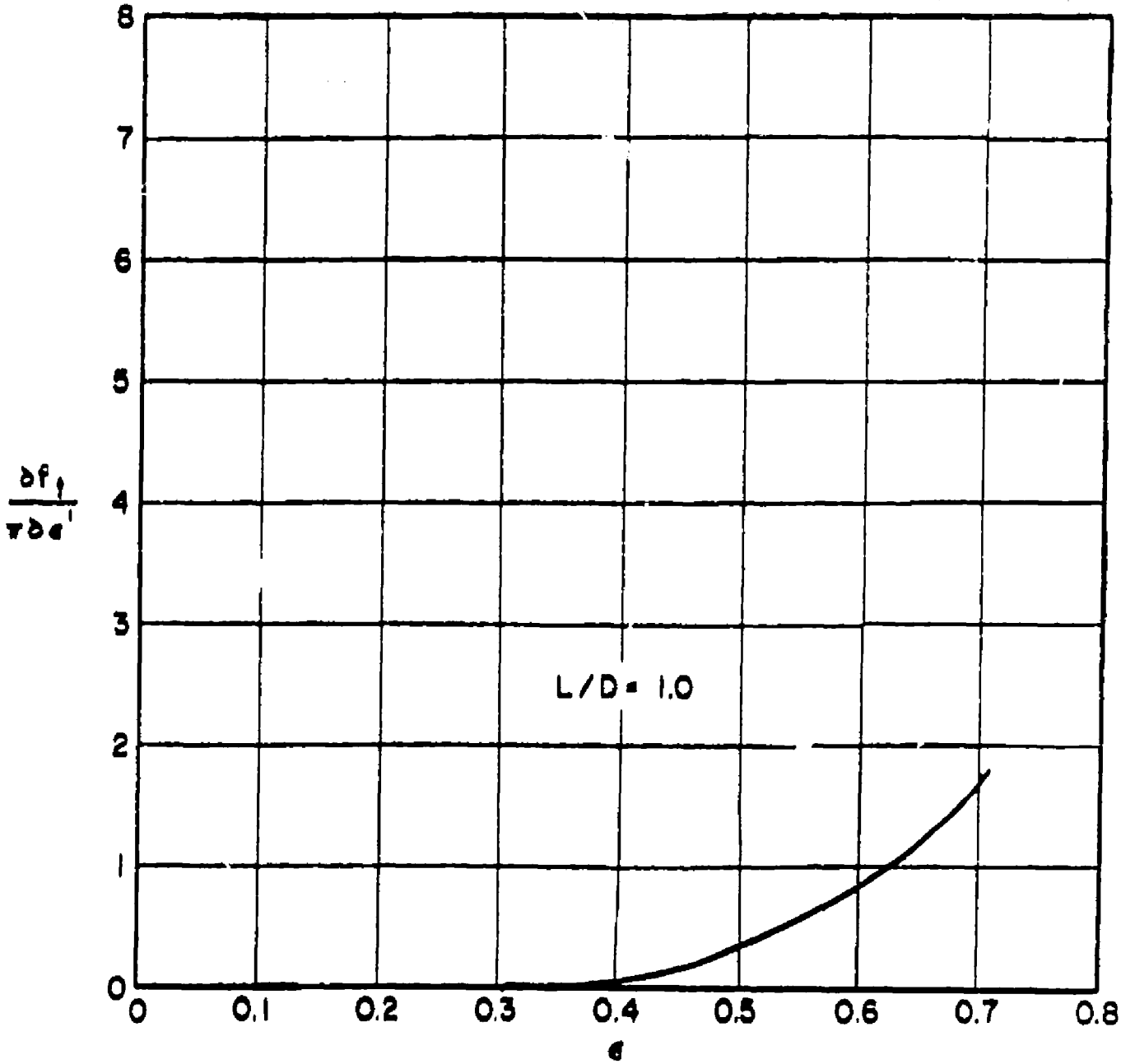

Fig. 25. $\frac{\partial f_t}{\pi \partial \epsilon'}$ vs ϵ (Compressible)

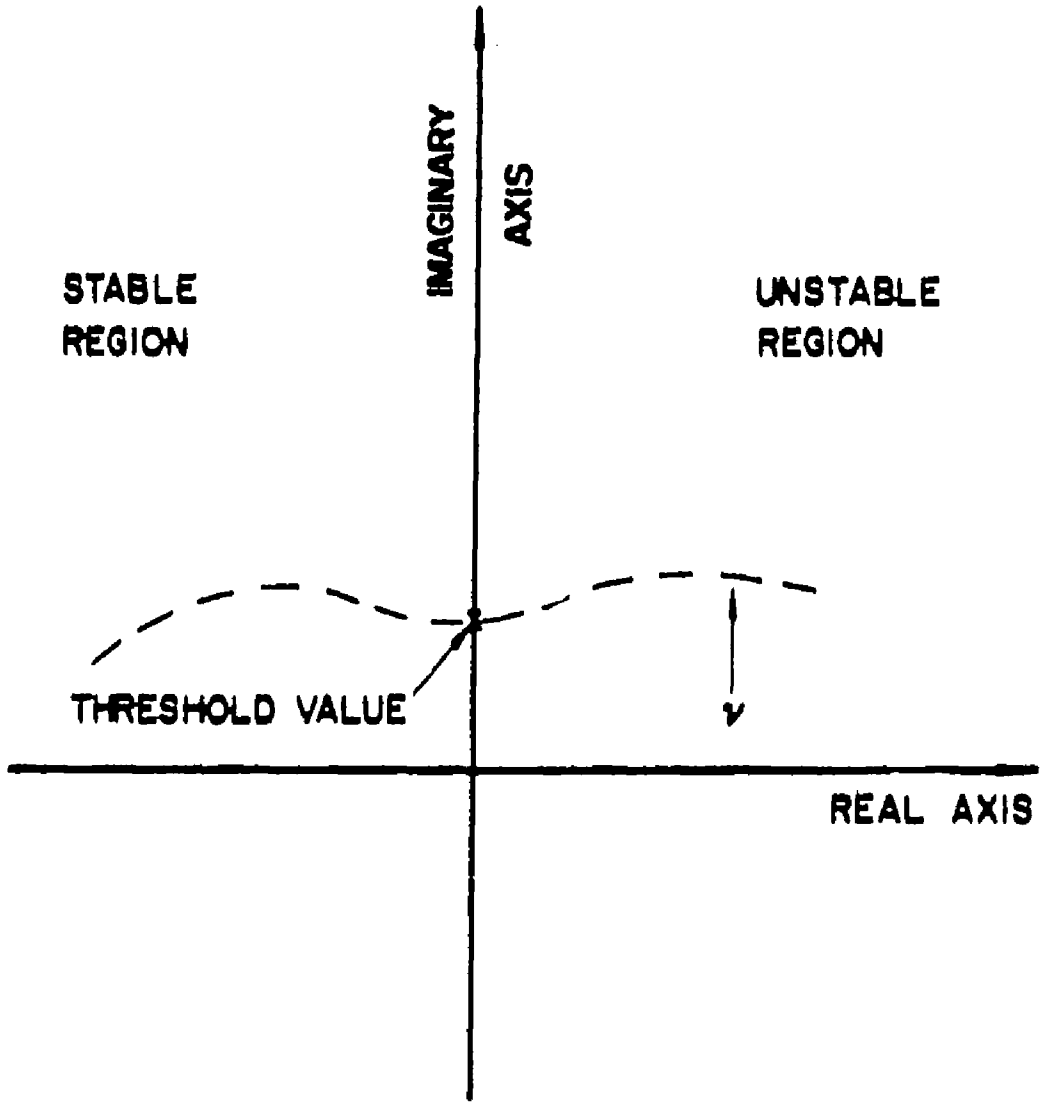

Fig. 26. Threshold of instability.

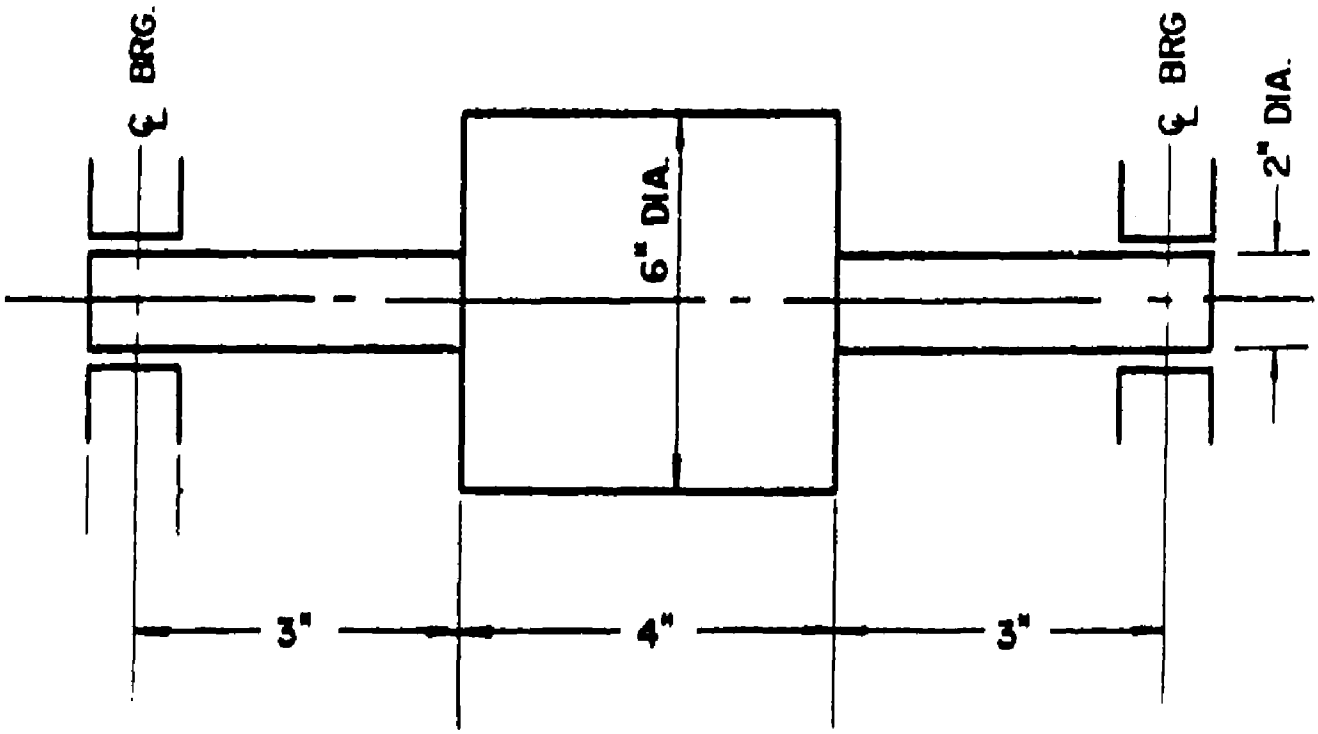

Fig. 27. Shaft rotor bearing system.

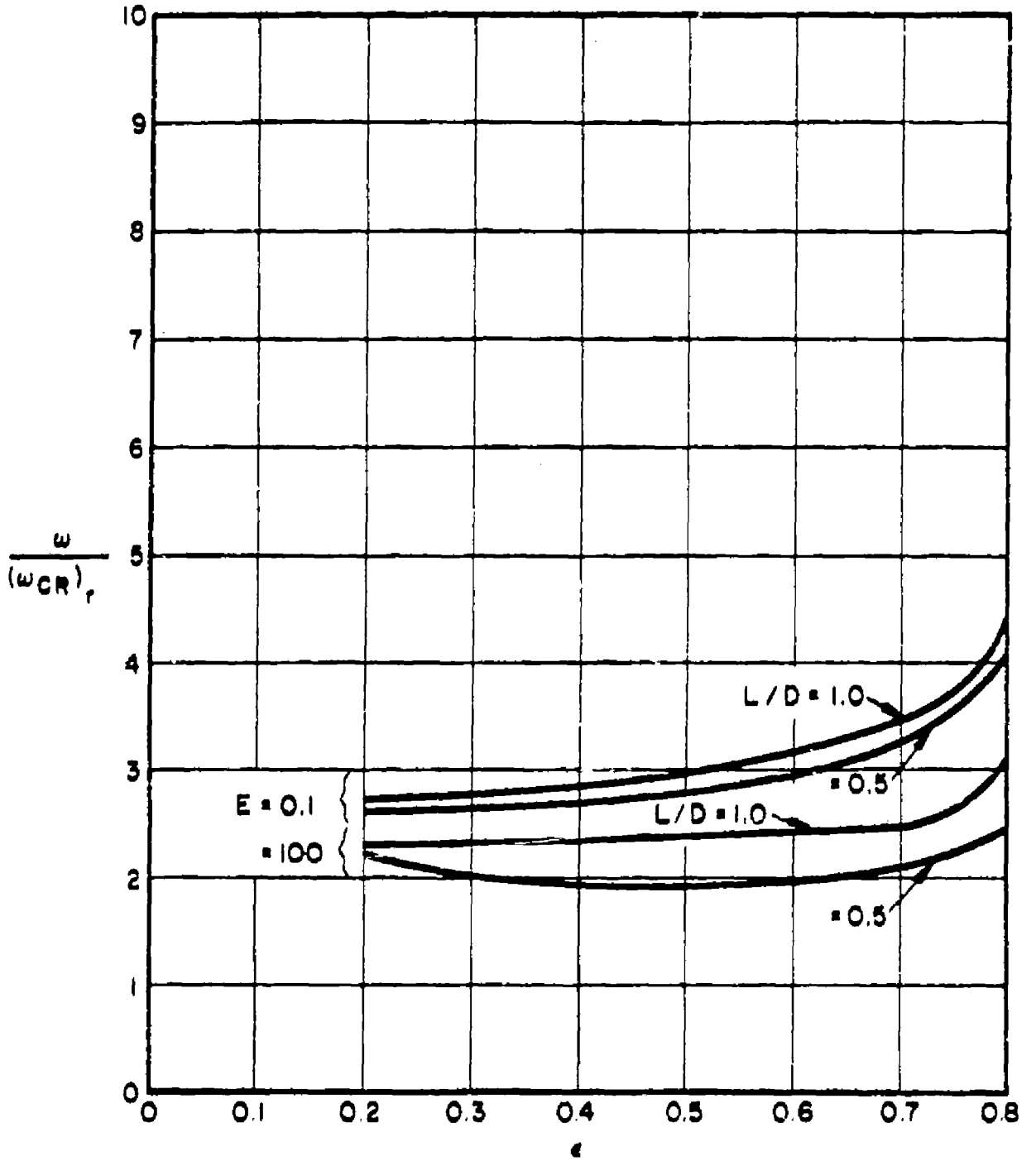

Fig. 28. $(\omega/\omega_{CR})_r$ vs ε for incompressible cases.

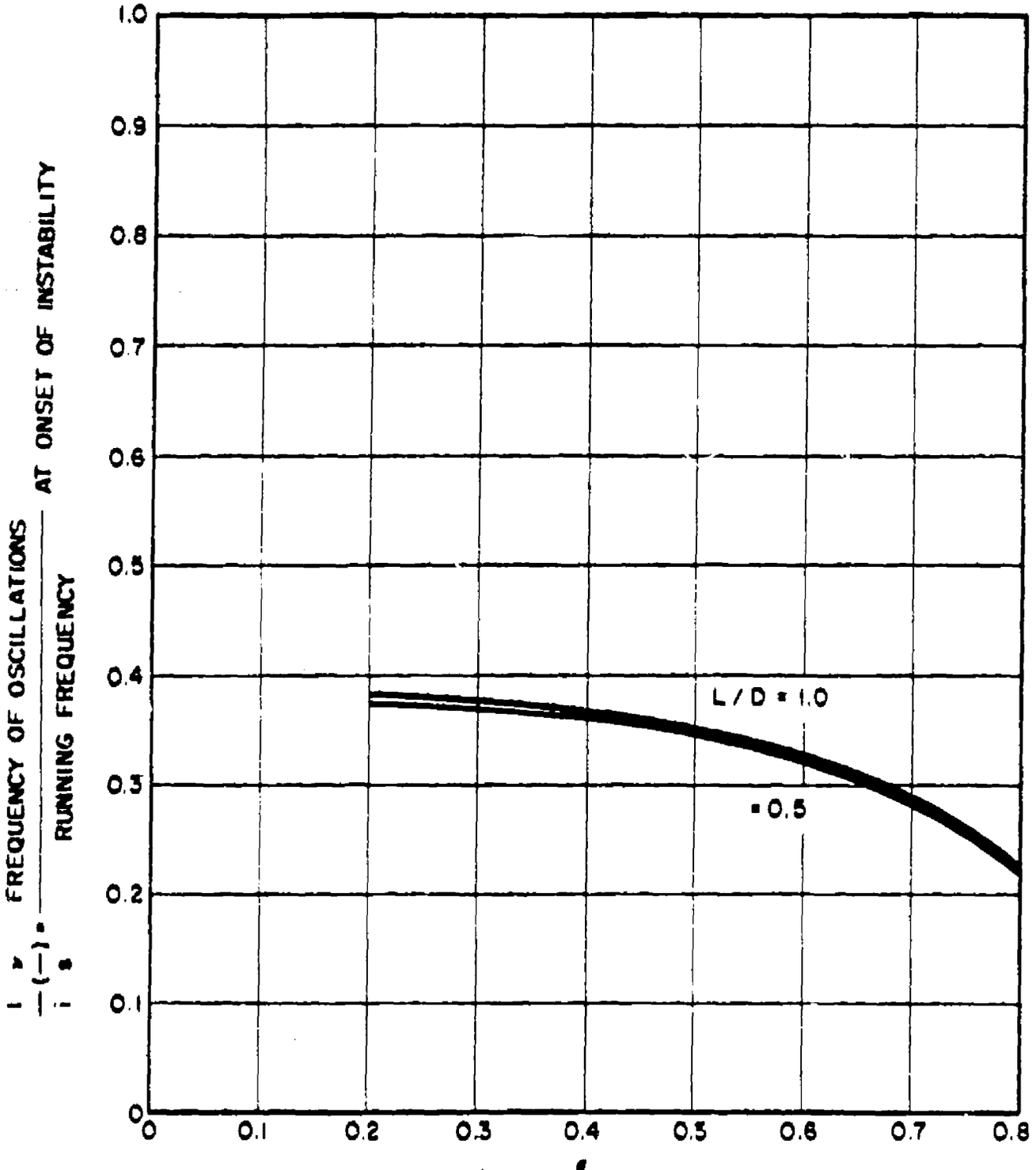

Fig. 29. $\frac{1}{i}\left(\frac{\gamma}{s}\right)$ vs ε for incompressible cases.

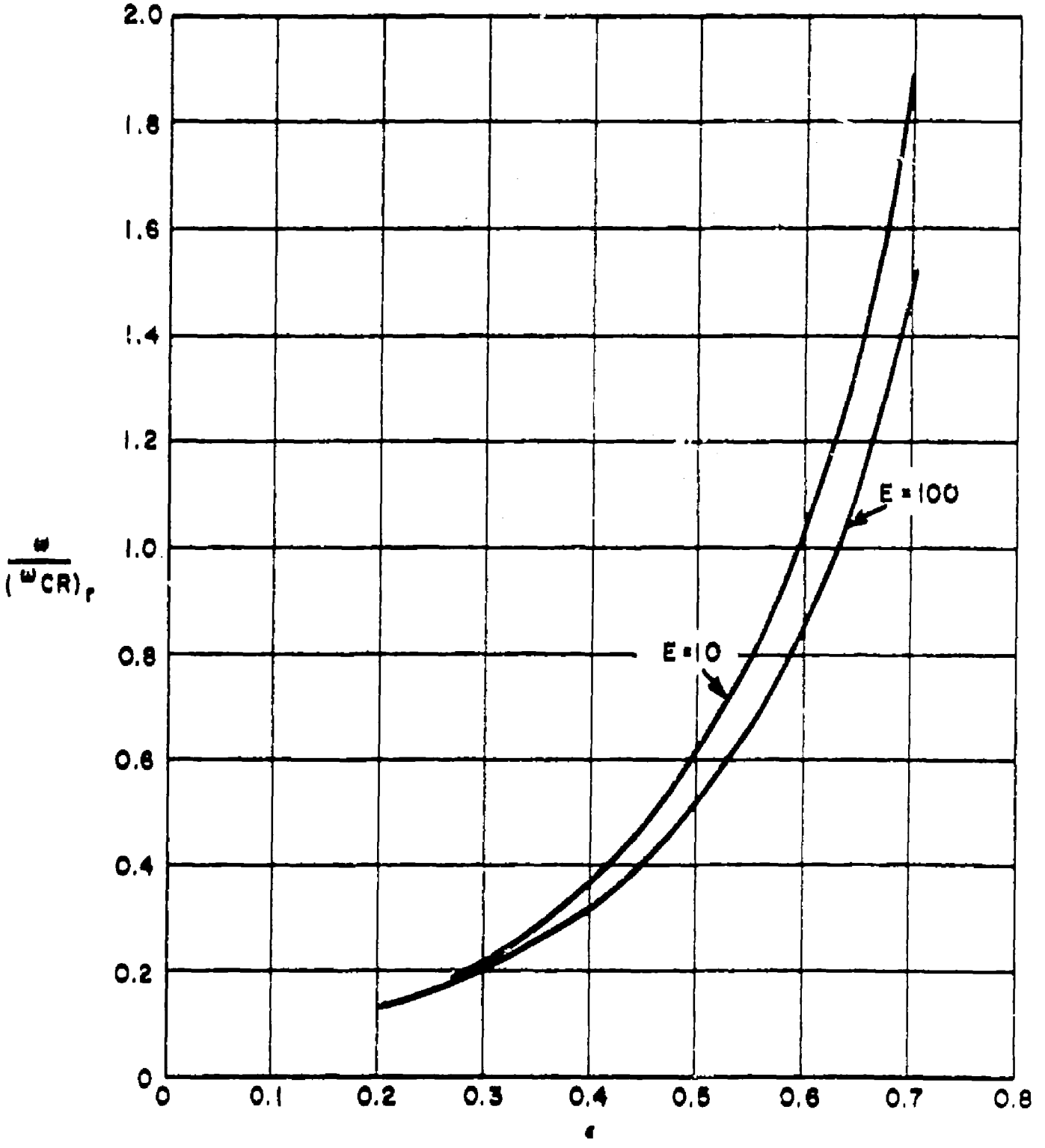

Fig. 30. $\frac{\omega}{(\omega_{CR})_r}$ vs ε for compressible cases.

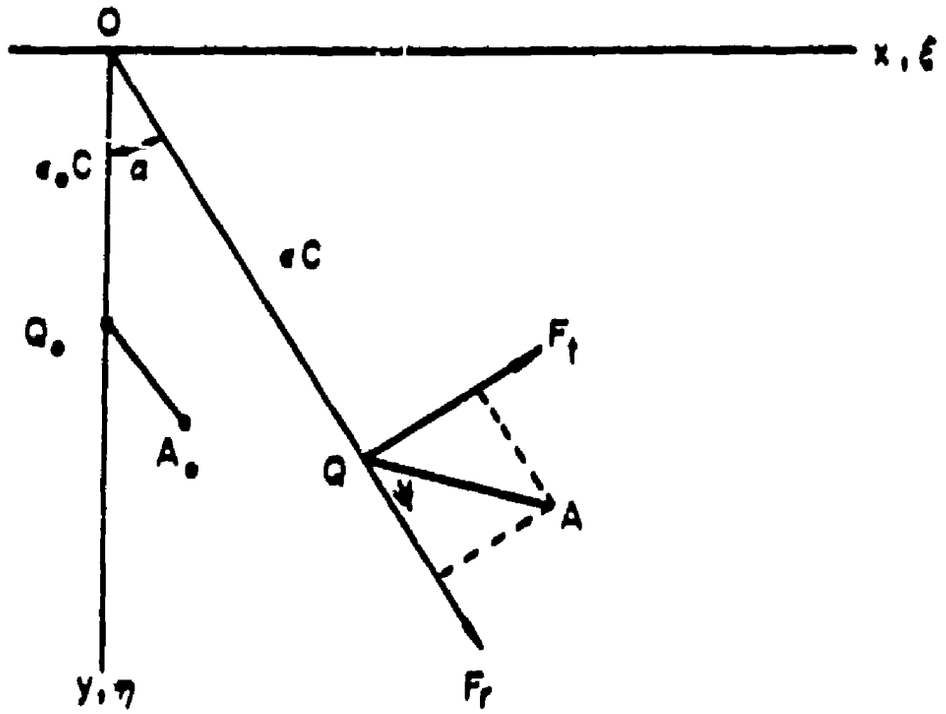

Fig. 31. Large displacements from equilibrium.

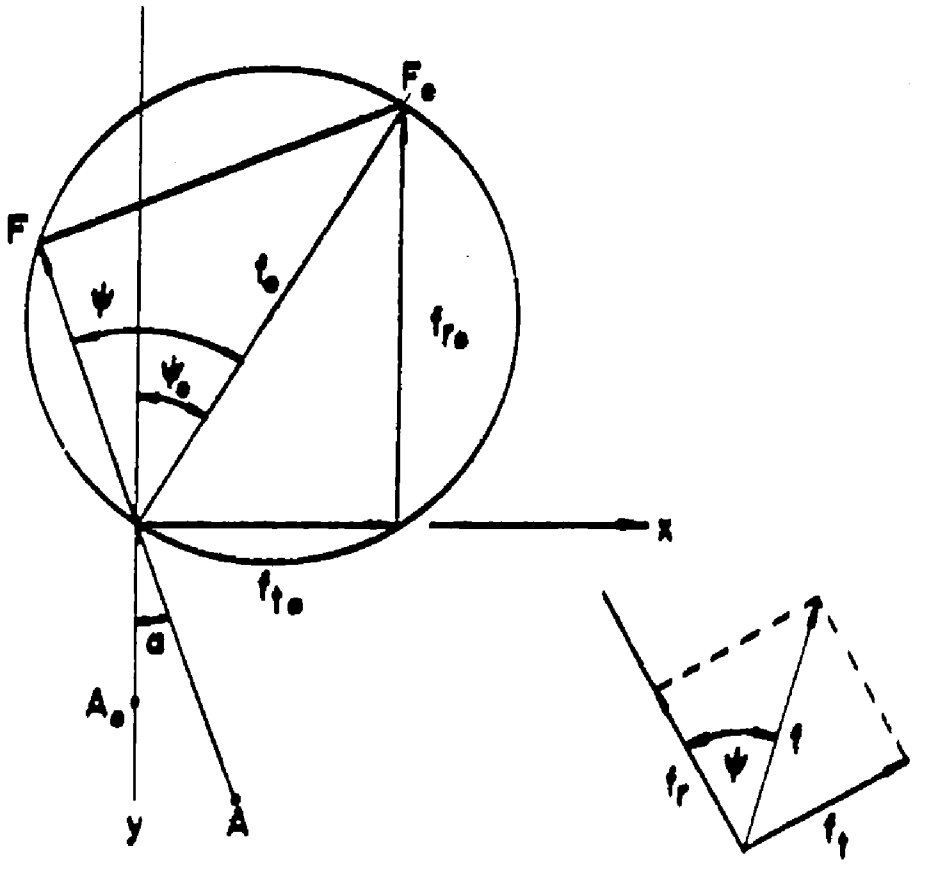

Fig. 32. Representation of resultant force.

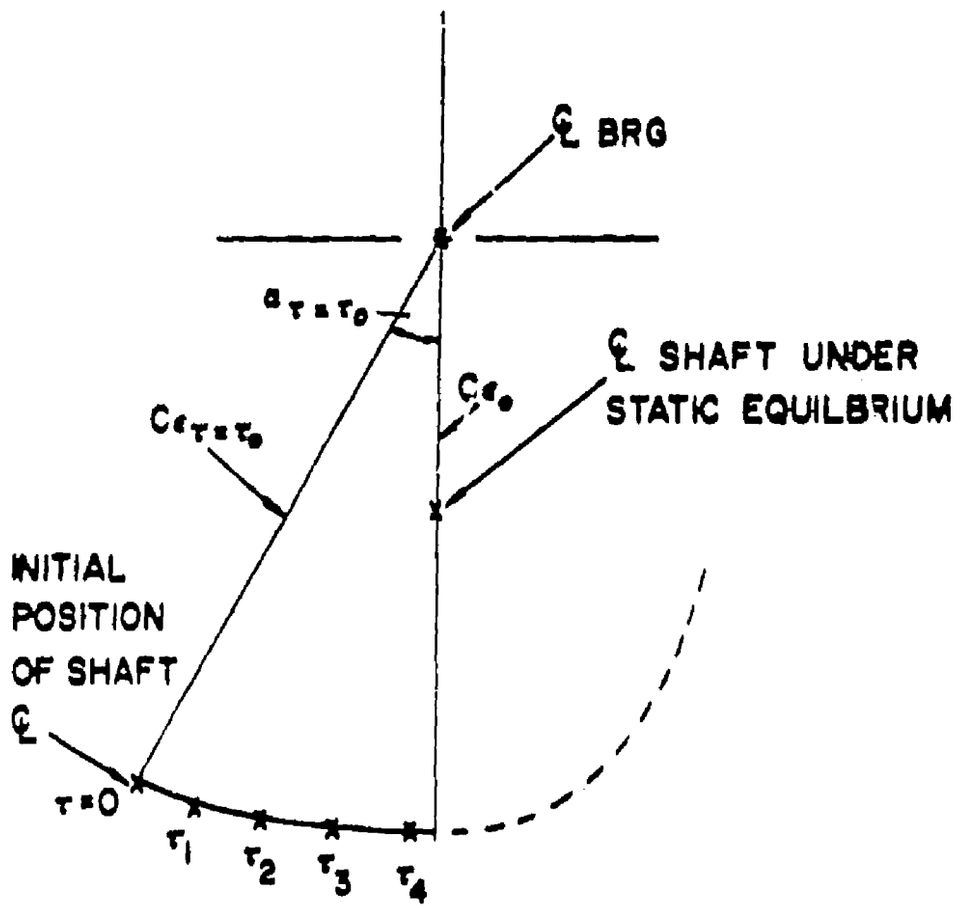

(a) PROCEDURE FOR DETERMINING LOCUS OF SHAFT ℄

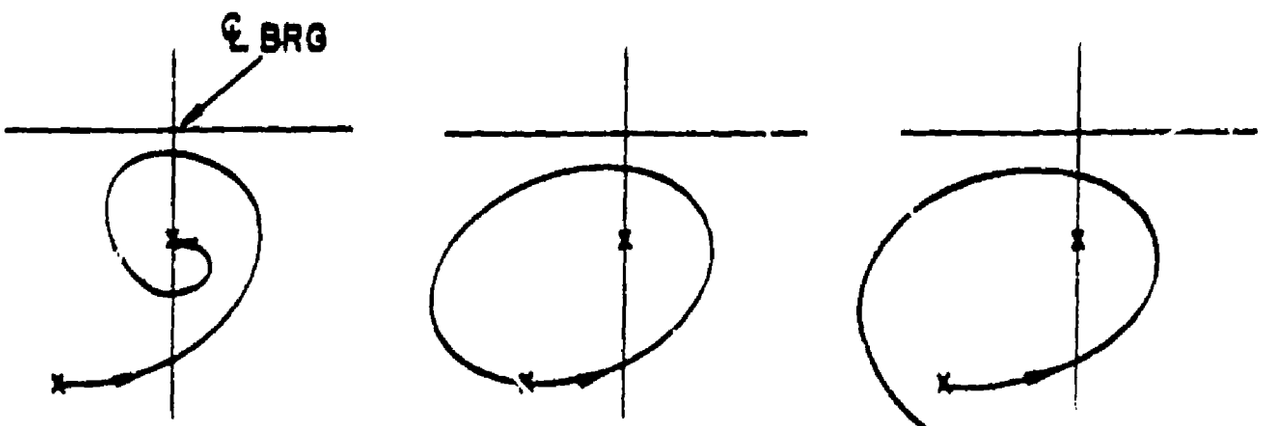

(b) STABLE CONDITION (c) STABLE OSCILLATION (d) UNSTABLE OSCILLATION

Fig. 33 Locus of journal center - massless rotor solution

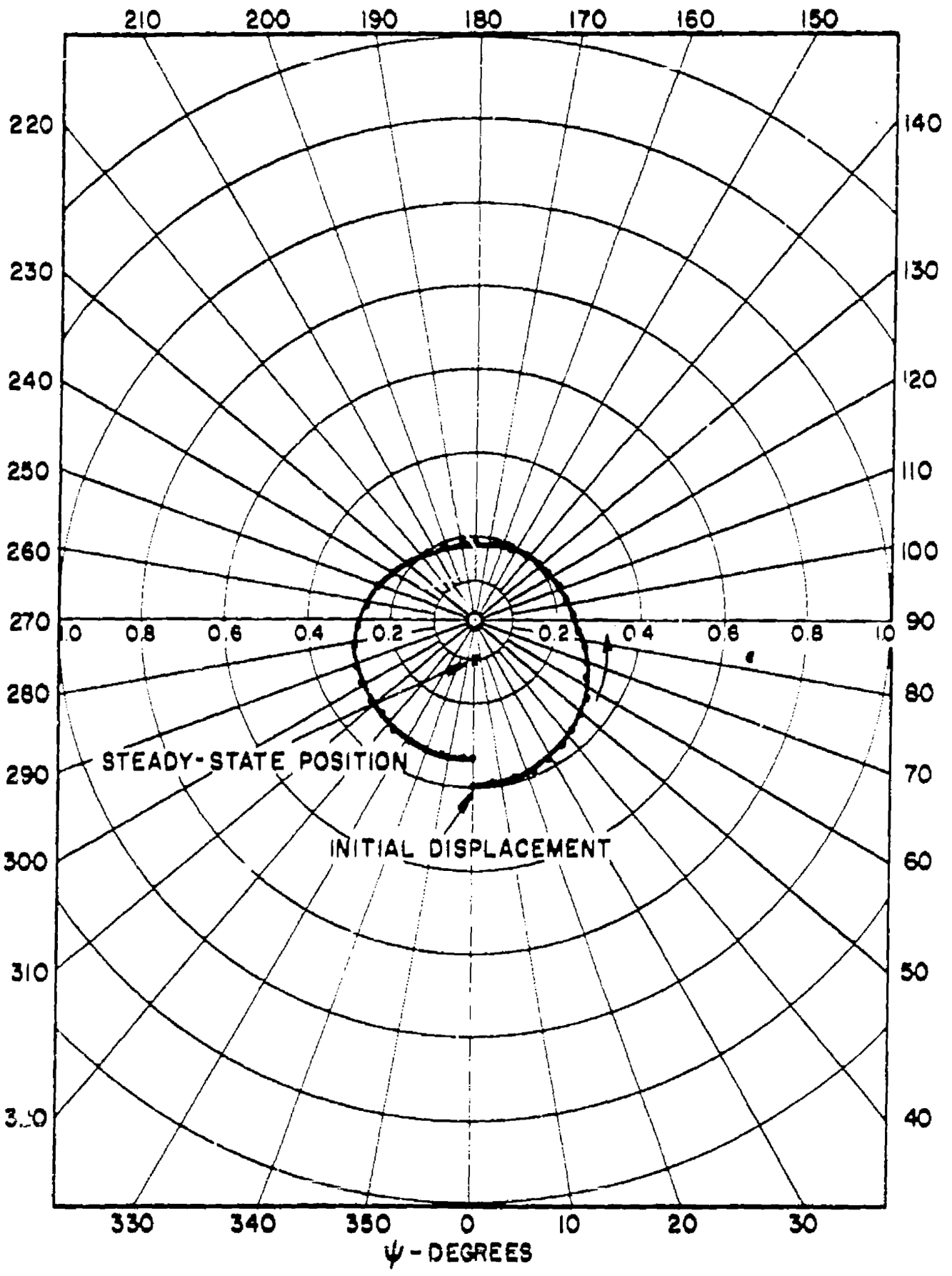

Fig. 34. Locus of journal center.

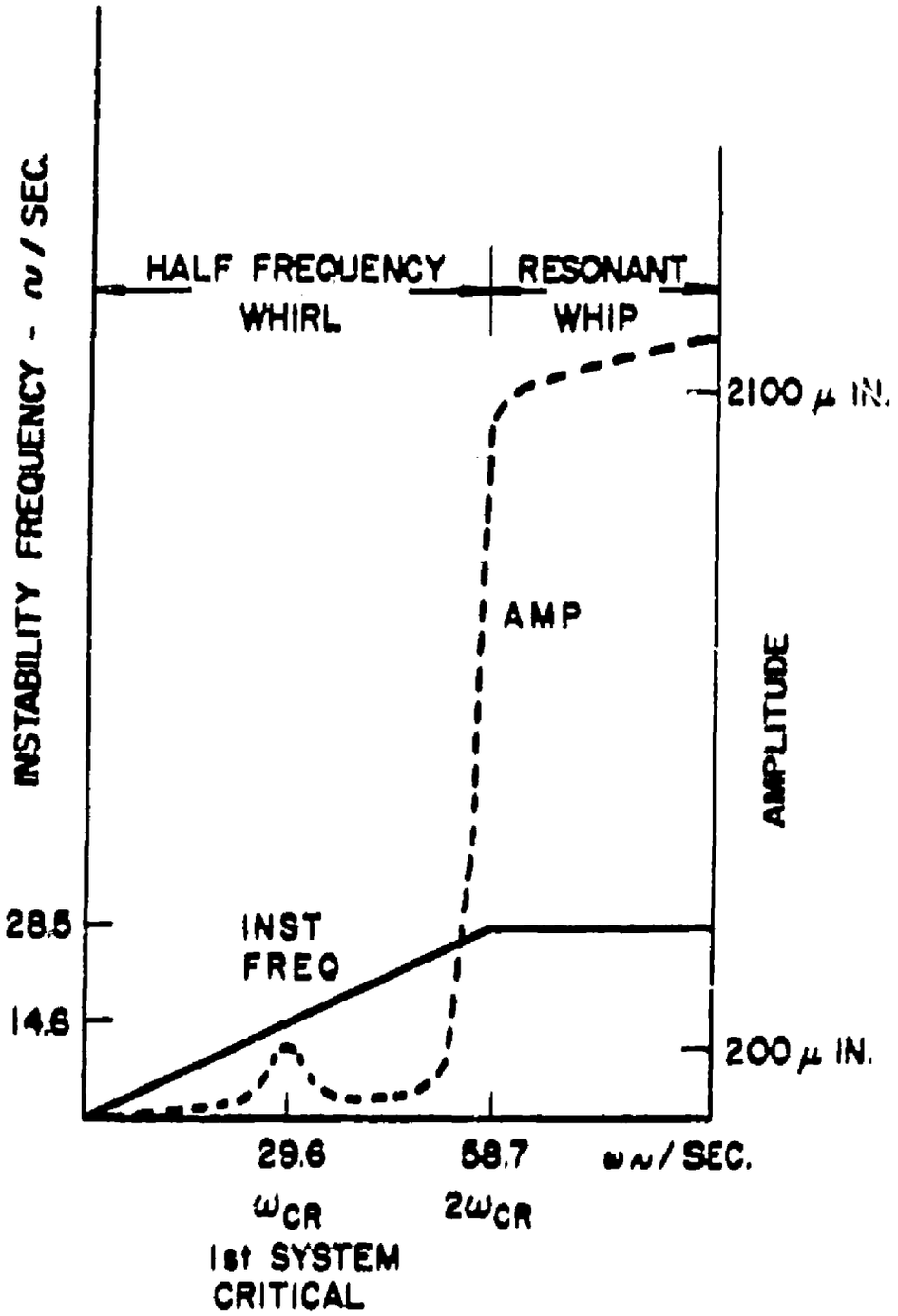

Fig. 35. Amplitude and frequency of instabilities.

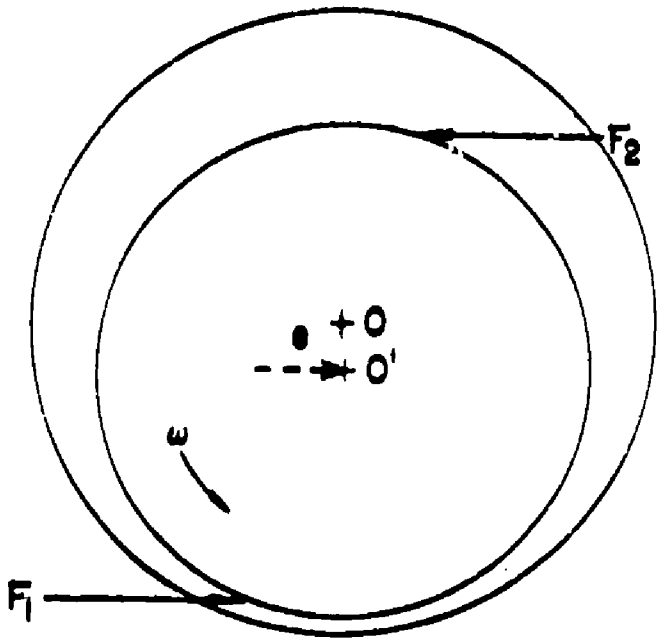

Fig. 36. Uneven torques due to eccentricity.

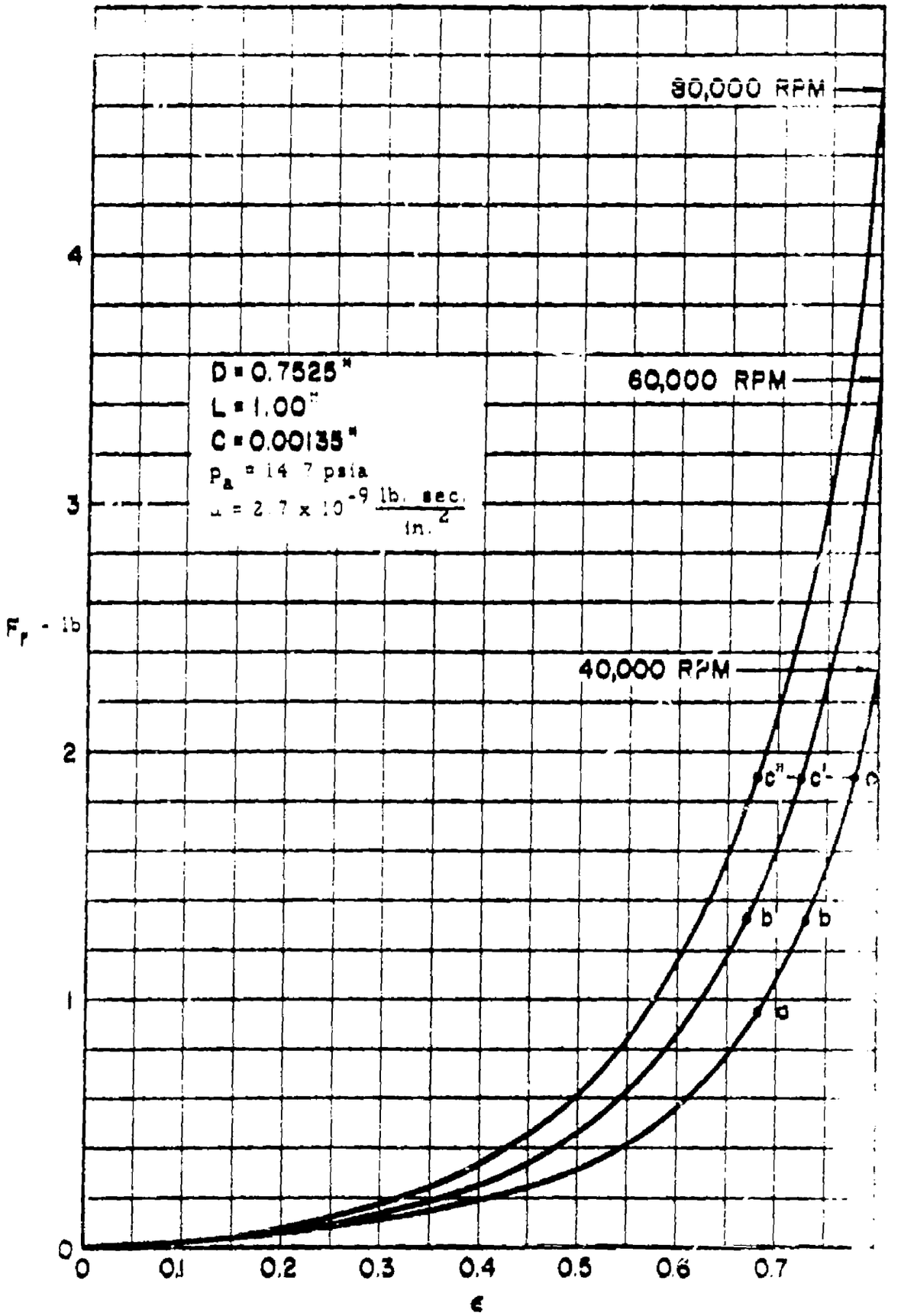

Fig 3: Self acting bearing radial force vs eccentricity ratio

SYMBOLS

C	radial clearance	in.
C_d	discharge coefficient (approx. equal to 0.6)	
D	diameter	in.
d	orifice diameter	in.
E	$\frac{h\pi}{2\mu L \omega_o}\left(\frac{C}{R}\right)^3$, also modulus of elasticity	
e	eccentricity	in.
F	Force	lb.
f	dimensionless force	
g	acceleration	in./sec.^{2}
h	film thickness	in.
I	moment of inertia	in.^{4}
K_2	radial fluid film stiffness	lb./in.
k	stiffness constant of the rotor shaft	lb./in.
L	bearing length	in.
l	length between bearings	in.
m	mass, also number of orifices/feeders Eq. 12	lb.-sec.^{2}/in.
N	speed	RPM
n	number of feeders/bearing Eq. 12	
P	pressure over projected area, also force Eq. 71	psi
p	pressure	psi

R	radius	in.
$\mathcal{R}$	gas constant	in./°F
s	ω/ω_o	
T	temperature	°F
t	time	sec.
U	velocity	in./sec.
V	velocity	in./sec.
W	load	lb.
X	disturbing force	lb.
x	coordinate, also displacement of rotor center	
Y	disturbing force	lb.
y	coordinate, also displacement of rotor center	
Z_t	dimensionless feeding parameter for turbulent flow	
z	coordinate	
α	angle	
$\dot{\alpha}$	$V_t/C\varepsilon$	
β	phase angle	
γ	variable Eq. 69	
δ	distance	in.
ε	eccentricity ratio	

$$\varepsilon' = \frac{d\varepsilon}{\omega\, dt} = \frac{V_R}{2\pi CN}$$

ζ	$\frac{E\nu}{1+\nu^2}$	
η	displacement of journal center from equilibrium	in.
θ	angle	radians
λ	$\frac{\mu L R}{w}\left(\frac{R}{C}\right)^2$	lb.-sec.
μ	viscosity	lb.-sec./in.^{2}
ν	complex number	
ξ	displacement of journal center from equilibrium	in.
ρ	mass density	lb.-sec.^{2}/in.
τ	$\omega_o t$	
ϕ	attitude angle	radians
ψ	angle	radians
Ω	whirling frequency	
ω	angular velocity	radians/sec.

Subscripts

a	ambient
o	equilibrium position, critical speed of rotor
opt	optimum
r	radial
s	supply
t	tangential
CR	critical
res	resonant frequency

Superscripts

—	dimensionless